AD NUMBER

ADB027935

LIMITATION CHANGES

TO:

Approved for public release; distribution is unlimited.

FROM:

Distribution authorized to U.S. Gov't. agencies only; Test and Evaluation; JUN 1976. Other requests shall be referred to Air Force Armament Lab., Eglin AFB, FL.

AUTHORITY

USADTC ltr 10 Dec 1979

FOR FURTHER TRAN

AFATL-TR-76-64

THE EFFECTS OF HIGH INTENSITY IMPULSE LOADING ON REINFORCED CONCRETE BEAMS

OKLAHOMA STATE UNIVERSITY
SCHOOL OF CIVIL ENGINEERING
STILLWATER, OKLAHOMA

JUNE 1976

FINAL REPORT FOR PERIOD
JANUARY 1973-MAY 1976

AIR FORCE ARMAMENT LABORATORY
AIR FORCE SYSTEMS COMMAND • UNITED STATES AIR FORCE
EGLIN AIR FORCE BASE, FLORIDA

UNCLASSIFIED

SECURITY CLASSIFICATION OF THIS PAGE (When Data Entered)

REPORT DOCUMENTATION PAGE

READ INSTRUCTIONS BEFORE COMPLETING FORM

1. REPORT NUMBER: AFATL-TR-76-64	2. GOVT ACCESSION NO.
3. RECIPIENT'S CATALOG NUMBER	Final rpt Jan 73 - May 76
4. TITLE (and Subtitle): THE EFFECTS OF HIGH INTENSITY IMPULSE LOADING ON REINFORCED CONCRETE BEAMS.	5. TYPE OF REPORT & PERIOD COVERED: FINAL--January 1973 through May 1976
	6. PERFORMING ORG. REPORT NUMBER
7. AUTHOR(s): J. N. Ingram, A. E. Kelly, O. P. Lloyd	8. CONTRACT OR GRANT NUMBER(s): F08635-73-C-0066
9. PERFORMING ORGANIZATION NAME AND ADDRESS: Oklahoma State University, School of Civil Engineering, Stillwater, Oklahoma	10. PROGRAM ELEMENT, PROJECT, TASK AREA & WORK UNIT NUMBERS: Program Element ESP 921H, JON 91340106
11. CONTROLLING OFFICE NAME AND ADDRESS: Air Force Armament Laboratory, Armament Development & Test Center, Eglin Air Force Base, Florida 32542	12. REPORT DATE: June 1976
	13. NUMBER OF PAGES: 145 (12) 164 p.
14. MONITORING AGENCY NAME & ADDRESS (if different from Controlling Office): (16) 9134 (17) 01	15. SECURITY CLASS. (of this report): UNCLASSIFIED
	15a. DECLASSIFICATION/DOWNGRADING SCHEDULE

16. DISTRIBUTION STATEMENT (of this Report)

Distribution limited to U. S. Government agencies only; this report documents test and evaluation; distribution limitation applied June 1976. Other requests for this document must be referred to the Air Force Armament Laboratory (DLYW), Eglin Air Force Base, Florida 32542.

17. DISTRIBUTION STATEMENT (of the abstract entered in Block 20, if different from Report)

18. SUPPLEMENTARY NOTES

Available in DDC

19. KEY WORDS (Continue on reverse side if necessary and identify by block number)

Impulse loaded reinforced concrete beams
Digital computer program IMPBC
Blast-structure interaction
Pentolite
Concrete beams
Blast loading
Vulnerability
Spherical charges

20. ABSTRACT (Continue on reverse side if necessary and identify by block number)

Presented in this report are the results of a study of the response of impulse loaded reinforced concrete beams. The objectives were to develop basic data of the blast-structural response phenomenon for the evaluation of structural survivability, and to compare these data with results of digital computer program, IMPBC, a simulation of the blast-structure interaction. Finally, the study included the definition of failure and a method for

* are presented - 267 pp

DD FORM 1 JAN 73 1473 EDITION OF 1 NOV 65 IS OBSOLETE

78 06 16 006

UNCLASSIFIED

SECURITY CLASSIFICATION OF THIS PAGE (When Data Entered)

assessing damage due to blast loading. The reinforced concrete beams were full-sized representations of members found in buildings.

There were twelve impulse tests, of which seven were performed on identical beams for which the material properties and steel percentage were typical of average construction practice. The remaining five were of beams having high strength concrete (two tests), high strength steel (one test), and greater steel percentage (two tests).

Impulse loading was obtained from the detonation of 214-pound spherical pentolite charges suspended above the beams. By adjusting the standoff distance of the charge to the upper surface of the beam, it was possible to vary the impulse and peak pressure. The test specimens were enclosed by a massive test frame which provided protection for the sides and lower surface of the test member. Only the upper surface of the beam was subjected to the pressure developed by the chemical explosion.

A damage assessment study followed the impulse tests. Static tests were performed to determine the change in beam strength, stiffness and ductility properties. These data were correlated with charge standoff distance to provide the failure criterion. For the members studied by this work, it was possible to correlate the total static work capacity with an estimate of the kinetic energy imparted to the structure by the impulse loading.

Finally, the high strength concrete beams exhibited the greatest resistance to damage from impulse loading. These members experienced little distress while the members with increased steel area and greater moment capacity suffered the greater damage. This was predicted by the damage criterion presented in this report.

PREFACE

This report is the result of an experimental and analytical study of reinforced concrete beams subjected to blast loading. The work was conducted by the Oklahoma State University, Stillwater, Oklahoma, from January 1973 through May 1976, under Contract No. F08635-73-C-0066, with the Air Force Armament Laboratory, Armament Development and Test Center (ADTC), Eglin Air Force Base, Florida. The project required the fabrication of test items at Oklahoma State University, with the blast tests performed by Eglin AFB. In addition to the performance of the impulse tests and supervision, Eglin AFB provided data reduction support for this work. The program was managed by Mr. Marvis Adams (DLYW) for the Armament Laboratory.

Included in this report are experimental data from the blast tests as well as correlation with an existing computer program and a proposed criteria for the evaluation of blast damage. The program managers at Oklahoma State University were Drs. Allen E. Kelly and John P. Lloyd. Mr. J. Nelson Ingram served as research project engineer, both in Stillwater, Oklahoma, and at Eglin AFB, Florida.

This technical report has been reviewed and is approved for publication.

FOR THE COMMANDER

J. R. MURRAY
Chief, Analysis Division

(The reverse of this page is blank)

TABLE OF CONTENTS

TABLE OF CONTENTS (Concluded)

LIST OF FIGURES

LIST OF FIGURES (CONTINUED)

LIST OF FIGURES (CONTINUED)

LIST OF FIGURES (CONCLUDED)

LIST OF TABLES

LIST OF ABBREVIATIONS, ACRONYMS, AND SYMBOLS

A	acceleration, in/sec^2
A_s	tensile steel area, in^2
b	beam width, in
d	effective depth of tensile steel, in
E	Young's modulus, psi
EI	beam flexural stiffness, $lb\text{-}in^2$
f'_c	static concrete ultimate strength, psi
f'_{Dc}	dynamic concrete ultimate strength, psi
f_{Dy}	steel yield stress under large strain rates, psi
f_y	steel yield stress under static loading, psi
g	unit of gravitational acceleration, 386 in/sec^2
i	total impulse, lb-sec
I	impulse per unit area, psi-ms
KE	kinetic energy, lb-in
L	beam span, in
m	beam mass per unit length, $lb\text{-}sec^2/in^2$
ms	millisecond
M	beam bending moment, lb-in
M_b	beam mass, $lb\text{-}sec^2/in$
M_y	beam yield moment. lb-in
M'_u	static ultimate moment, lb-in

LIST OF ABBREVIATIONS, ACRONYMS, AND SYMBOLS
(Continued)

$M'_u(D)$	static ultimate bending moment for damaged beam, lb-in
$M'_u(T)$	theoretical ultimate bending moment, lb-in
P_o	peak reflected pressure, psi
P_{ult}	beam static failure load
R_m	maximum member resistance, lb
t	time, ms
t_d	pressure loading duration, ms
T	period of motion, ms/cycle
$T\emptyset$	tabulated data reference time
w	weight of beam per unit length, lb/in
W_p	work performed on beams in forcing them from yield to failure displacement, kip-in
X_G	vertical distance between steel and concrete strain gages, in
α	ratio of dynamic to static ultimate compressive strength, f'_{Dc}/f'_c
δ	beam load point displacement during static load test, in
δ_{max}	load point displacement at beam failure, in
δ_P	plastic load point displacement
δ_y	maximum elastic load point displacement
ε	strain
$\dot{\varepsilon}$	strain rate, sec^{-1}
ε'_c	static ultimate concrete strain
ε'_{Dc}	ultimate concrete strain under dynamic loads

LIST OF ABBREVIATIONS, ACRONYMS, AND SYMBOLS
(Concluded)

γ	ductility, ratio of maximum plastic to maximum elastic displacement
μ	micro, 10^{-6} (unit prefix)
ρ	steel reinforcing ratio, $A_s/(bd)$
ϕ	curvature, rad/in

SECTION I

INTRODUCTION

The development of analytical methods to predict survivability of complex structures has been enhanced by the digital computer. When accuracy of weapon placement was uncertain, the need for accurate determination of structural survivability to a single weapon was hardly justified when one considered possible weapon placement. However, with sophisticated weaponry, not only the size of the weapon but also its placement may be accurately specified. Furthermore, it is likely the impulse produced by the weapon will be due to high pressure over a small time increment, typical of chemical explosion.

In recent years considerable data has been developed on the response of complex structures to nuclear blast loading. A significant characteristic of the loading is the relatively large duration of the loading as compared with fundamental frequencies of the structure. Furthermore, the nuclear blast can engulf the total structure. A chemical explosion, on the other hand, has a limited zone of influence and may be directed at a single critical structural member. Although the damage produced by the chemical explosion is very localized, by causing the failure of a critical structural member, the subsequent total structural damage may be severe. This study is focused on chemical explosions and the resulting structural damage to reinforced concrete beams.

To evaluate the survivability of a structure subjected to chemical explosions, it is necessary to study the survivability of the structural elements and the nature and location of the blast. Although a structure may survive the detonation of a weapon at the center of a wall or floor slab, the structure might collapse if the same weapon were detonated near a girder or column in the structure.

To develop data of the phenomenon, the Warhead Effectiveness Branch (DLYW) of the Air Force Armament Laboratory, Eglin Air Force Base, Florida, entered into a contract in 1973 with Oklahoma State University to develop survivability data for reinforced concrete beams.

1.1 OBJECTIVES

Reinforced concrete beams, similar to those found in conventional office buildings or warehouses, were subjected to high intensity impulse loads and the structural response measured by accelerometers, load cells, and strain gages. The high intensity impulse was provided by spherical pentolite

suspended over the beams. Five different beams were studied and included a typical beam, a typical beam without shear reinforcement, a beam with high strength concrete, a beam with high strength steel, and a beam with a large reinforcement ratio.

The first objective of these tests was to determine the impulse necessary to fail a given beam. By adjusting the distance from the charge to the test item, it was possible to vary the impulse. Data from Goodman (Reference 1) were utilized to select the charge size for the desired range of impulse.

The second objective of the program was to generate test data for the evaluation of a numerical method (IMPBC) (Reference 2) which was developed for the nonlinear analysis of impulse-loaded reinforced concrete beams.

1.2 PROGRAM DEVELOPMENT

The work summarized in this report was conducted over a 3½-year period at Oklahoma State University, Stillwater, Oklahoma, and Eglin AFB, Florida, from January 1973 until May 1976. The design and construction of the test beams and a supporting frame were performed at Stillwater, Oklahoma, and shipped to Eglin AFB, Florida. The impulse test program conducted by Eglin AFB began in May and was completed in September 1974. The explosive charges which generated the impulse were spherical pentolite provided by the Naval Weapons Station, Yorktown, Virginia. Following the blast tests, the beams were returned to the Oklahoma State University, Stillwater, Oklahoma, for final damage inspection and static tests.

The analysis of test data began in February 1974 and continued through January 1976. Three tapes, containing 304 data files, were assembled by the Eglin AFB Computer Sciences Laboratory and forwarded to Oklahoma State University for processing and analysis. The Oklahoma State University Field Office, Eglin AFB, Florida, provided valuable assistance in the modification of the data tapes for compatibility with the OSU (Stillwater) IBM 360/65 computer system.

Data analysis was divided into five stages, conducted simultaneously whenever possible. First, pressure data were reviewed for reliability and accuracy. This was performed by the review of pressure-time curves and digitized data listings provided by Eglin AFB. Second, methods for the integration of accelerometer data were studied to provide a suitable integration technique to obtain beam velocity and displacement. Third, the strain data were processed and studied: load cell data to determine beam reactions and strain gage data to calculate curvature. Fourth, data from a final static test program were used to evaluate the level of damage sustained during impulse tests. Finally, a correlation study was performed to compare test data

with results predicted by IMPBC (Reference 2), a program devoted to the nonlinear structural response of reinforced concrete beams subjected to impulse loading.

1.3 PROGRAM RESULTS

In general, the data developed by these tests were suitable for both the evaluation of computer program IMPBC and the definition of member damage. The acceleration data did not prove reliable for the analysis required in this work. Pressure data, from which the measured impulse was determined, indicated both pressures and impulses less than those predicted by Goodman (Reference 1).

Laboratory static tests following the impulse tests provided a means to estimate damage. The method for damage assessment is based on an extension of a design procedure of Biggs (Reference 3) in which the impulse to produce failure is related to the static plastic work capacity of the member.

In this report, each type of data is presented and discussed. However, a complete analysis for each test is not given because of similarities in data between tests and the quantity of data generated by this work. The test data are available for review in Appendix A. These curves were prepared by the Eglin AFB Computer Sciences Laboratory.

Of the beams tested, the one fabricated with high strength concrete sustained the least damage and the one with the greatest flexural strength, the beam with increased tensile steel, suffered the greatest damage. As a result of these tests, it was found that a member subjected to high intensity impulse loads should be fabricated using high strength concrete and modest quantities of ductile steel reinforcement.

SECTION II

PREVIOUS STUDIES OF IMPULSE LOADED REINFORCED CONCRETE BEAMS

The response of impulse loaded reinforced concrete beams is a function of several variables, among which are the strain rate, the material properties, and the cross section geometry. Under impulse loading, portions of a member experience high rates of change of curvature, which produce high strain rates in the steel and concrete. The net effect of high strain rates is to increase the strength and toughness of steel and the strength and crushing strain of concrete. These properties lead to increased member strength and ductility.

A number of studies of rapidly-loaded reinforced concrete beams with both full- and model-sized specimens have been reported. Although loads were applied mechanically, more recent studies have used explosives. The literature cited herein provides some information on both material and member behavior under rapid loading.

2.1 EFFECTS OF STRAIN RATE ON THE PROPERTIES OF STEEL

The strain rates discussed in the literature are based on average rates. Manjoine (Reference 4) investigated the effect of large strain rates on mild steel at temperatures varying from room temperature to 600°C. The stress-strain curves from room temperature experiments are given in Figure 1 for strain rates which vary from 9.5×10^{-7} to 300 per second. It was concluded in this study that increased strain rates cause the lower yield point, the yield strain, the strain at which strain hardening began, and the ultimate strength to increase. The influence of strain rate on significant parameters are summarized in Figure 2 as a function of strain rate. The steel used in that study was a low-carbon, open-hearth, mild steel, not a reinforcing steel.

The dynamic yield stress ratio, f_{Dy}/f_y, is presented in two studies (References 5 and 6). These ratios are shown in Figure 3 as a function of strain rate. Also shown in Figure 3 is a mathematical model of the relation between strain rate and dynamic yield stress ratio given by Perrone (Reference 7):

$$f_{Dy}/f_y = 1 + (\dot{\varepsilon}/D)^{1/n} \qquad (1)$$

where n and D are material dependent constants and $\dot{\varepsilon}$ is the strain rate. For mild steel these values are D = 40.4 per second and n = 5.

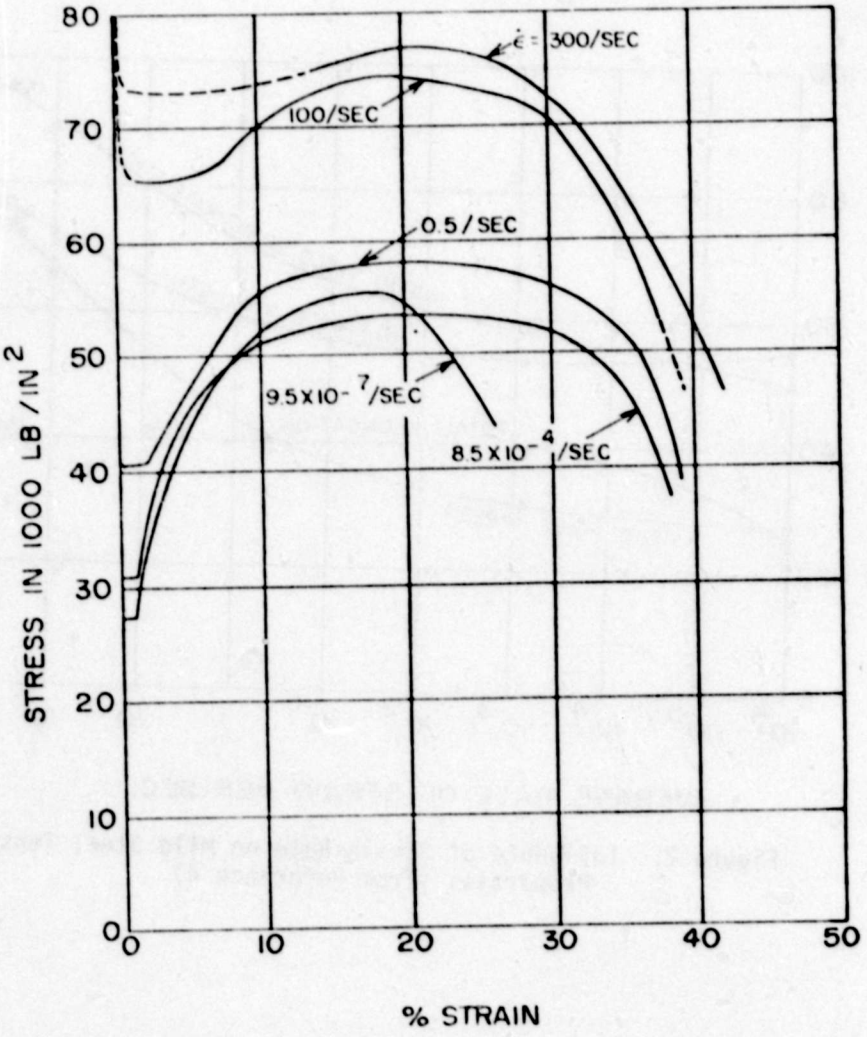

Figure 1. Stress-Strain Curves for Mild Steel for Various Strain Rates (From Reference 4)

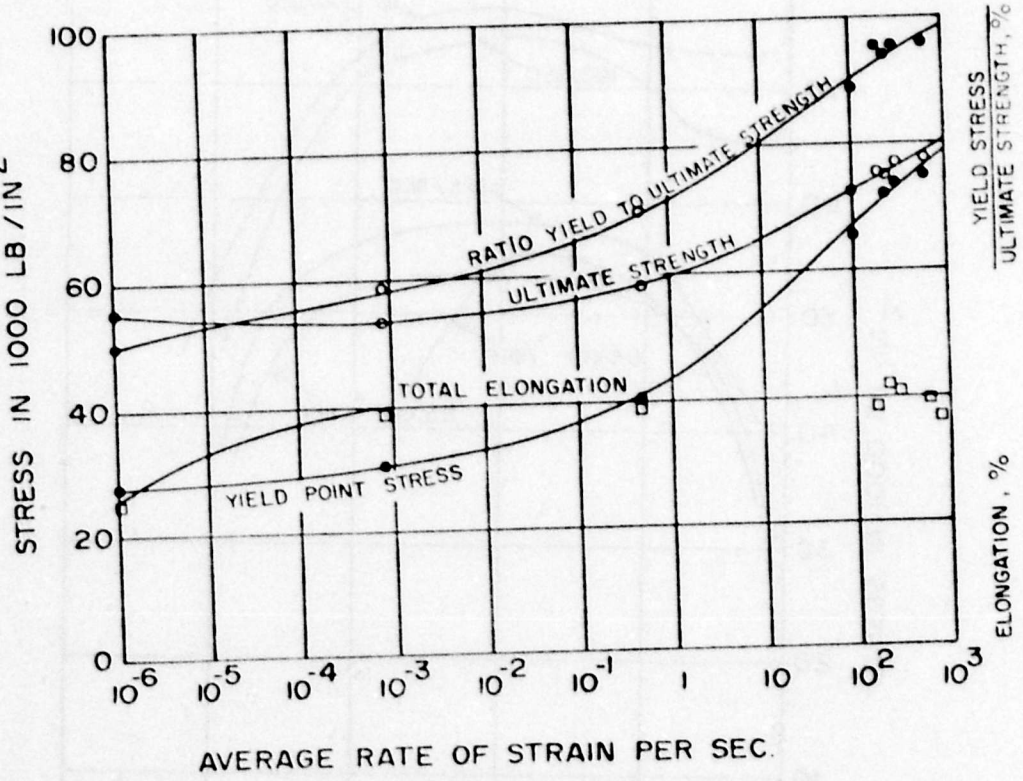

Figure 2. Influence of Strain Rate on Mild Steel Tensile Properties (From Reference 4)

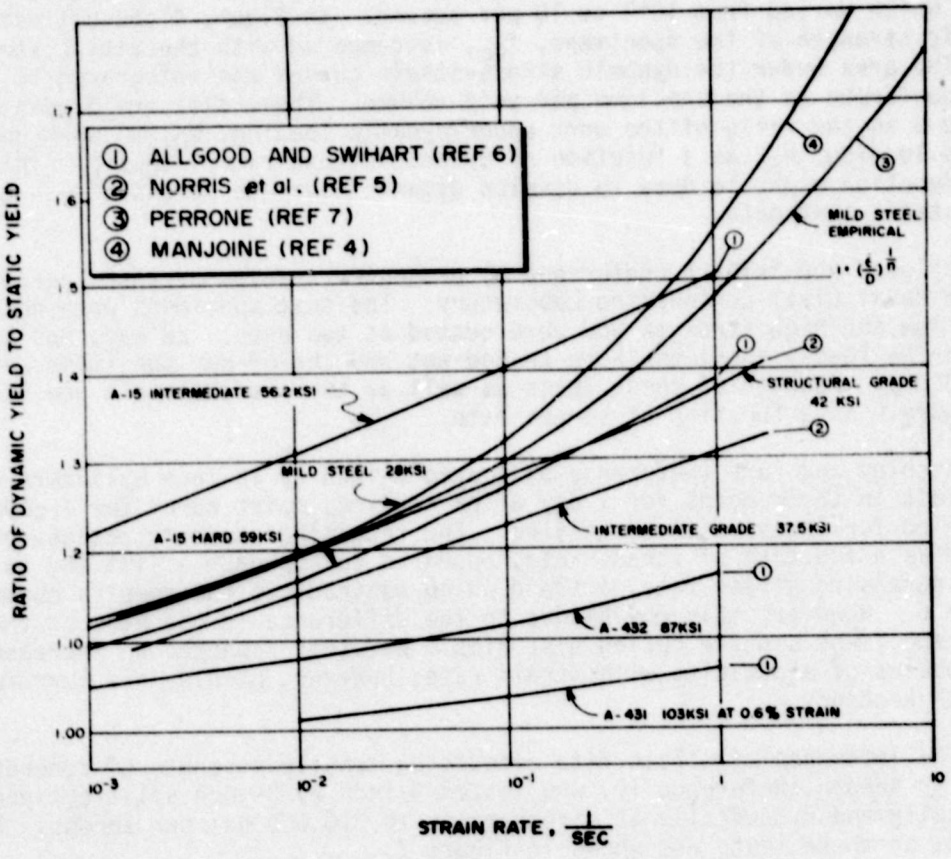

Figure 3. Influence of Strain Rate on Stress

2.2 EFFECTS OF STRAIN RATE ON THE PROPERTIES OF CONCRETE

A large compressive strain rate increases the ultimate strength, the strain at ultimate strength, and the strain energy. Watstein (Reference 8) tested 3-inch by 6-inch cylinders of 2000 and 6500 psi concrete at strain rates which varied from 10^{-6} to 10 per second. In Figure 4 the ultimate dynamic strength of the specimens, f'_{Dc}, is compared with the static strength, f'_c. The area under the dynamic stress-strain curves was integrated to yield work performed on the specimen per unit volume. These data are presented in Figure 5 as the ratio of the work under dynamic loading, W_D, to work under static loading, W_s, as a function of dynamic stress ratio, f'_{Dc}/f'_c. This work function might be used to develop dynamic concrete stress-strain curves from static test data.

Allgood and Swihart (Reference 6) presented results of tests performed at the Naval Civil Engineering Laboratory. The test specimens were noted as being low and high strength and were tested at two ages: 28 days and 49 days. The 28-day specimens were tested wet and the 49-day specimens were tested dry. Results of these tests as well as those of Watstein are shown in Figure 6 as a function of stress rate.

Atchley and Furr (Reference 9) tested 6-inch by 12-inch cylinders which were left in their molds for 1 day after casting, moist cured for 7 days, and air dried for 1 day prior to testing. The resulting strength ratios, presented as a function of stress rate, appeared to approach a limiting value with increasing stress rate, a trend which contradicts the results shown in Figure 6. However, this may be due to the difference in the ages of the concrete specimens and the curing histories. Watstein reported an increase for the modulus of elasticity with strain rate; however, Atchley and Furr found no such tendency.

The influence of strain rate effects on tensile strength of concrete was given by Keenan (Reference 10) who tested 4-inch by 8-inch split cylinders statically and dynamically at stress rates to 210,000 psi per second. The results of these tests are shown in Figure 7.

Fox (Reference 11) and Galloway and Rathby (Reference 12) performed rapid load tests on plain concrete beams to assess the effects of transient loads on the modulus of rupture. They reported increases in the modulus of rupture as large as 66 percent. There is some indication that their results, which are dependent on measured reactions, have not been corrected for inertial forces of the specimens and supports.

2.3 RESEARCH ON REINFORCED CONCRETE BEAMS SUBJECTED TO HIGH LOAD RATES

Over the years a number of studies (e.g., References 10 and 13 through 29) have been performed to determine the performance of reinforced concrete

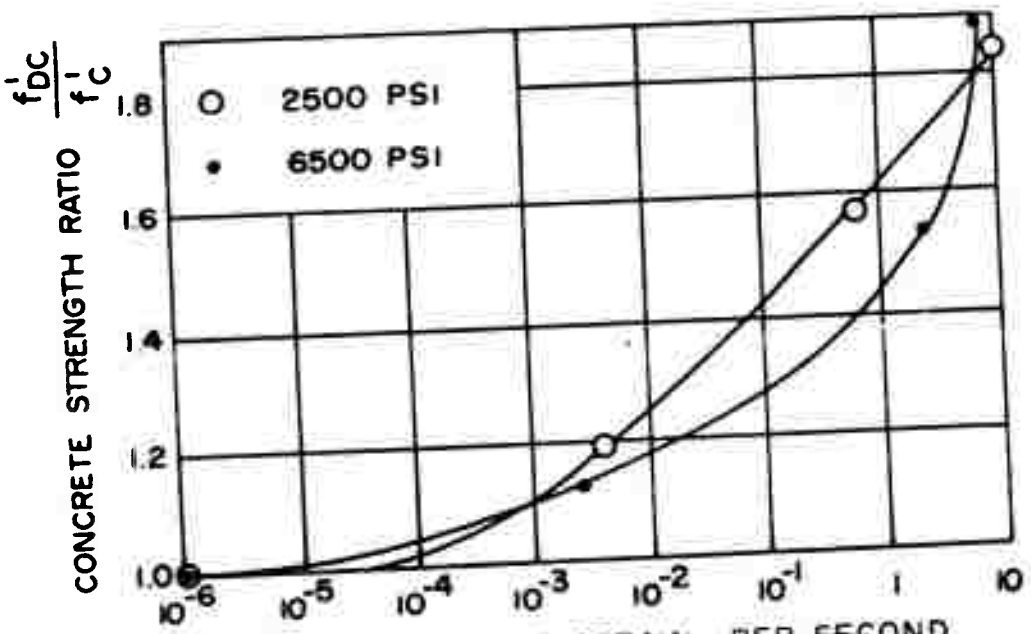

Figure 4. Influence of Strain Rate on Concrete Cylinder Strength (From Reference 8)

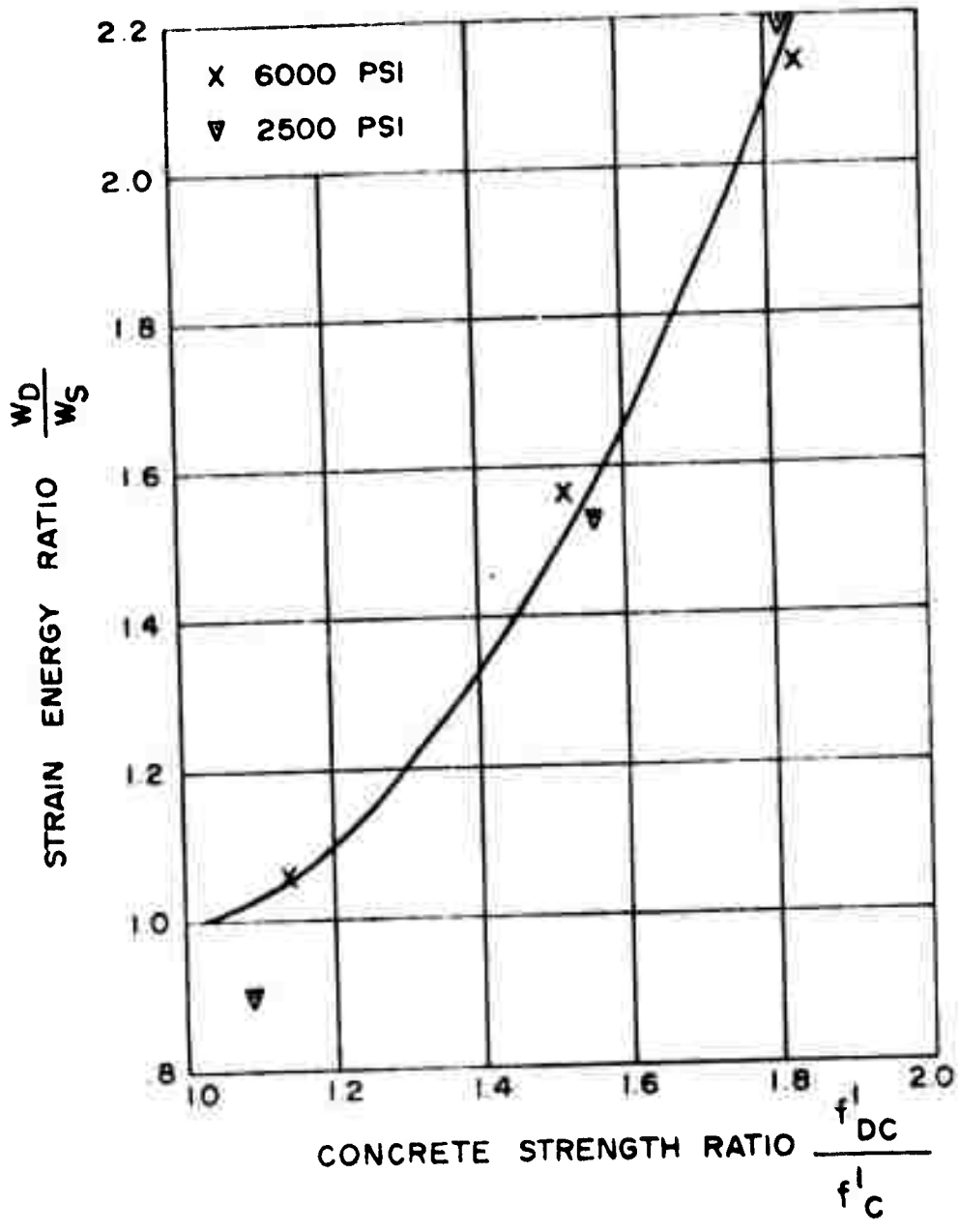

Figure 5. Relation Between Strain Energy Capacity and Concrete Strength Ratio (From Reference 8)

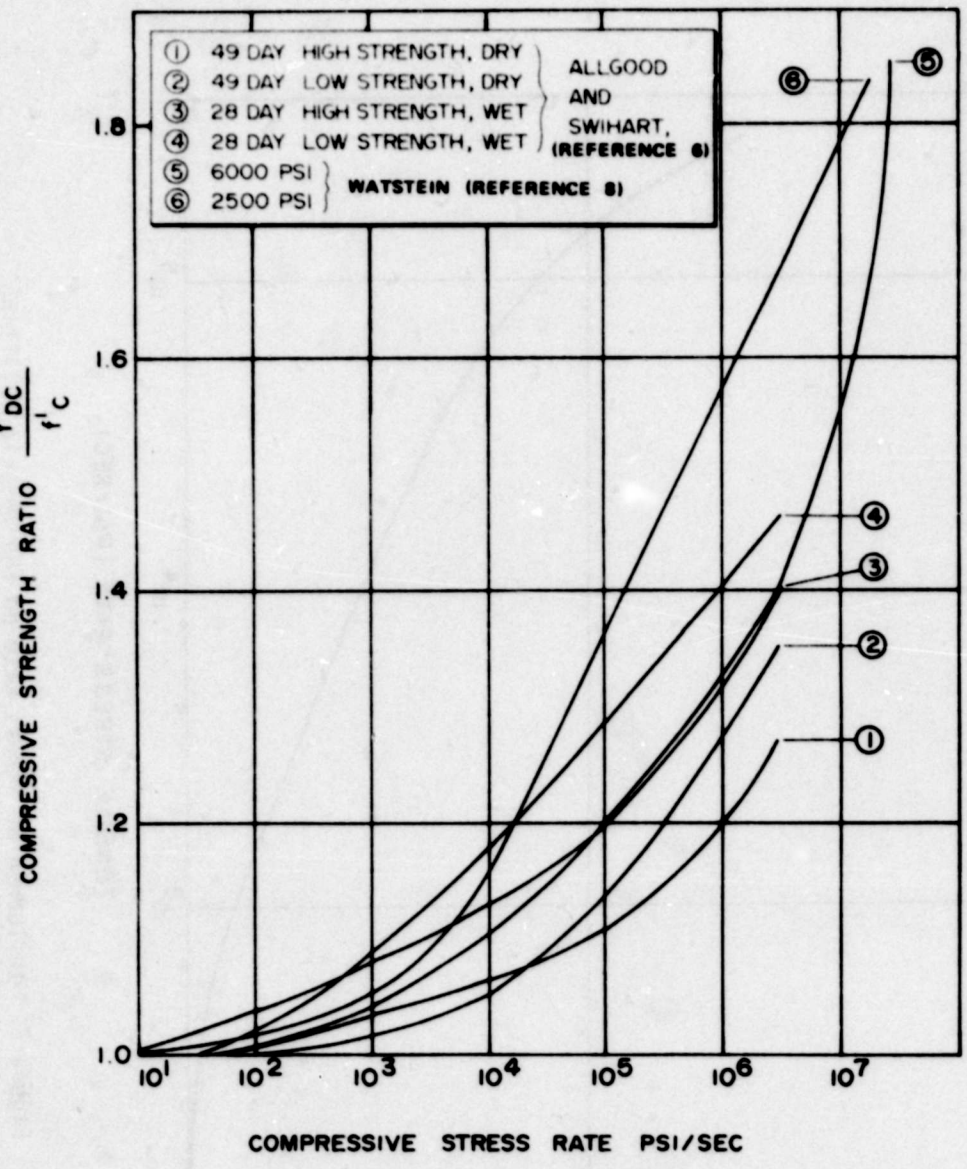

Figure 6. Comparison of Experimental Concrete Strength Ratios

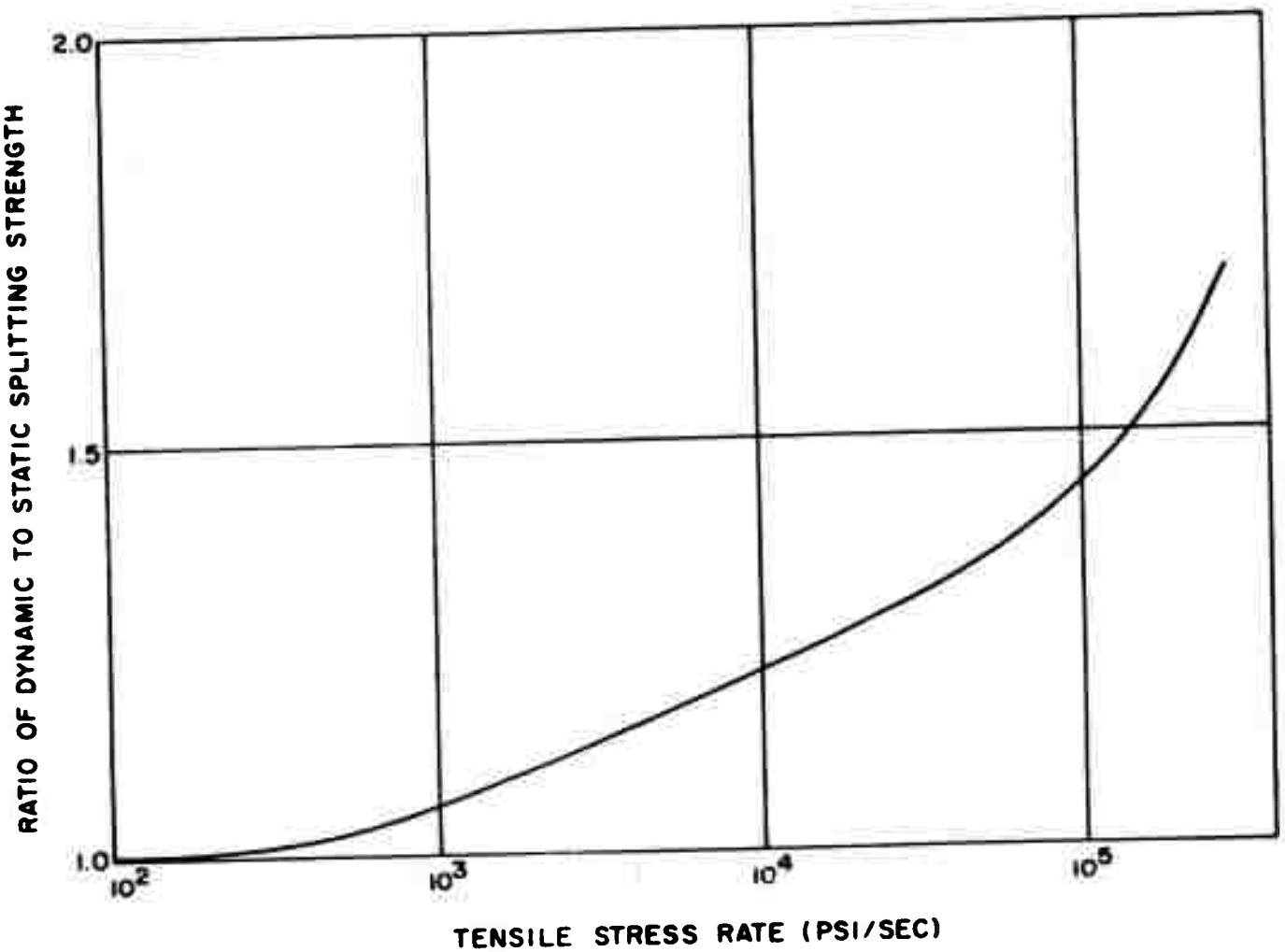

Figure 7. Influence of Stress Rate on the Tensile Splitting Strength of Concrete Cylinders (From Reference 10)

elements under rapid loading. Although the tests often involve ingenious experimental techniques, deficiencies in instrumentation and other test details limit the value of the results from these efforts to this program.

2.4 DISCUSSION

From the available literature, a number of factors relative to the behavior of reinforced concrete members subjected to impulse loading have been presented. Both concrete and reinforcing steel are influenced by large strain rates. For concrete, the effect is for the stress and strain at crushing to increase with strain rate. This would cause corresponding increases in the curvatures at which a beam segment experiences concrete distress. For steel, large strain rates cause the yield stress to increase and consequently, the yield moment, M_y. The increase in dynamic yield stress relative to the static yield stress is larger for the intermediate and structural grade steels than for the high strength steels. These properties were verified by tests of the materials and reinforced concrete beams.

Material properties are presented as a function of average strain rates. There was no discussion of possible effects of variable strain rates; however, this phenomenon may be of significance. The strain rate varies from a maximum value, following the application of the impulse loading, to zero at the maximum deflection.

During the planning stages of the program, it was recognized that the experiments which would be conducted with explosives would entail many uncertainties. If a test was conducted with the charge too far from the specimen, only minimal damage would occur, data would be of little value, and the specimen would not be useful for further tests. On the other hand, if the charge was placed too close, the impulse would not only fail the beam but possibly the test frame and instrumentation.

For these reasons, a number of specimens were fabricated to be as identical as possible; these specimens were to permit several tests to be performed under increasing impulse. Several other beams were fabricated with certain properties significantly different than the typical beams; however, the properties of all beams were chosen to be within the scope of actual construction practice.

SECTION III

TEST SPECIMENS

The objective of this investigation was to subject reinforced concrete beams to very short duration pressure loads, to study the blast-structure interaction, and to assess the resulting damage. Test specimens were fabricated to be representative of full-sized beams used in typical building construction.

The test specimen was selected so that it was large enough to preclude similitude problems, yet small enough to minimize cost and procurement of test fixture and explosives. A member 8 inches by 12 inches appeared to satisfy these requirements.

3.1 BEAM GEOMETRY

The overall geometry proposed above was found acceptable and was used to plan beams in five different configurations, Table I. At the time of fabrication, the number of explosive charges available to the project was unknown. For these reasons, more beams were originally fabricated than subsequent budget restrictions permitted to be included in the test program. This report considers only beams subjected to impulse loading on detailed static tests. Figure 8 shows the general beam dimensions as well as the details of reinforcing steel and the end support connection.

A steel end angle (L 6x6x3/8) was cast in the beam to provide a connection and bearing seat for the end support mechanism. The end angle also provided anchorage for the reinforcing bars to insure development of steel strength near the end of the beam.

3.2 BEAM INSTRUMENTATION

Accelerometers, strain gages, and load cells were used to measure the response of the beam. Three accelerometers and four pairs of strain gages were installed in each beam. Two pairs of strain gages and one accelerometer were installed at the midspan of the beam. The other pairs of strain gages and accelerometers were installed at quarterpoints. The strain gage installation is shown in Figure 9. The quarter station instrumentation provided a check of symmetry and greater reliability for quarter station data.

The concrete gages were applied to the beam sides approximately 1.6 inches below the top surface. The gages were placed in a shallow 2-inch by 8-inch depression for protection from mechanical damage. Figure 10 shows a

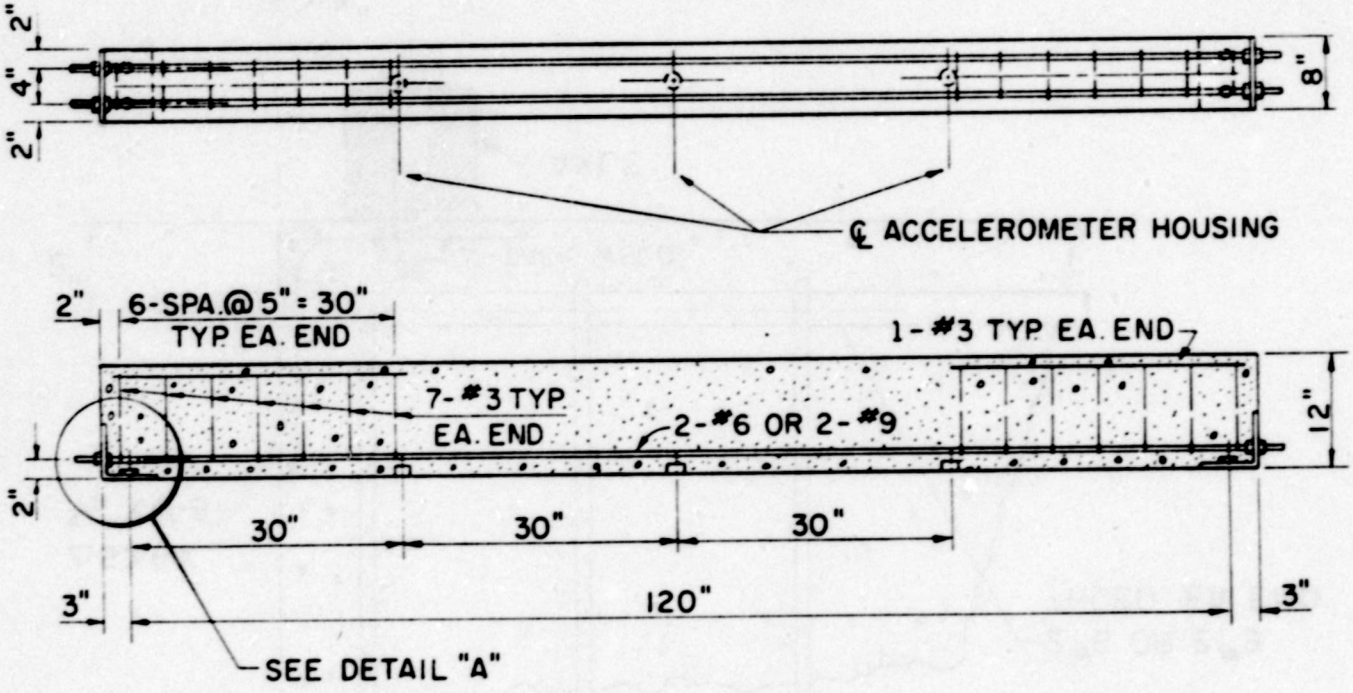

Figure 8. Test Beam Details

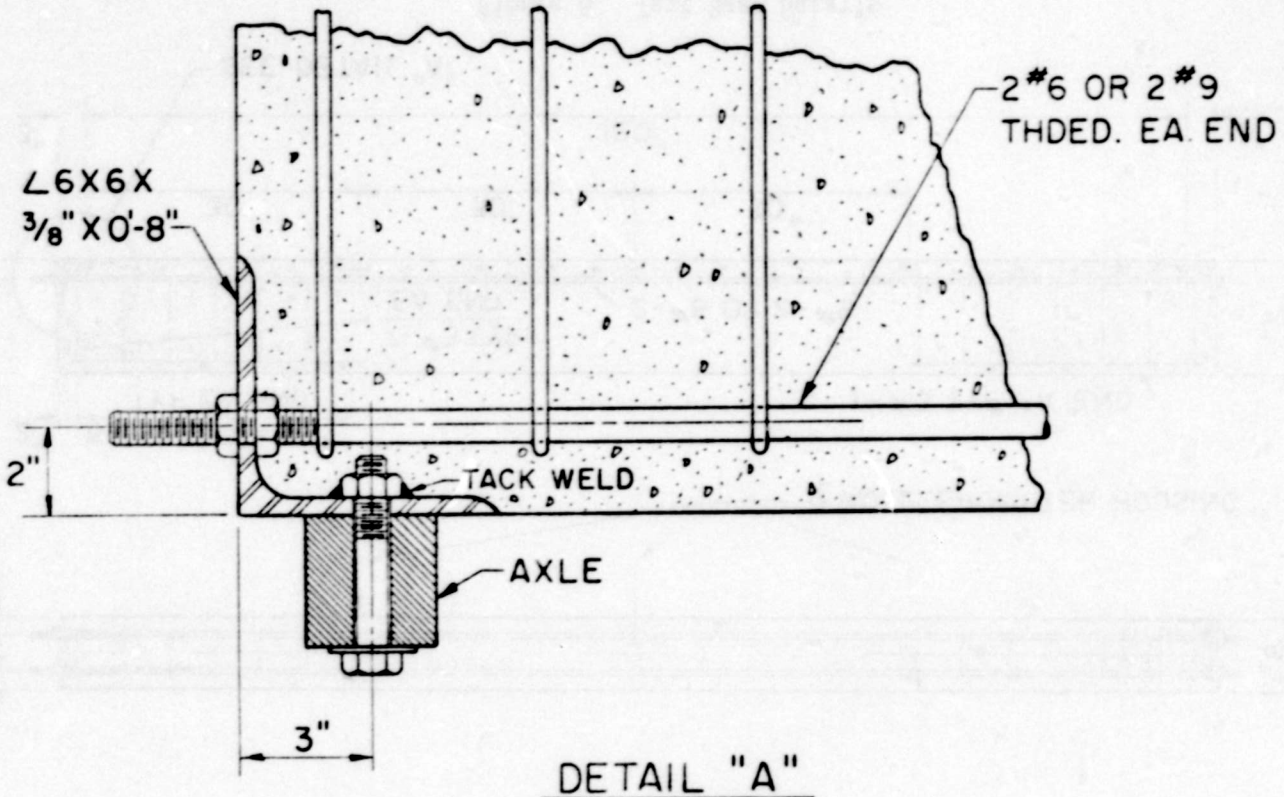

Figure 8. Test Beam Details (Concluded)

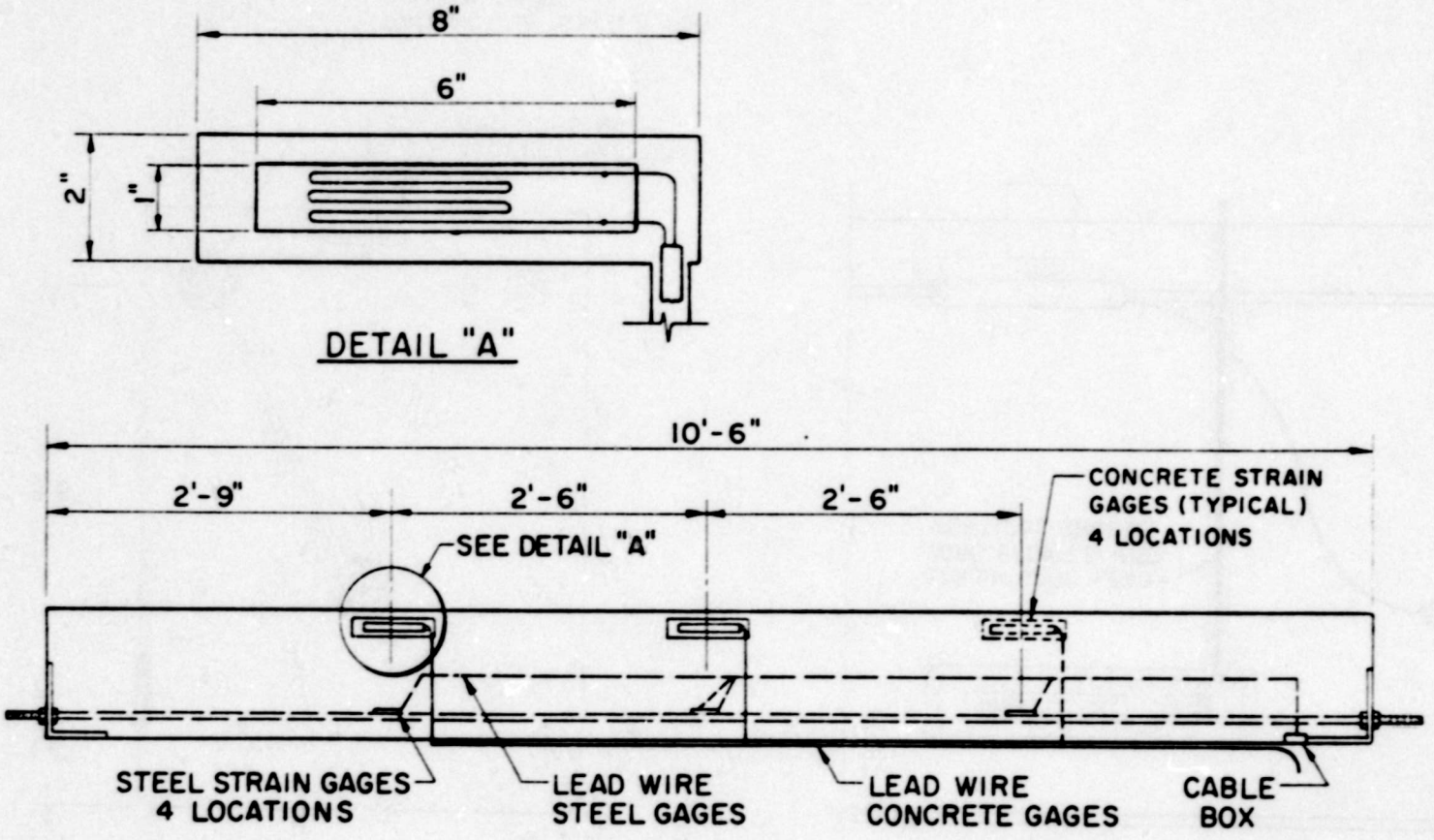

Figure 9. Strain Gage and Lead Wire Installation Details

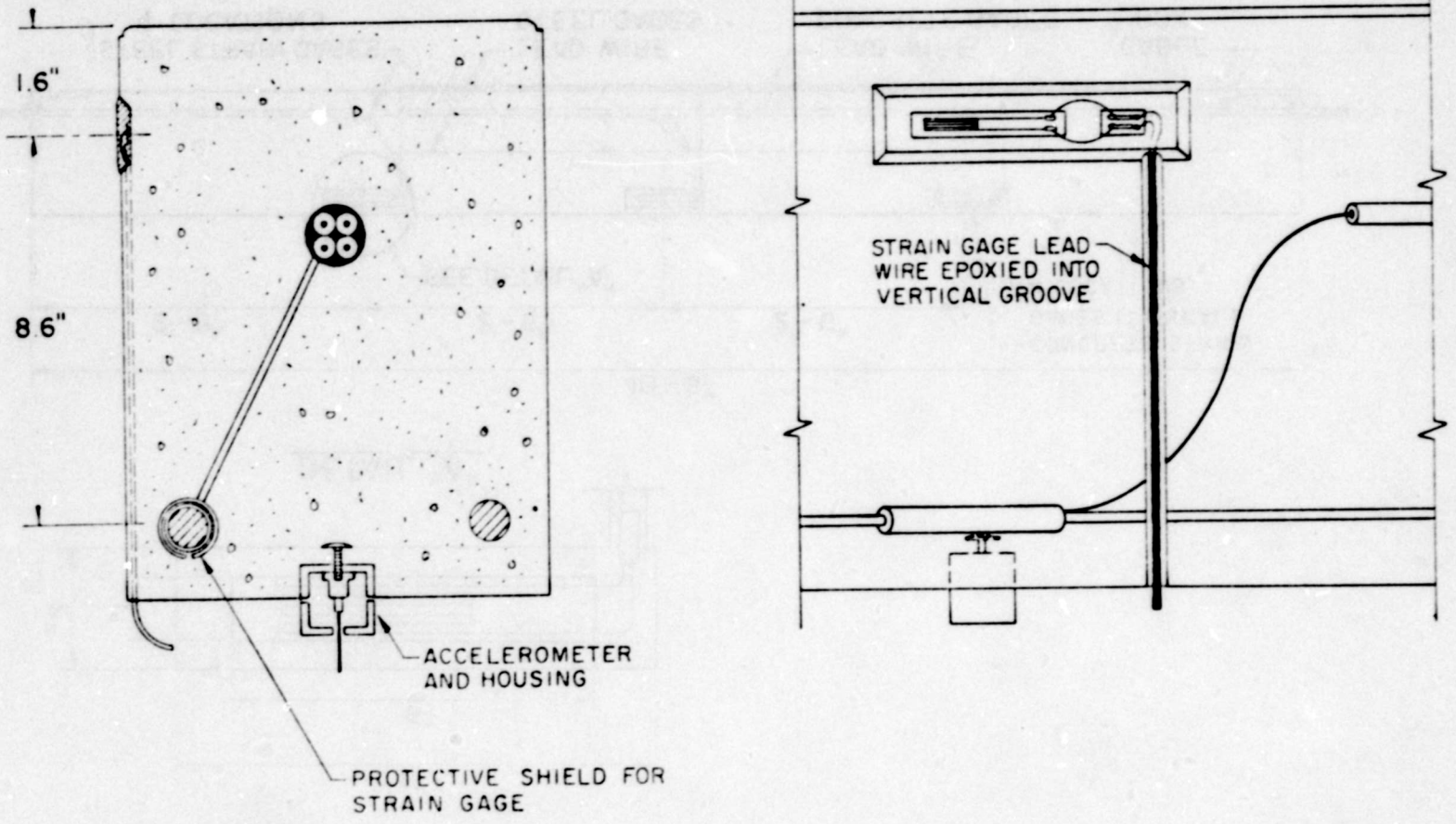

Figure 10. Typical Instrumentation at Beam Quarter Point

TABLE I. BEAM CONFIGURATION SCHEDULE

Beam Numbers	Beam Type	Nominal Design Parameters				
		f'_c (ksi)	f_y (ksi)	A_{s_2} (in^2)	Reinforcing Ratio	Shear Stirrups
1,2	High strength concrete	6	40	0.88	0.0104	Yes
3,4	Increased steel area	3	40	2.00	0.0239	Yes
5	Increased steel strength	3	60	0.88	0.0104	Yes
6,7	Shear stirrups removed	3	40	0.88	0.0104	No
8-13	Typical	3	40	0.88	0.0104	Yes

TABLE II. PROPERTIES OF REINFORCING STEEL

Beam Numbers	Bar Size	f_y (ksi)	f_{ult} (ksi)	Percent Elongation
1,2,6-13	No. 6	51.95	82.85	22.15
5	No. 6	62.50	100.00	---[a]
3,4	No. 9	50.50	81.80	24.00

[a]Data not obtained.

side view of a beam-quarterpoint station and illustrates the placement of the concrete strain gage and its connecting lead wire. The cross section shows the steel gage installation with its lead wire passing up to a harness near the center of the beam. Also illustrated in this figure is the accelerometer housing with an accelerometer and lead wire in place. The steel strain gage installation is illustrated in Figure 11.

3.3 MATERIAL DESCRIPTION

Properties of the steel, fine aggregate, coarse aggregate, cement and concrete, are presented in this section. Static tensile test results for the reinforcing bars are given in Table II. The coarse aggregate was 3/4 inch crushed limestone from the Quapaw Quarry, Drumright, Oklahoma. The fine aggregate was Cimmaron River sand from the Dolese Quarry, Guthrie, Oklahoma. Type I portland cement was manufactured by the Dewey Division of Martin-Marietta. The aggregate properties are given in Tables III and IV.

The properties of the concrete for each beam are given in Table V. In addition to these data, the strain at ultimate load was recorded for a limited number of compression cylinders. For concrete with a compressive strength of 3000 psi, the average strain, ε_c', from four samples was 0.0022, while a sample of concrete with a compressive strength of 6000 psi gave a value of 0.0021. These data are required for the construction of the concrete stress-strain curves for dynamic loading.

3.4 TEST SPECIMEN FABRICATION

Beam fabrication and instrumentation was performed in three stages:

(1) Application of strain gages to the reinforcing bars
(2) Casting and curing beams and control cylinders
(3) Application of the strain gages to the surface of the beams.

The beams were cast in a steel form. The beams were 8.2 inches wide and 12.2 inches deep. Each beam was cast in three 4-inch lifts; each lift was from a separate batch. A portion of each batch was cast into control cylinders: four 6x12-inch cylinders and four 6x6-inch cylinders. The 12-inch cylinders were compressive strength specimens while the 6-inch cylinders were used for the Brazil indirect tensile strength test. Half of these cylinders were moist cured and were tested for ultimate strength at the age of 28 days. The other half were cured with the beam and were tested as soon after the beam field test as was practical.

After casting, the beam and control cylinders were covered with wet burlap and a layer of plastic for about 16 hours. At this time the beam and half of the control cylinders for each batch were removed from the forms and set aside to moist cure under wet burlap and plastic for an additional 6 days.

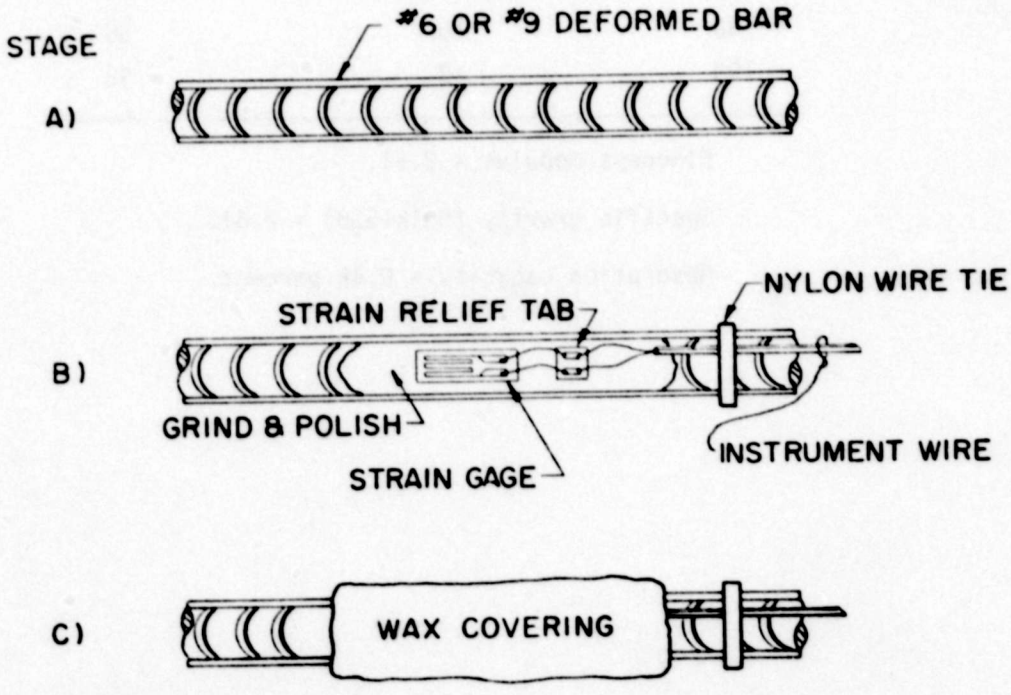

Figure 11. Typical Strain Gage Installation on Reinforcing Steel

TABLE III. GRADATION OF FINE AGGREGATE

Sieve Size Numbers	Percent Retained	Cumulative Percent Retained
4	1	1
8	4	4
16	12	16
30	30	46
50	40	86
100	12	98

Fineness modulus = 2.51.

Specific gravity (bulk-SSD) = 2.61.

Absorption capacity = 0.46 percent.

TABLE IV. GRADATION OF COARSE AGGREGATE

Sieve Size (inches)	Percent Retained	Cumulative Percent Retained
1 1/2	0	0
1	5	5
3/4	40	45
1/2	35	80
3/8	11	91
4	5	95

Fineness modulus = 7.31.

Specific gravity (bulk-SSD) = 2.79.

Absorption capacity = 0.90 percent.

TABLE V. CONCRETE PROPERTIES

Beam Numbers	Water-Cement Ratio	Unit Weight (lbs/ft^3)	Percent Entrapped Air	28-Day Strength f'_c(psi)	28-Day Strength f'_{sp}(psi)	Strength at Test f'_c(psi)	Strength at Test f'_{sp}(psi)	Modulus of Elasticity at 28 Days (ksi)
1	0.44	155	2.5	5710	505	5870	413	5640
2	0.44	154	1.9	5760	432	5960	425	5780
3	0.71	154	2.1	3660	415	4350	372	4750
4	0.72	154	1.5	3500	392	3960	322	4680
5	0.72	154	1.6	3420	367	3820	343	4600
6	0.72	154	1.8	3470	362	3650	331	4450
7	0.71	153	2.0	3810	390	3900	346	5020
8	0.71	152	2.5	3770	382	3590	327	---[a]
9	0.71	152	2.1	3710	389	3690	331	---[a]
10	0.72	150	2.0	3660	369	3860	323	5050
11	0.71	155	1.3	3740	393	---[b]	---[b]	5020
12	0.72	151	4.3	3440	363	3880	345	4560
13	0.72	151	3.7	3046	386	4160	394	4690

[a]Modulus not taken for beams 8 and 9.

[b]Strength at time of test not determined.

followed by air drying. The remaining cylinders were placed in a moist cure room and were strength tested at 28 days.

SECTION IV

TEST PROGRAM

The test program extended from October 1973 through November 1974 and was conducted in three phases. The initial tests were conducted at Oklahoma State University, Stillwater, Oklahoma, and were designed to check instrument performance. The second phase was conducted at Eglin AFB, Florida, from May through September 1974, where the impulse tests were performed. Finally, the beams were returned to Stillwater, Oklahoma for final tests.

4.1 PRELIMINARY STATIC LOAD TESTS

Tests were conducted with the beams mounted in a test fixture as shown in Figure 12. Symmetrical static loads were applied to produce constant moment in the center 48-inch span of the beam. Steel and concrete strains, along with the curvature of the constant moment region were recorded. The purposes of these tests were:

(1) To precrack the beam prior to application of the impulse loads so its stiffness would be similar to that of a beam with a prior service load history,

(2) To determine flexural stiffness of the beam in the constant moment span, and

(3) To compare curvature calculated from steel and concrete strains with measured curvature.

The beams were cyclically loaded, from one to three cycles, with progressively larger maximum loads, as shown in Figure 13. In each cycle the load was increased to a peak value and then gradually decreased to zero. The maximum load was equal to or slightly larger than half the theoretical ultimate load. Following the preliminary load cycling, a load which was 40 percent of the theoretical ultimate was applied. The data from this last cycle were used to estimate the flexural stiffness and are presented in Table VI.

Strains measured at the midpoint were used to calculate the curvature, ϕ_S, at the maximum load of each loading cycle. These were compared with the measured curvature, ϕ_D, as shown in Figure 14. The curvatures calculated from strains tended to be less than those found by displacements.

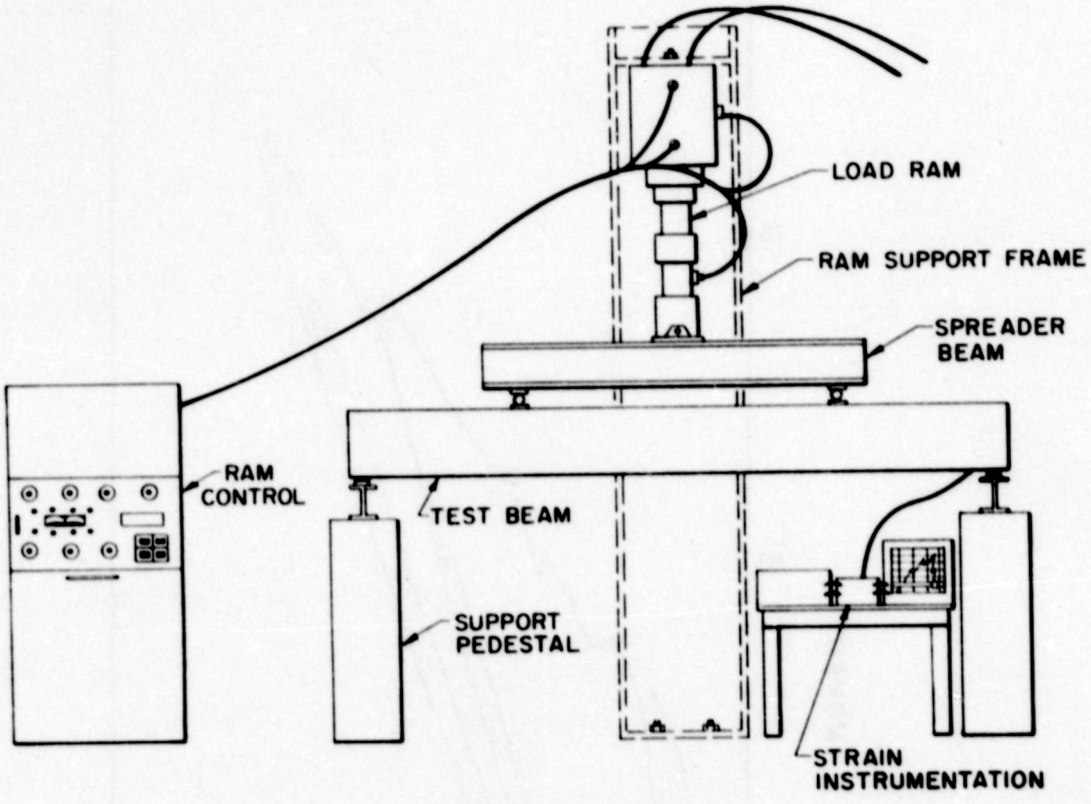

Figure 12. Beam Installed in Laboratory Test Fixture for Preliminary Static Load Tests

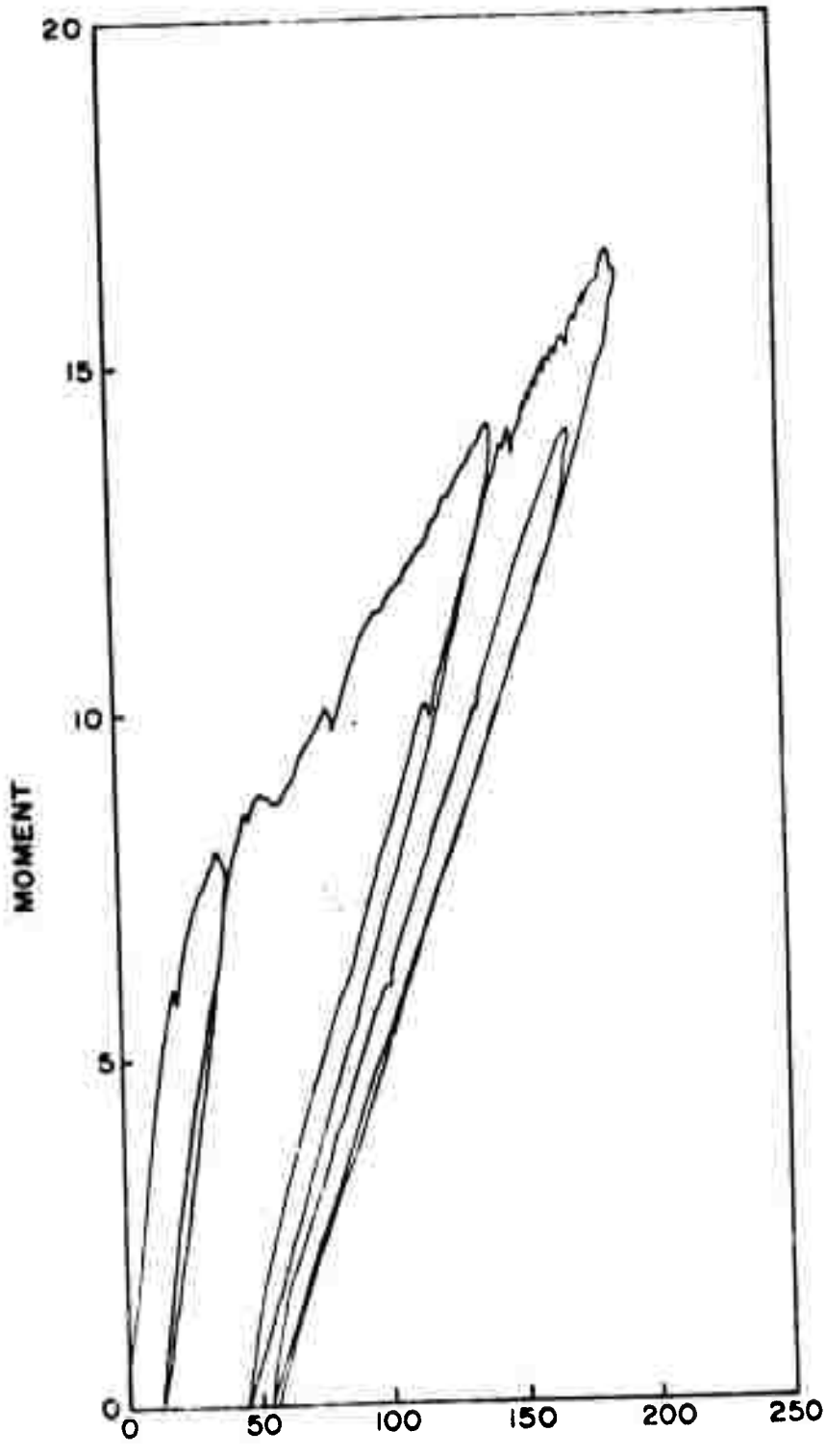

Figure 13. Typical Moment-Curvature Plot From Preliminary Static Load Tests

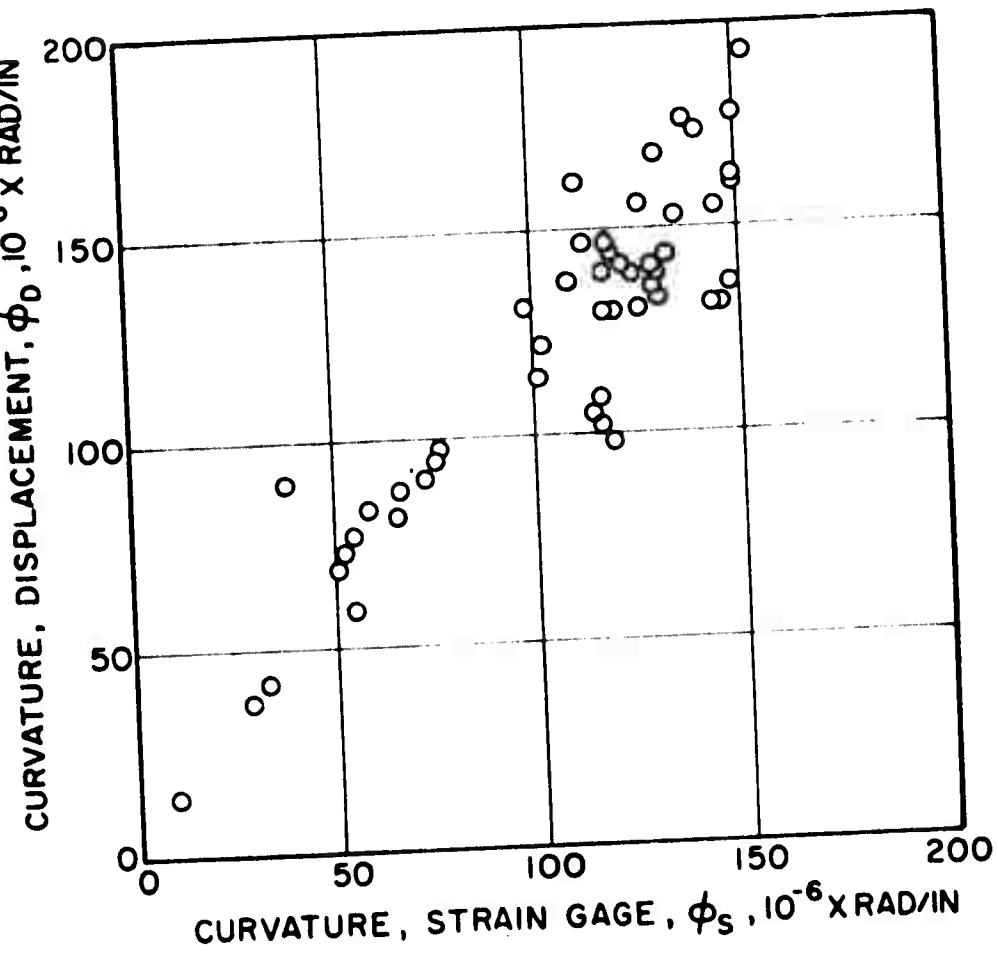

Figure 14. Correlation Between Curvature Measurements

TABLE VI. MEASURED FLEXURAL STIFFNESS

Beam Numbers	Measured Stiffness ($lb\text{-}in^2$)
1	1.32×10^9
2	1.34×10^9
3	2.06×10^9
4	1.91×10^9
5	1.50×10^9
6	1.38×10^9
7	1.36×10^9
8	1.40×10^9
9	1.53×10^9
10	1.36×10^9
11	1.17×10^9
12	1.44×10^9
13	1.44×10^9

4.2 IMPULSE TESTS

The test beams and the support equipment were shipped to Eglin AFB, Florida, following the preliminary static load tests. The test fixture was installed in Test Site C-80A and 12 tests were conducted there between 17 May and 19 September 1974. Data obtained in these tests were documented by Reichstetter (Reference 29).

4.2.1 Test Facilities

4.2.1.1 Test Site. A plan view of the test site, Figure 15, shows a test arena located a quarter mile from a control bunker. The elevation view in Figure 15 shows the arrangement of the major test components. Cables stretched between a pair of 30-foot guyed poles supported the explosive charge above the center of the test fixture. The charge standoff distance was adjusted by a winch attached to one pole. Instrumentation lead-wires were buried in a shallow trench leading to an arena instrumentation bunker about 200 feet away. This bunker housed data acquisition equipment for the strain gage and load cell signals. The accelerometer and pressure transducer signals were transmitted to data acquisition equipment in the control bunker.

4.2.1.2 Test Fixture. The test beams were installed in a massive instrumented test fixture which rested on a 3-foot-thick concrete slab. The test fixture was designed so that only the top surface of the test beam was loaded by the shock wave. The test fixture, shown in Figure 16, was constructed for the purpose of protecting the test beam, the instrumentation, and the beam support assembly. It consisted of a base slab with key-ways cast into each end. In each key-way a beam support mechanism was positioned over three load cells as shown in Figure 17. Four concrete blocks were placed on the base slab to enclose the beam and its support assemblies. The four blocks were fastened to each other and to the base slab by horizontal and vertical tie rods.

Steel plates were placed on top of the fixture flush with the top surface of the beam as shown in Figure 18. A small gap was left between the plate and the beam to prevent the plate from interfering with the beam motion. This gap was sealed with a light gage steel sheet.

The top plate incorporated machined receptacles to hold the pressure transducer mounts, as shown in Figure 19. These mounts positioned the pressure transducers flush with the top surface of the plate. The transducer lead wires passed through conduits in the siderails and base slab to one key-way to shield them from blast effects.

4.2.1.3 Explosive Charges. Twelve charges were procured by Eglin AFB, Florida for the test program. They were 18.75-inch-diameter spheres of pentolite weighing 214 pounds. Each charge was suspended from the overhead

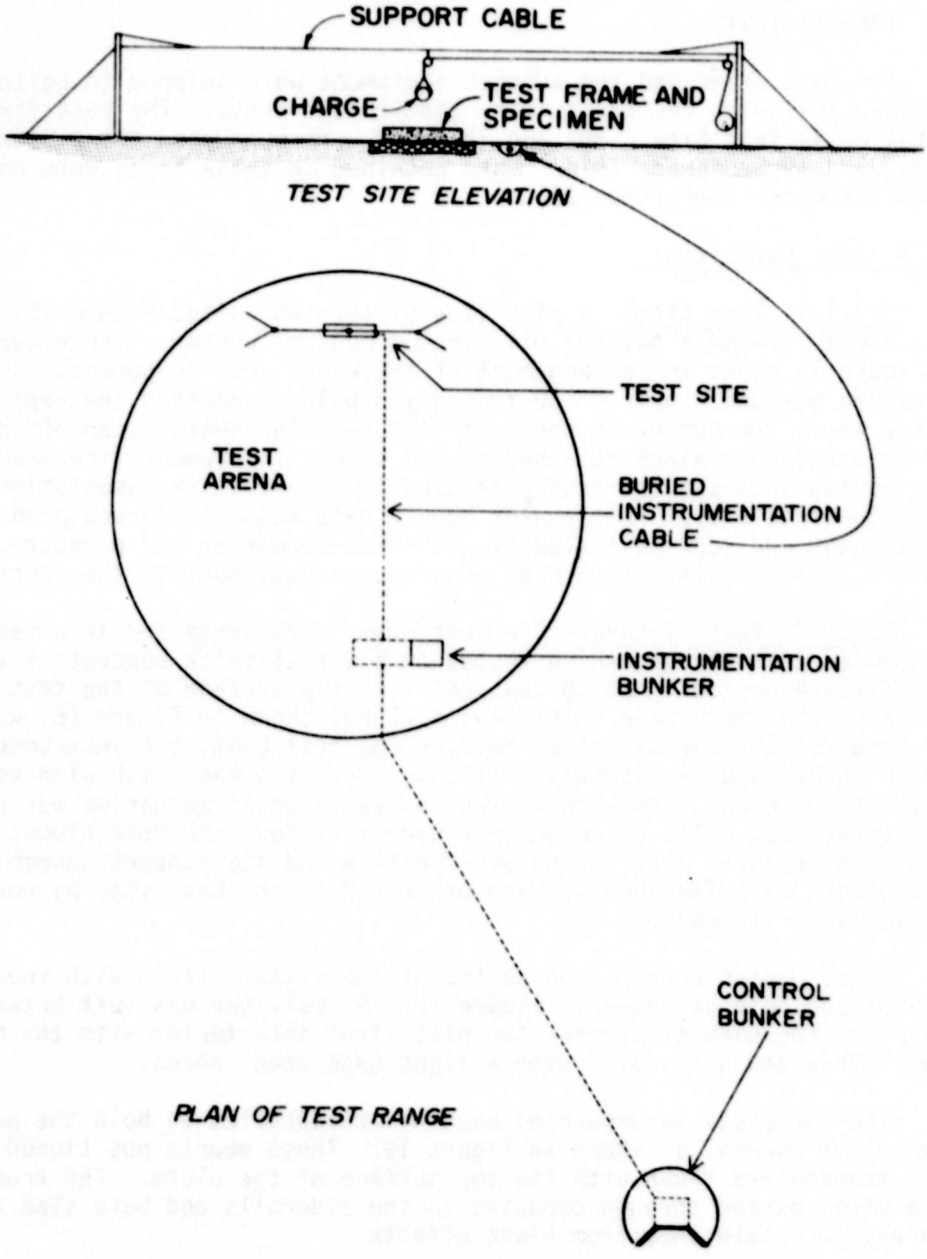

Figure 15. Test Site

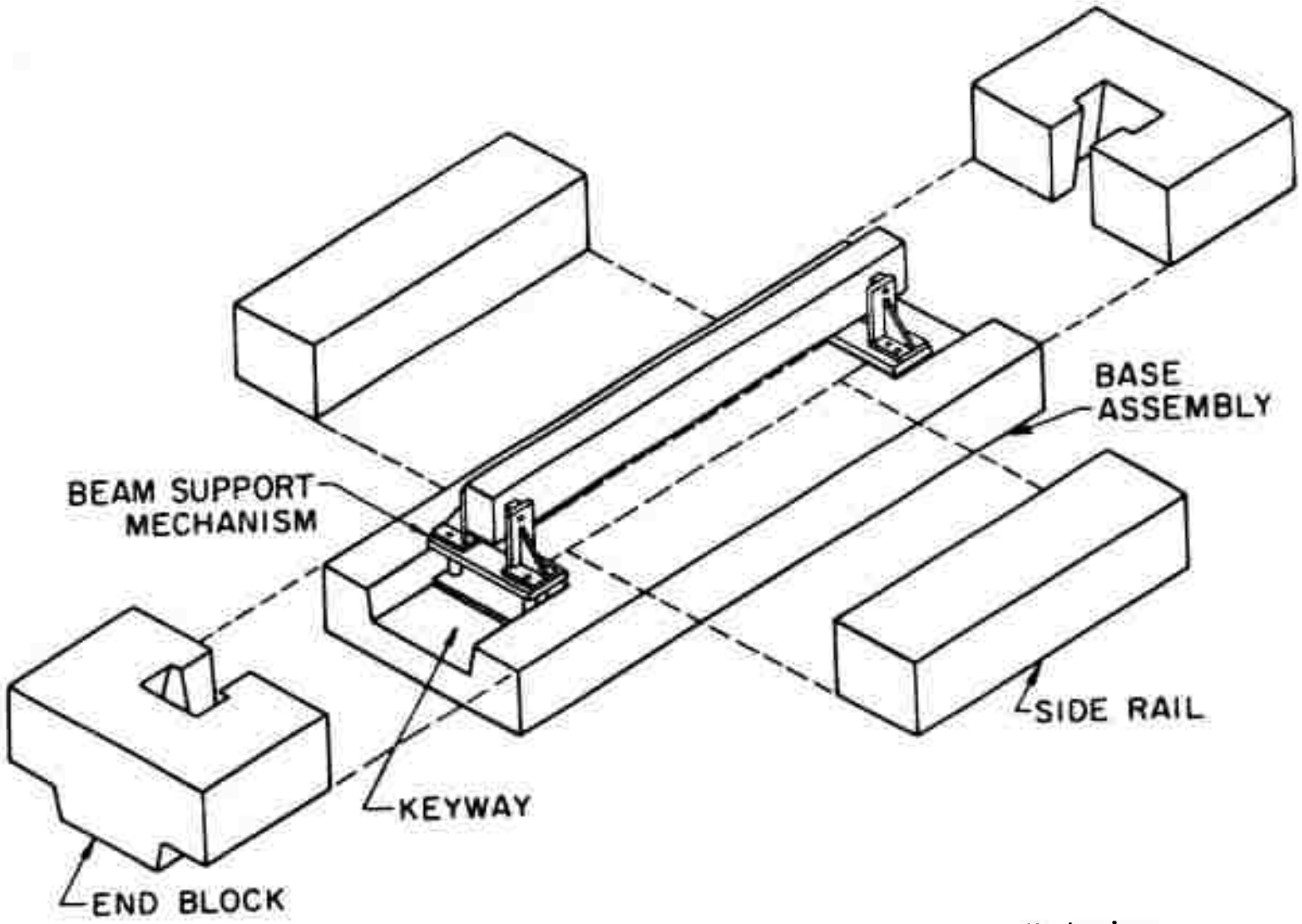

Figure 16. Test Fixture With Beam Installed on Support Mechanisms

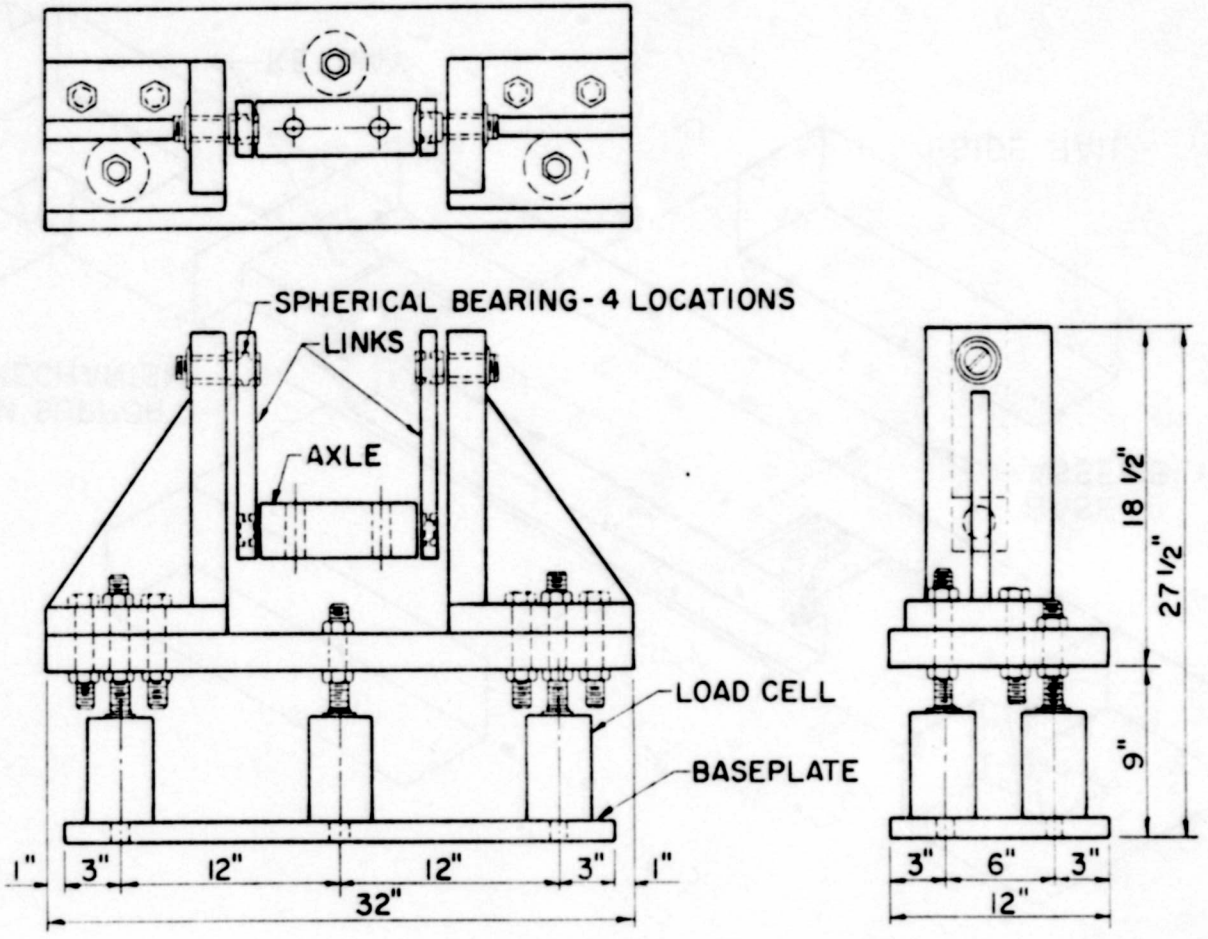

Figure 17. Beam Support Assembly

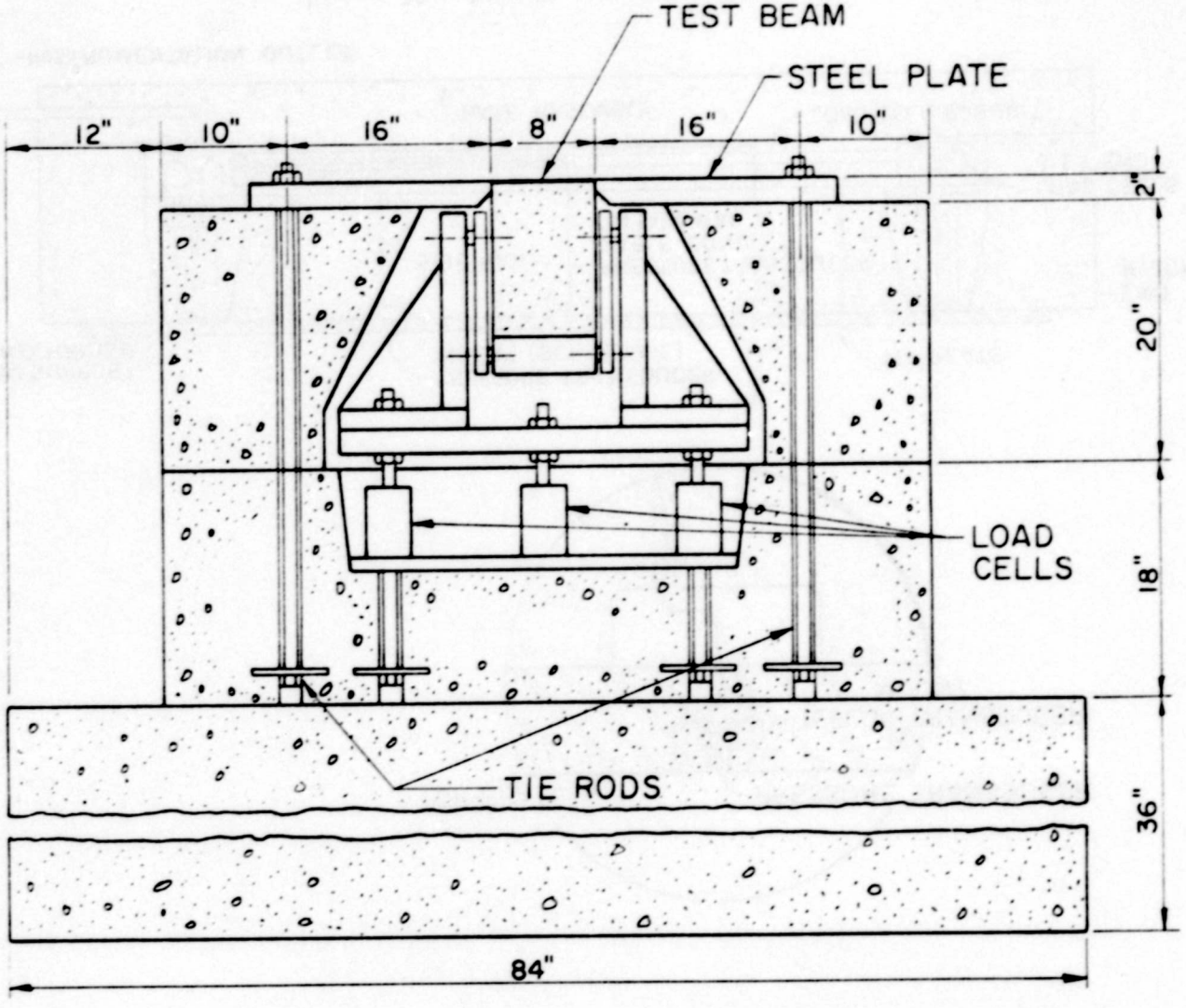

Figure 18. Cross Section Through End of Test Fixture With Top Plates, Beam Support Mechanism, and Load Cells in Place

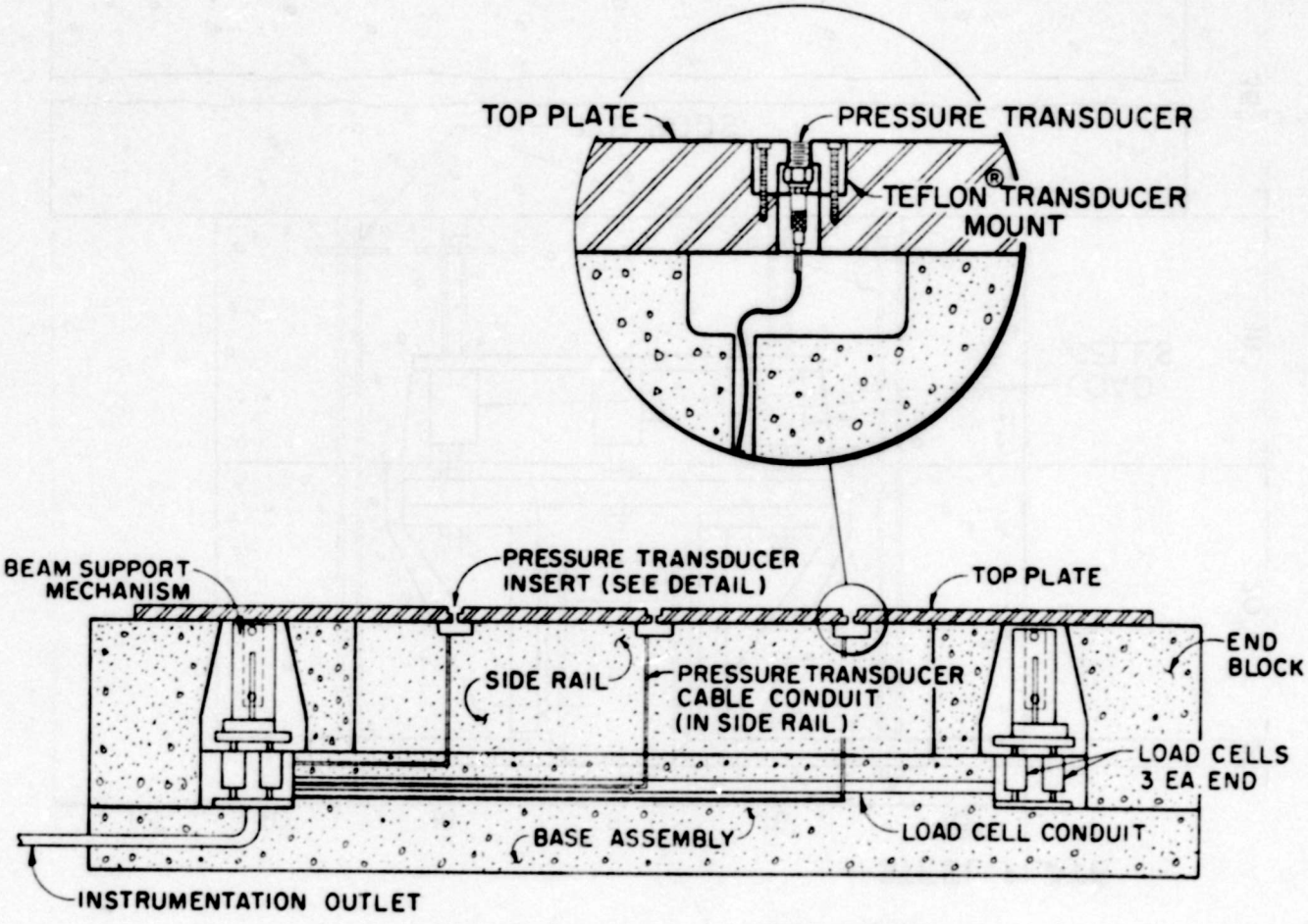

Figure 19. Test Fixture Cross Section

cable with a nylon harness, as shown in Figure 20. An M-6 detonator was placed into the center of each charge through a drilled hole. The charge was encircled by a break-wire to produce a time of detonation mark for telemetry time reference. This time is designated TØ in the reduced data shown in Appendix A.

4.2.1.4 Data Acquisition. During a test, data were obtained from six load cells, eight strain gages, five accelerometers, and four pressure transducers. Table VII lists the manufacturer, model and specifications for these devices. The data were taken on the two sets of data acquisition equipment mentioned above. The pressure and accelerometer data were recorded on magnetic tape by the VALTS Signal Conditioning and Recording system in the C-80A control bunker (Reference 30). The strain gage and load cell signals were recorded with similar equipment temporarily installed in the instrument bunker.

4.2.2 Test Procedures

Each impulse test was conducted in three stages: (1) beam installation and instrument calibration; (2) impulse test; and (3) post-test examination of the beam. In stage one, two static loads were applied to the beam to produce constant moment of 15 kip-feet in the center 48-inch span of the member. Strains in steel, concrete and load cells were manually recorded. The strain gages and load cells were connected to the signal conditioning and recording equipment and the calibration repeated and data recorded.

The charge was positioned at the required standoff distance directly over the center of the test beam. The charge was secured against wind drift with lines connecting its harness to the test fixture. Following the explosion the test specimen was examined for the effects of the blast and photographed before removal from the test fixture. Qualitative measurements of the beam center displacement were made to estimate the amount of permanent deformation. The specimen was then removed from the test fixture and the damaged area in the center of the beam was examined and photographed in greater detail.

The analog signals on magnetic tape were digitized by the Eglin AFB Computer Sciences Laboratory. Pressure data were integrated with respect to time to obtain the impulse per unit area. Digitized strain, load and acceleration data were copied on magnetic tape and transmitted to Oklahoma State University for analysis.

The tests conducted early in the program revealed important features which required modification of some aspects of the test procedure on equipment. Following the first test, calibration levels were adjusted upward in anticipation of larger strains, pressures, and loads. The peak accelerations were many times those estimated and the high calibration levels required to

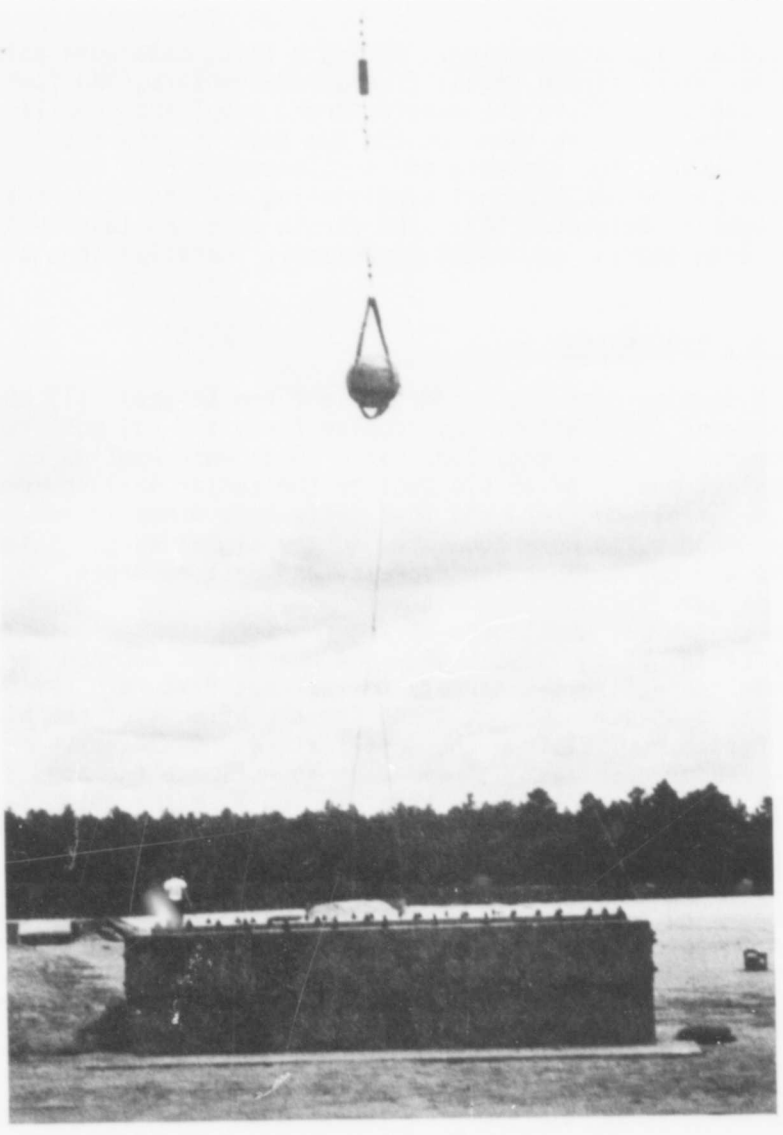

Figure 20. Charge in Place Over the Text Fixture Prior to Test

TABLE VII. INSTRUMENTATION SCHEDULE

Instrument	Manufacturer and Model	Specification	Provided By
Accelerometers	ENDEVCO 2225	20,000 g	ADTC
Pressure Transducers	Kistler 202A1	5,000 psi	ADTC (Test Nos. 1-5)
	PCB 102M24	5,000 psi	ADTC (Test Nos. 6-12)
Strain Gages			
Concrete	BLH Electronics BLH A9-4	120 ± 1.5 OHMS Gage Factor = 2.14	OSU
Steel	Budd Corporation C6-181B	120 ± 0.2 OHMS Gage Factor = 2.09	OSU
Load Cells	BLH Electronics U1	10,000 lb	OSU

accommodate these peak accelerations caused the much smaller, free vibration accelerations of the beam to be the same order of magnitude as the instrumentation line noise errors. This reduced accuracy of test data severely. To reduce this problem, on the fifth test a thin gasket was placed underneath a quarterpoint accelerometer and the calibration on that channel was changed from 10,000 g's to 1000 g's. The calibration level change improved the signal-to-noise characteristics of data. However, the magnitude of peak accelerations was still sufficient to produce zero shifts in the output of transducer which could not be eliminated from the accelerometer data. After the first test, axle pins were found to be bent and a second set of axles was fabricated using higher strength steel. By the time of the third test modified axles, with accelerometers attached to monitor the motion of the support mechanism, were in use.

After the first four tests a different style of pressure transducer was utilized in an effort to obtain more reliable pressure-time data. The test configuration was further modified by burying the test fixture so that the top surface of the beam, the test frame, and the ground level were at the same level. This was done to eliminate pressure relief which may have been present due to the vertical faces of the long narrow test fixture.

The beams of the fifth and sixth tests exhibited signs that the sides of the beam had impacted with the test frame during the test, even though the steel plates had been initially placed at least 0.2 inch away from the beam. It was felt that high lateral soil pressure might be causing displacements of the siderails during the blast. For this reason a pair of 4-inch by 6-inch posts were placed at the bottom of the cavity to brace the two siderails against such motion.

Prior to Test No. 7 one load cell was found to be inoperable. A replacement could not be obtained and the damaged load cell was left in place.

A log of all tests is given in Table VIII. Included are the test dates, the beam numbers, and post-test measurements.

4.2.3 Post-Test Observations

The beams suffered little damage in the first two tests. A vertical crack ran through the beams to their top surface as shown in Figure 21. These cracks were clean, straight tensile fractures on the top surface and appeared to have resulted from beam rebound. Longitudinal hairline cracks were noted on the sides of these two beams about 1/2 inch below the top surface for 3 to 4 inches on either side of the centerline. These cracks appeared to be the beginning of spalling of the top layer. In later tests, with smaller charge standoff distances, the top layer (1/2 to 3/4 inch thick) exhibited crushing damage 6 to 8 inches on either side of the centerline. In Figure 22 the extent of damage indicates a massive spalling was

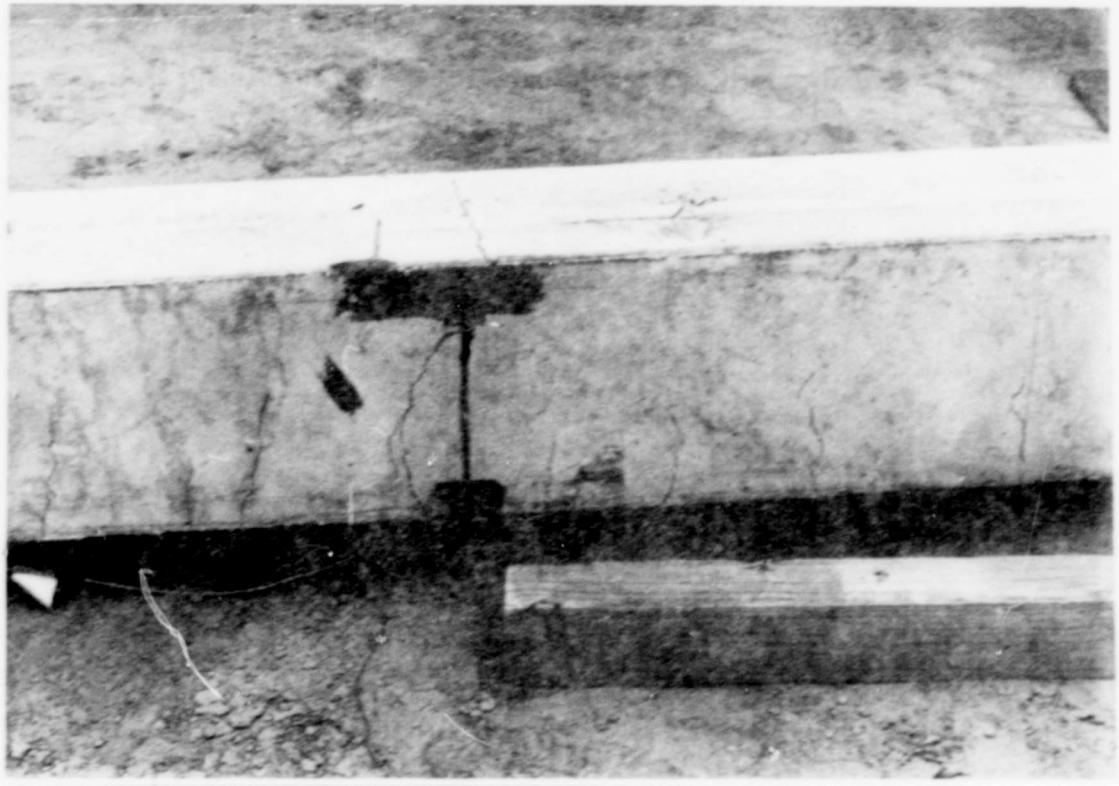

Figure 21. Center Section of Beam 12 After Test No. 1

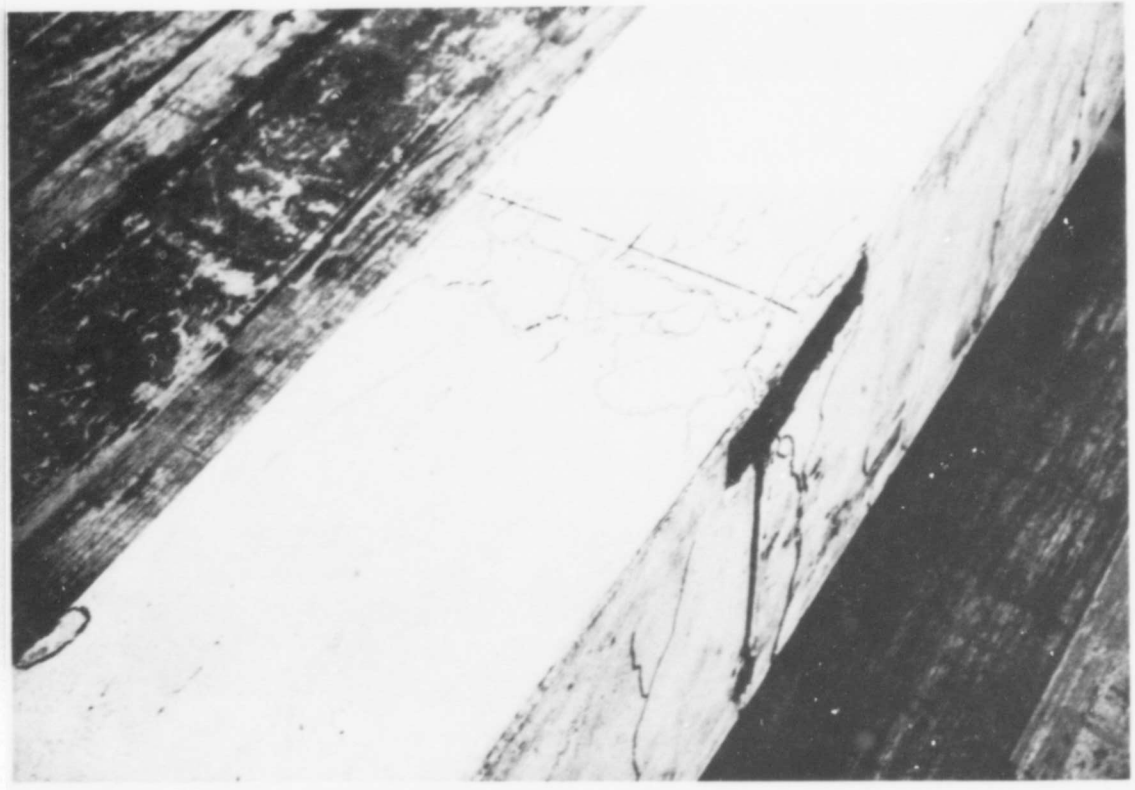

Figure 22. Center Section of Beam 10 After Test No. 3

TABLE VIII. TEST PARAMETERS AND POST-TEST MEASUREMENTS

Test Number	Beam Number	Test Date (1974)	Charge Distance[a] (ft)	Age at Test (days)	Estimated Permanent Center Displacement (in)	Maximum Crack[b] Width (in)
1	12	17 May	16.00	310	0.45	---[c]
2	13	29 May	15.25	317	0.34	---[c]
3	10	19 Jun	12.75	358	0.72	0.135
4	3	21 Jun	12.25	308	0.04	---[c]
5	8	21 Aug	11.75	434	0.88	0.147
6	6	23 Aug	11.75	378	0.80	0.168
7	5	10 Sep	11.25	397	0.72	0.101
8	1	12 Sep	11.25	393	1.02	0.203
9	4	13 Sep	11.25	389	0.31	0.076
10	7	16 Sep	10.75	398	0.99	0.171
11	2	18 Sep	10.25	398	0.78	0.120
12	9	19 Sep	11.25	457	0.90	0.155

[a]Measured from center of charge to top surface of beam.

[b]Width of largest crack at level of reinforcing steel.

[c]Data not obtained.

eminent. For still smaller standoff distances the concrete was crushed in a wedge-shaped zone about 2 inches long and 1/2 to 3/4 inch deep as shown in Figure 23. For the smallest standoff distances, the crushed zone was about 4 inches long and 1 to 1½ inches deep. This crushing behavior did not occur in beams with high strength concrete, as can be seen, for example, in Figure 24. In contrast with the typical strength beams tested with the same standoff distance, the high strength concrete appeared to be more damage resistant.

Beam 5, which was reinforced with high strength steel, sustained more damage than other test specimens. Figure 25 shows this beam immediately after testing and prior to removal from the test fixture. Figure 26 shows the same beam after removal from the test fixture. Furthermore, the beams with a higher reinforcing ratio experienced greater top surface crushing than typical beams with similar charge standoff distances.

The crack widths at the level of the reinforcing steel were measured after the beams were removed from the fixture. Figure 27 illustrates typical cracking in the center section. The crack spacing was on the order of 6 to 8 inches. The maximum crack widths occurred in the center section. The smallest measurable cracks were between 12 and 18 inches from the center. Beams 6 and 7, in which the shear stirrups had been omitted, did not exhibit diagonal tension cracks.

Beams 3 and 4 with a high reinforcing ratio had prominent longitudinal splitting cracks at the level of the reinforcing steel, as shown in Figure 28. For beam 3 these cracks extended 12 to 18 inches on either side of the centerline. Splitting of this type is frequently associated with bond failure. Also shown in Figure 28 is some significant surface crazing which was highlighted by test personnel; these random cracks were not a result of impulse testing.

4.3 DAMAGE ASSESSMENT TESTS

Although the impulse loadings caused significant crushing and permanent displacements in some beams, visual inspections could not define the extent of the damage. To quantify the damage and to relate it to delivered impulse, the beams were returned to Oklahoma State University for further testing.

The test configuration for the final load tests was identical to the preliminary static tests. Loads were applied as shown in Figure 12 and both loads and displacements were recorded on an X-Y recorder. The test procedure was to load a beam progressively to failure. Yielding was considered to have occurred in the reinforcement when load-displacement plots ceased to be linear. The ultimate moment, M'_u, was the largest measured moment. Failure was defined as a sudden, large loss of capacity due to the crushing of a significant zone of concrete on the top surface of the beam. Additional displacements were imposed and progressive failure continued until the resistance of

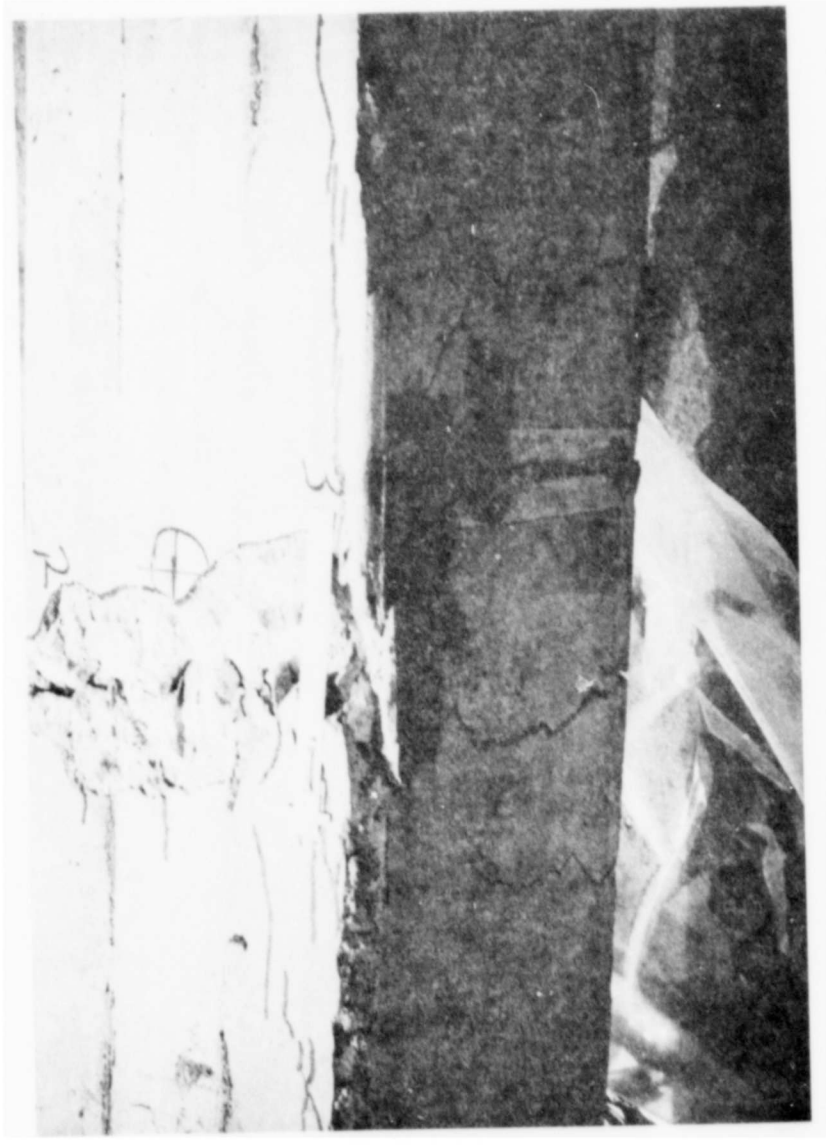

Figure 23. Center Section of Beam 7 After Test No. 10

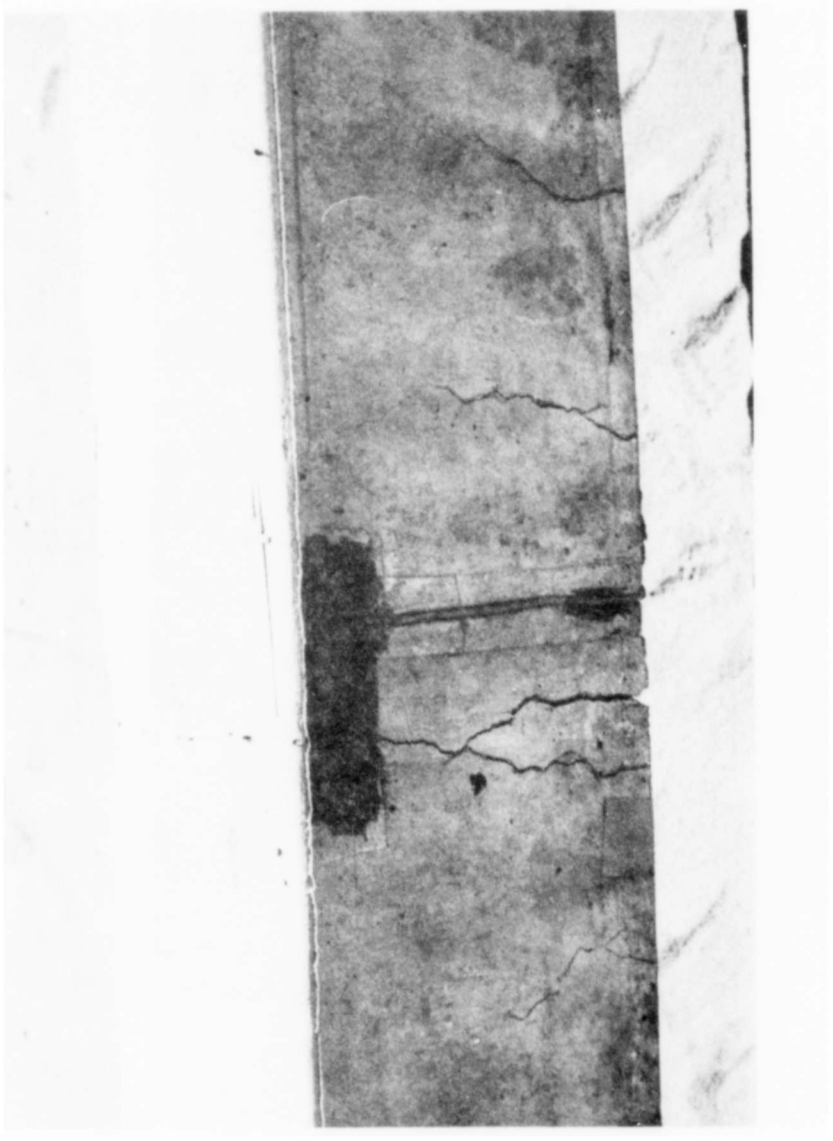

Figure 24. Center Section of Beam 2 After Test No. 11

Figure 25. Center Section of Beam 5 After Test No. 7

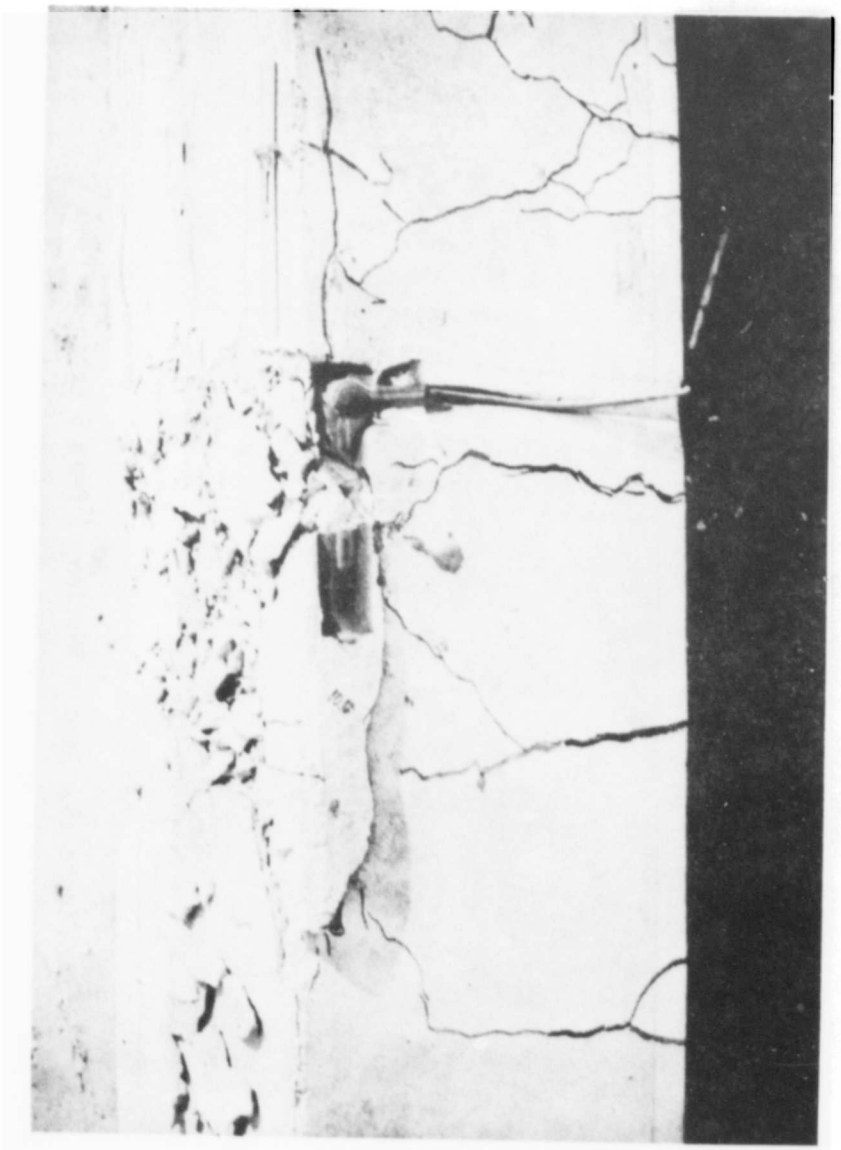

Figure 26. Side View of Beam 5 After Test No. 7

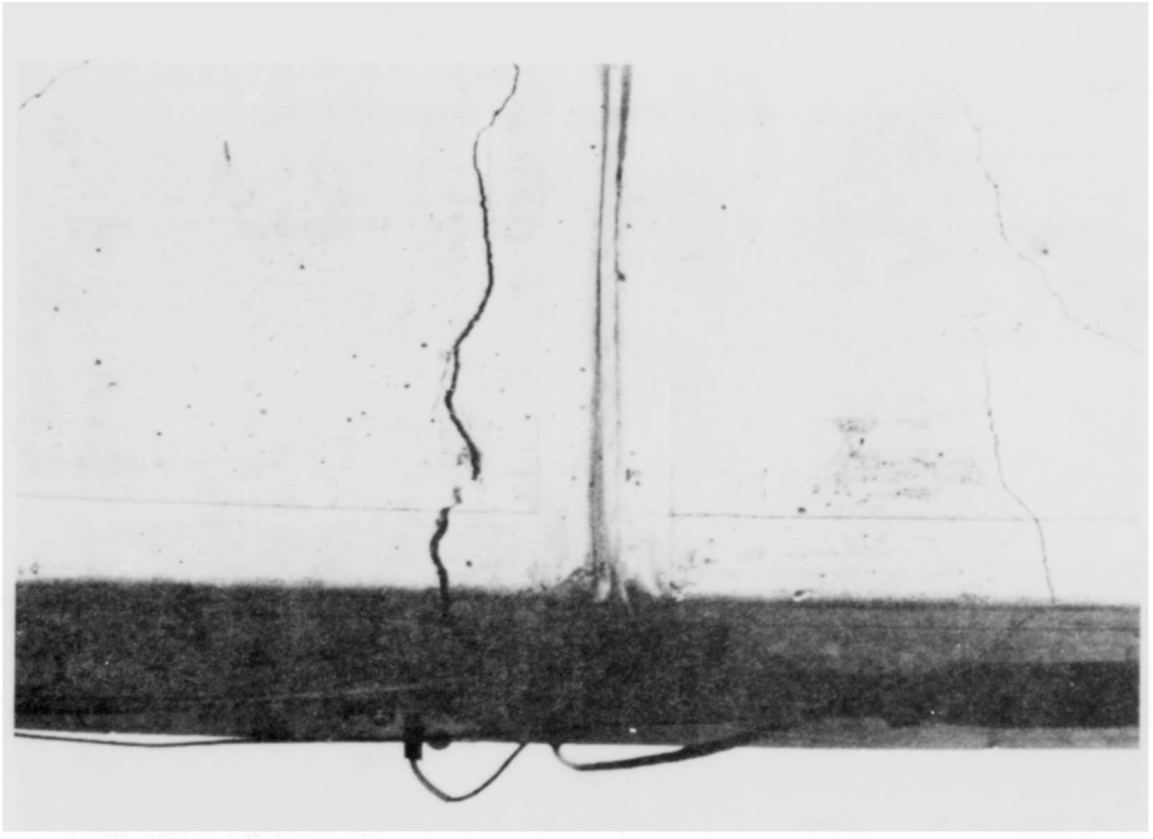

Figure 27. Side and Bottom Views of Beam 2 After Test No. 11

Figure 28. Side View of Beam 3 After Test No. 4

the beam was reduced to about 50 percent of the maximum load. Typical data from final static tests are shown in Figure 29. The response of an undamaged typical beam (beam 11) and a similar impulse-damaged beam (beam 9) are shown for comparison. Variations between the static behavior of the damaged and undamaged beams are attributed to the impulse loading.

Load, strain, and deflection data were recorded at regular intervals during these tests. Small, sharp reductions of load noted in the load-deflection curves of Figure 29 occurred during the manual recording of data and occasionally coincided with small failures in the compression zone of the beam.

Parameters used to evaluate the effects of impulse load are shown in Figure 29. These parameters which are recorded in Table IX by beam and test number are used in Section IX to assess the effect of the impulse load on the damaged sustained by the beams.

Two quantities which may be related to damage are the ductility ratio γ, δ_{max}/δ_y, and W_p, the work dissipated during plastic displacement. The static ductility ratio relates the ability of the beams to undergo plastic deformation. Note that the undamaged beam (beam 11) has a static ductility ratio of 6.30 whereas typical beams subjected to impulse loading exhibited much smaller values. The work, W_p, was obtained by integrating the area under the load-deflection curve between δ_y and δ_{max}.

TABLE IX. SUMMARY OF RESULTS OF STATIC STRENGTH TESTS OF DAMAGED BEAMS

Test Number	Beam Number	Ultimate Moment M'_u (kip-ft)	Work Performed on Beam, Plastic Range W_p (kip-in)	Displacement of Load Point at Yield, δ_y (in)	Displacement of Load Point at Failure, δ_{max} (in)	Ratio of Failure to Yield Displacement $\mu = \delta_{max}/\delta_y$
1	12	35.7	25.8	0.40	1.53	3.8
2	13	38.2	27.9	0.41	1.90	4.6
3	10	35.4	17.2	0.57	1.12	2.0
4	3	70.3	2.8	0.58	0.64	1.1
5	8	30.0	16.7	0.60	1.30	2.2
6	6	35.8	25.2	0.56	0.97	1.7
7	5	34.9	12.3	0.60	1.08	1.8
8	1	35.8	18.9	0.55	1.32	2.4
9	4	54.5	1.4	0.54	0.58	1.1
10	7	33.8	12.4	0.55	1.03	1.9
11	2	39.5	25.4	0.42	1.49	3.6
12	9	33.4	13.5	0.52	1.05	2.0
---[a]	11	38.5	40.8	0.37	2.33	6.3

[a]Static test member.

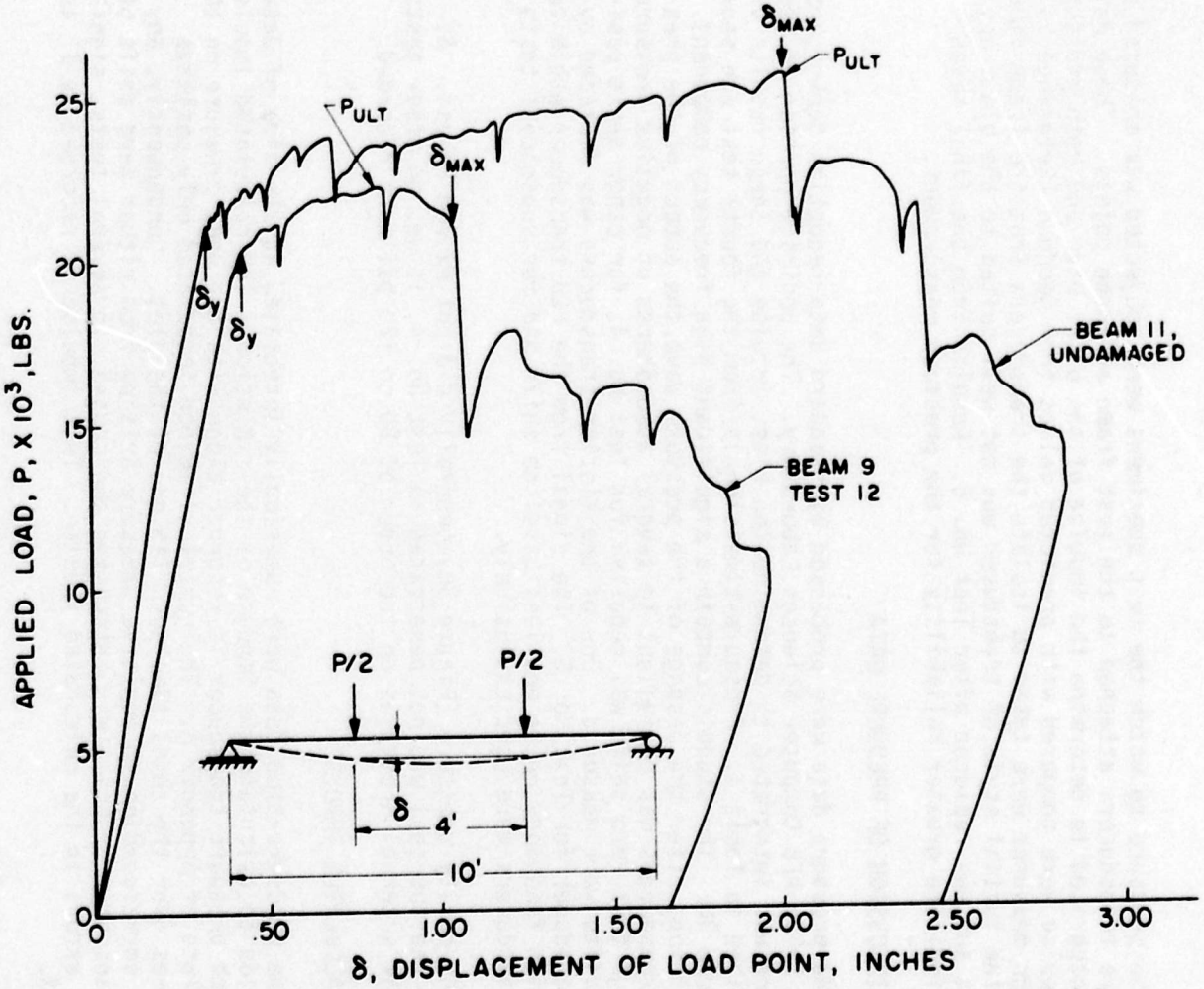

Figure 29. Comparison of Load-Displacement Curves of Impulse Damaged Beam and Undamaged Beam

SECTION V

PRESSURE MEASUREMENTS

The pressure to which the test specimens were subjected was measured by pressure transducers attached to the test frame at three points. These data were integrated to determine the impulse of the blast wave and both pressure and impulse were compared with predicted values from Goodman (Reference 1). Although measures were taken to isolate the transducers from the frame vibration, the initial style of transducer was not well suited to the blast environment and was replaced after Test No. 5. Results from the final seven tests indicate greater reliability for the pressure measurement.

5.1 DISCUSSION OF PRESSURE DATA

The pressure data were processed by standard data reduction techniques of the Eglin AFB Computer Sciences Laboratory. The positive portion of the pressure was integrated to determine the blast impulse and these results are summarized in Table X. Pressure-time signals from the fourth test are shown in Figure 30. The signals contain a significant high frequency component. In addition, after the passage of the pressure wave, the output of the pressure transducers was equivalent to several atmospheres of negative pressure. Although this zero shift was negative for Test No. 4, for other tests positive shifts were measured. One of the Kistler transducers was replaced by a PCB transducer for Test No. 5. The signal from the PCB transducer exhibited less high frequency noise and less baseline shift and for subsequent tests PCB transducers were used exclusively.

The cavity pressure (Figure 30) generally did not exceed 20 psi. Although the top seal was not penetrated on Test No. 4, it was on other tests and peak internal pressures on the order of 80 to 120 psi were recorded.

5.2 CALCULATED IMPULSE

The pressure-time data were numerically integrated at the time of data reduction to calculate the impulse of the explosion. The calculated impulse for each pressure transducer is recorded along with the peak pressure on the data plots of Appendix A. The numerical method integrated only positive pressures over the total time span (15 ms) of the plot. Consequently, any signal corresponding to positive pressure arising from either zero shift of the transducer or noise was integrated and caused, in several tests, significant errors in the calculated impulse. This impulse is recorded as I' in Table X.

To calculate a more accurate estimate of impulse, a review of pressure-time curves indicated an average duration of the positive pressure to be

TABLE X. TEST IMPULSES AND PEAK PRESSURES

Test No.	Stand-off (ft)	PF1 (Quarter) Impulse, psi-ms I'[a]	PF1 (Quarter) Impulse, psi-ms I[b]	PF1 (Quarter) p_o, psi	PF2 (Center) Impulse, psi-ms I'	PF2 (Center) Impulse, psi-ms I	PF2 (Center) p_o, psi	PF3 (Quarter) Impulse, psi-ms I'	PF3 (Quarter) Impulse, psi-ms I	PF3 (Quarter) p_o, psi	PF4 (Cavity) Impulse, psi-ms Tabulated	PF4 (Cavity) Impulse, psi-ms 1.25 ms	PF4 (Cavity) p_o, psi	Avg.[c] I', psi-ms	Avg.[e] I, psi-ms
1	16.00	397	342	683	402	351	660	435	309	672	---[d]	---[d]	---[d]	411	334
2	15.25	335	325	1259	324	309	1167	498	389	1416	---[d]	---[d]	---[d]	386	341
3	12.75	555	365	1843	228[e]	172[e]	1413	---[d]	---[d]	---[d]	---[d]	---[d]	---[d]	555	365
4	12.25	260[e]	260[e]	1130	187[e]	187[e]	1202	336	334	1614	7.3	0	25	336	334
5	11.75	190[e]	191[e]	1227	284[e]	284[e]	1854	354	311	1166	63.0	3	22	354	311
6	11.75	445	405	1803	1008[e]	502	1796	530	410	1668	88.0	21	53	487	441
7	11.25	---[f]	---[f]	---[f]	---[f]	---[f]	---[f]	---[f]	---[f]	---[f]	---[f]	---[f]	---[f]	---[f]	---[f]
8	11.25	600	380	1453	131[e]	131[e]	1700	588	470	1447	29.0	2	18	594	425
9	11.25	467	445	1344	138[e]	132[e]	1418	418	413	941	49.0	6	19	442	429
10	10.75	529	422	2148	578	395	1983	784	390	3259	102.0	8	86	630	402
11	10.25	480	350	1132	621	431	1342	---[f]	---[f]	---[f]	200.0	14	135	550	398
12	11.25	407	351	1872	442	370	1807	414	364	1675	112.0	11	91	421	362

[a] I' = impulse at 15 ms.

[b] I = impulse at 1.25 ms after shock wave arrival.

[c] Average impulses are for results from transducers PF1, PF2 and PF3.

[d] Transducer not present for Test Nos. 1, 2 and 3.

[e] Omitted from average.

[f] Transducer or recording system failure resulted in absence of data.

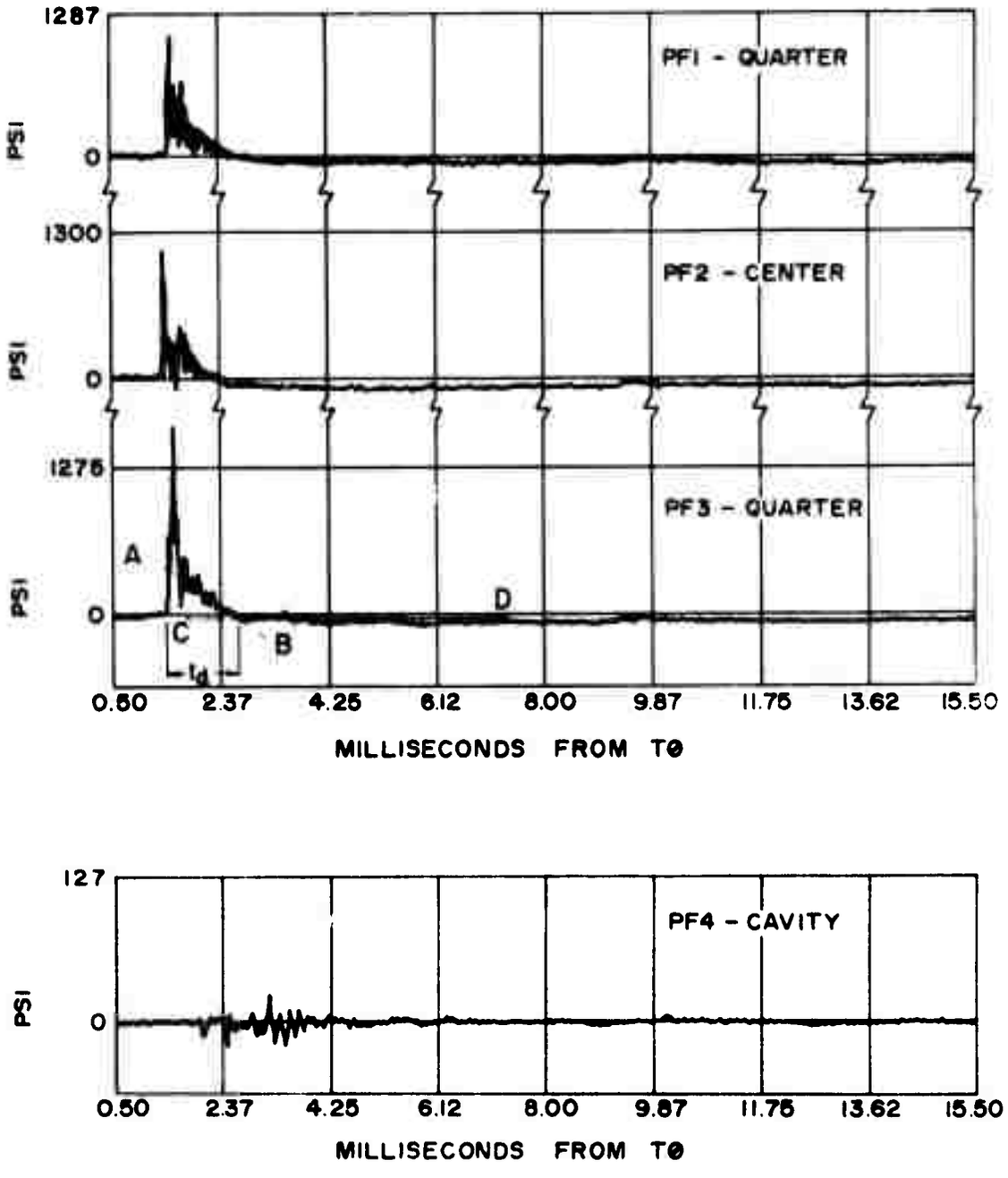

Figure 30. Plots of Typical Pressure Data From Test No. 4

approximately 1.25 ms. The construction shown on PF3 of Figure 30 illustrates the evaluation of the positive pressure duration, t_d. The value of impulse at 1.25 ms is recorded as I in Table X. Future reference to impulse will refer to the value related to 1.25 ms.

5.3 CORRELATION WITH PREDICTED VALUES

Peak pressures and calculated impulse are shown as a function of standoff distance in Figures 31 and 32. Also shown on these figures are values predicted by Goodman (Reference 1). Note that the calculated impulse at 1.25 ms is always less than the predicted value. These data should be accepted as qualitative, and not precise values of pressure and impulse. In later sections the charge standoff distance, which was measured accurately, will be used to represent pressure and impulse characteristics of the chemical explosion.

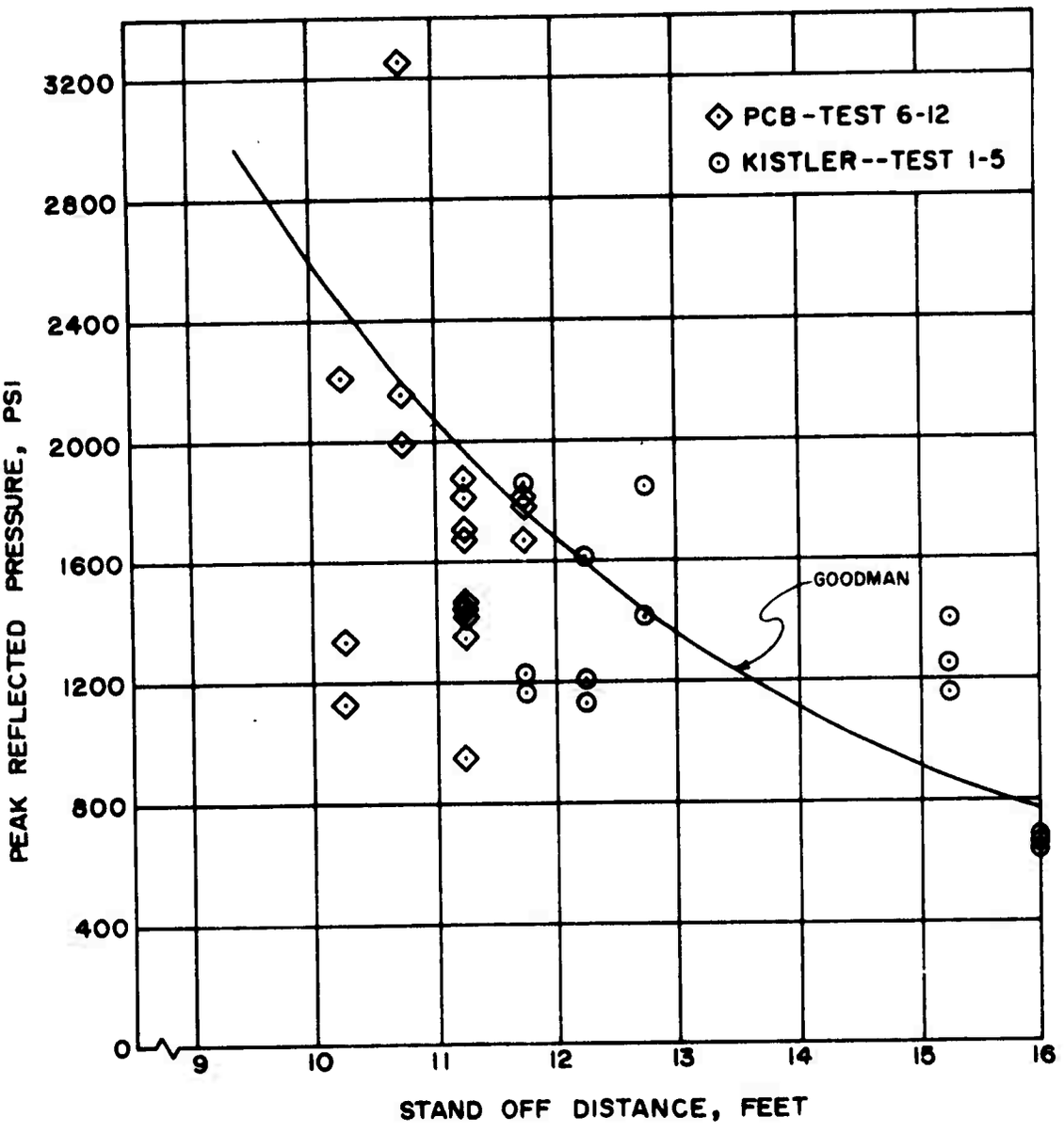

Figure 31. Comparison of Peak Reflected Pressure With Predictions From Reference 1

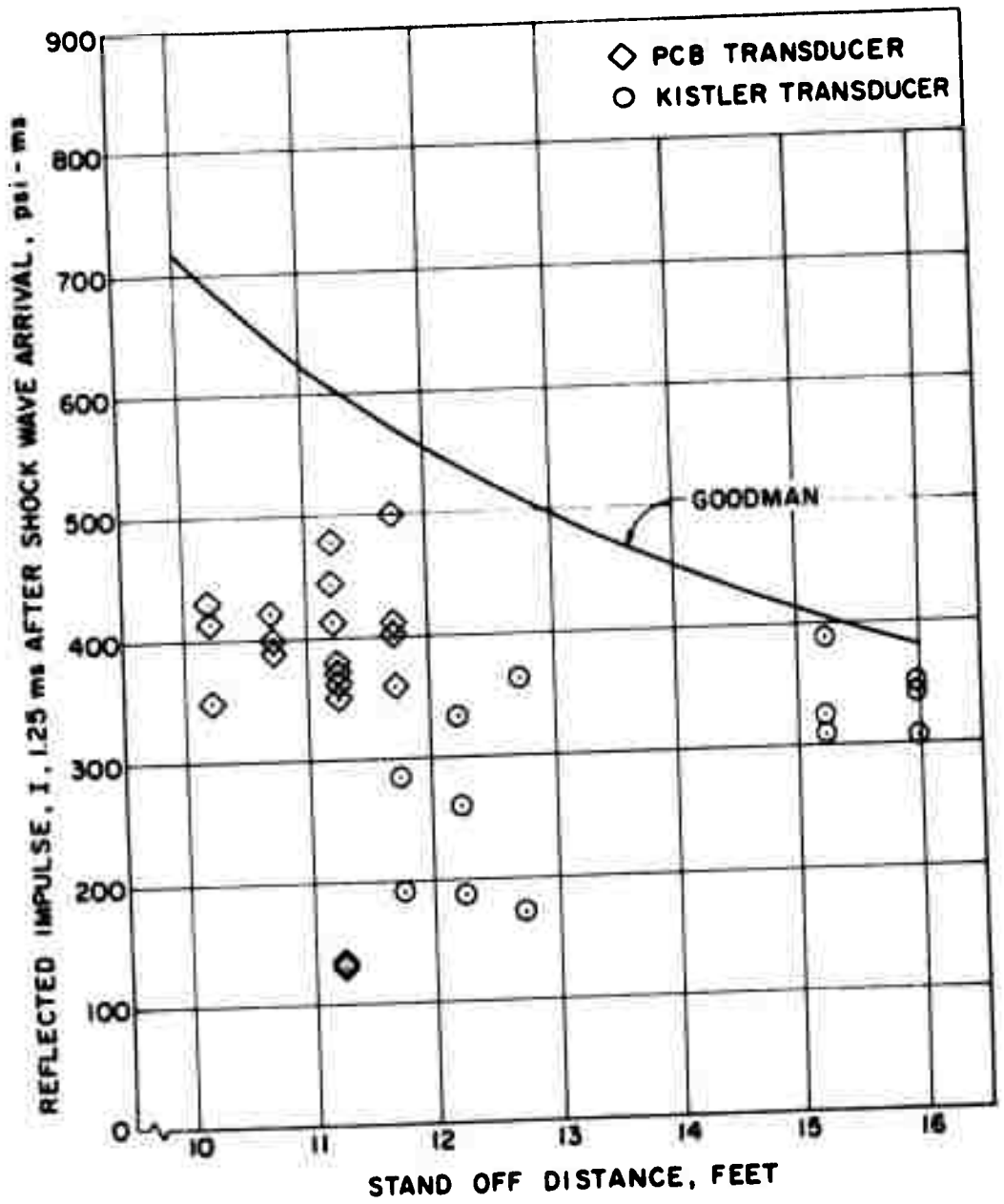

Figure 32. Comparison of Primary Reflected Impulse With Predictions From Reference 1

SECTION VI

ACCELERATION MEASUREMENTS

The vertical motion of the beams was measured by accelerometers. However, the shock loading produced high frequency acceleration signals which were approximately an order of magnitude greater than those corresponding to actual beam acceleration. Furthermore, the very short rise time experienced by the transducers produced a shift in the zero baseline of the instrument. A preliminary data analysis which followed Test No. 3 indicated calculated velocities and displacements to be in error. It was presumed that the initial high frequency acceleration was responsible for the error and a damping material was installed between the accelerometer base and the beam. At the same time accelerometers were installed on the beam end support members to provide a time history of the end motion of the member. Because of an accelerated test schedule and the absence of timely data reduction, the qualitative nature of the acceleration data could not be established until impulse tests were completed. Following the impulse tests, a variety of methods were used to calculate the time-velocity and time-displacement characteristics of the beam with no success.

Because of the high accuracy required of acceleration data to correctly establish time-displacement characteristics by double integration, the lack of success encountered in this program is not atypical. The acceleration measurements are included in Appendix A to provide the reader a means to evaluate the data.

6.1 DISCUSSION OF DATA

The response of a typical digitized accelerometer signal is shown in Figure 33. While the magnitude of the measured high frequency acceleration was significantly reduced by inserting damping material between the beam and the accelerometer base, the initial acceleration was an order of magnitude greater than the beam acceleration. Therefore, very accurate measurements were required to provide data which would be suitable for velocity and deflection calculations. However, accelerometer signals were influenced by the very high initial acceleration signals which significantly reduced the quality of the data. The shift of the instrument zero baseline was the order of magnitude of the acceleration experienced by the beam in free vibration.

6.2 DATA ANALYSIS

Several methods were employed to integrate digitized accelerometer records for time histories of velocity and displacement. Although none of the

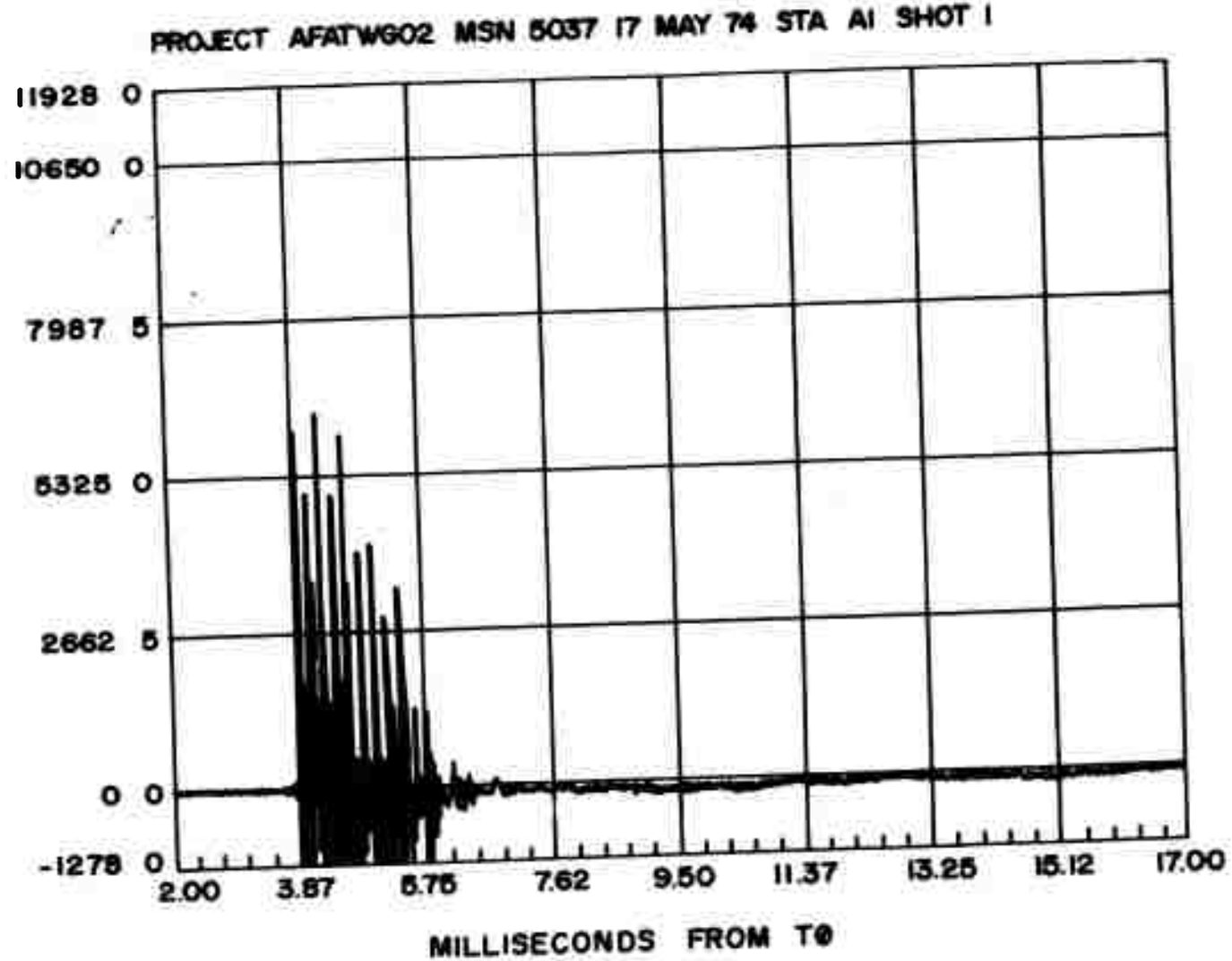

Figure 33. Plot of Typical Acceleration Record for a Quarter Station, Test No. 1

methods studied gave reasonable values of velocity and displacement for all tests, a method which assumed a constant shift of the zero baseline gave values of velocity and deflection which were the order of magnitude of the anticipated beam response for several tests. Shown in Figures 35 and 36 are integrated velocities and displacements for the accelerometer record shown in Figure 34. It must be emphasized that these results are not typical for calculated beam response.

While time and funds were not available for more extensive data analysis, it is doubtful that more reasonable or accurate results could be obtained by further study. First, the large magnitude, high frequency signals produced a baseline shift which may be variable with time. While this phenomenon might be approximated by acceptable data reduction techniques, the digitizing rate may limit the accuracy of the data. A digitizing rate of 12.5 microseconds which was used in the program may be too large for an accurate representation of the acceleration signal. It should be emphasized that there was no precedence for this type of impulse test, and the accelerometers did not provide a reliable means for the measurement of beam motion. For future studies of the response of structures to high intensity impulse loading, other methods for deflection measurements should be considered. Without significant advances in the design of accelerometers, the use of either optical or direct measuring devices, such as the LVDT, should be investigated.

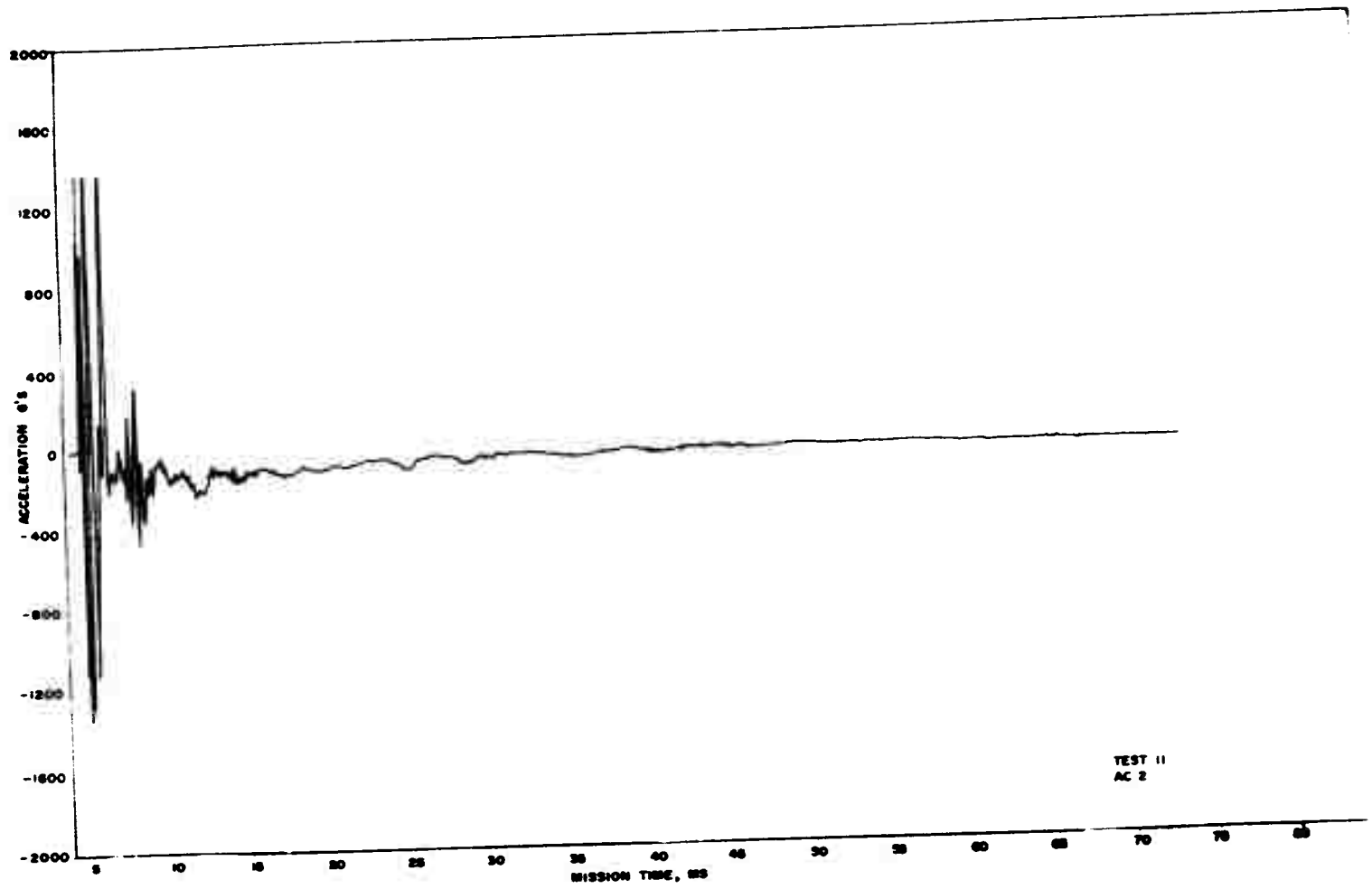

Figure 34. Quarterpoint Accelerometer--AC-1, Test No. 11

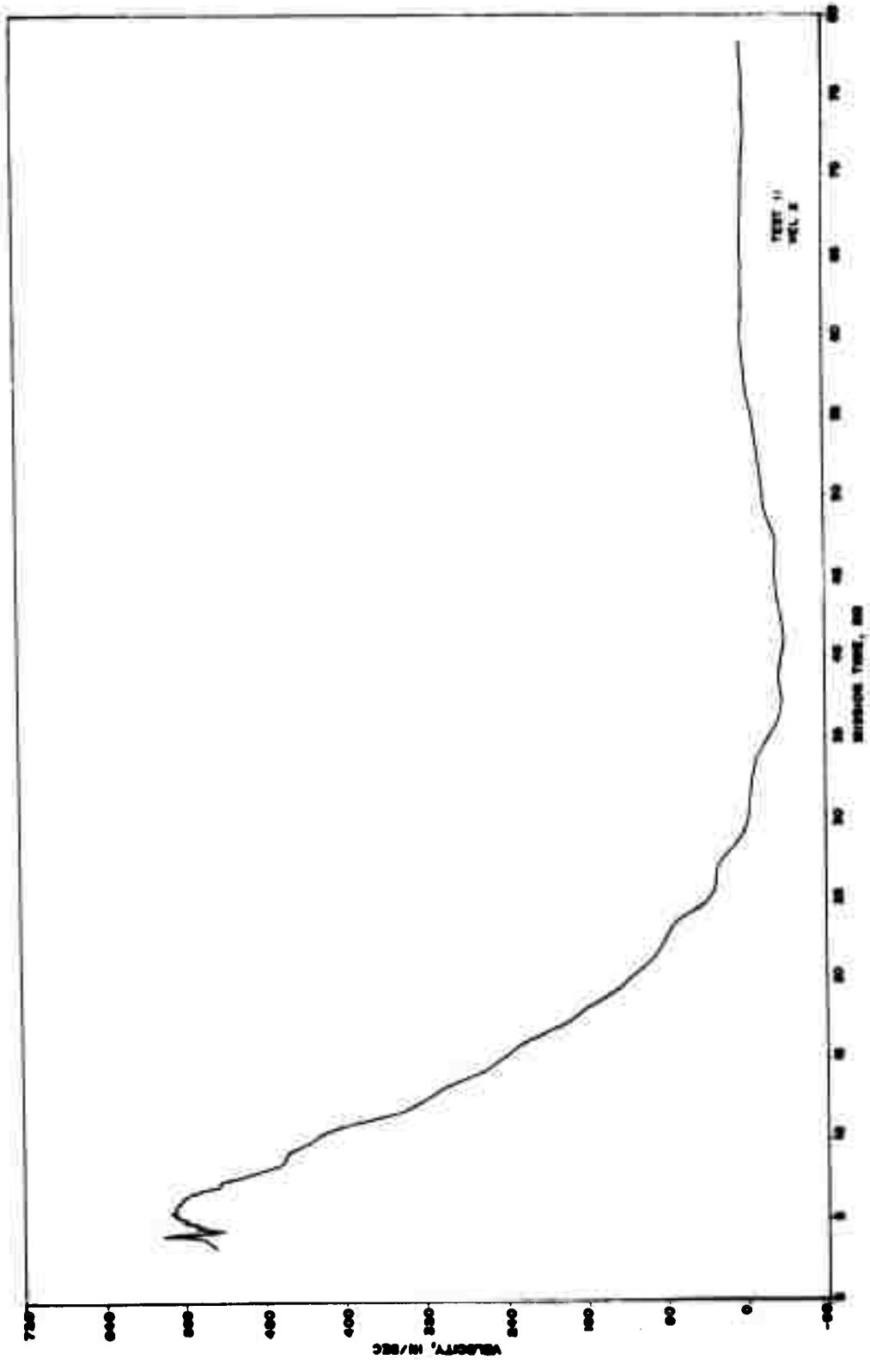

Figure 35. Calculated Center Velocity From AC-2, Test No. 11

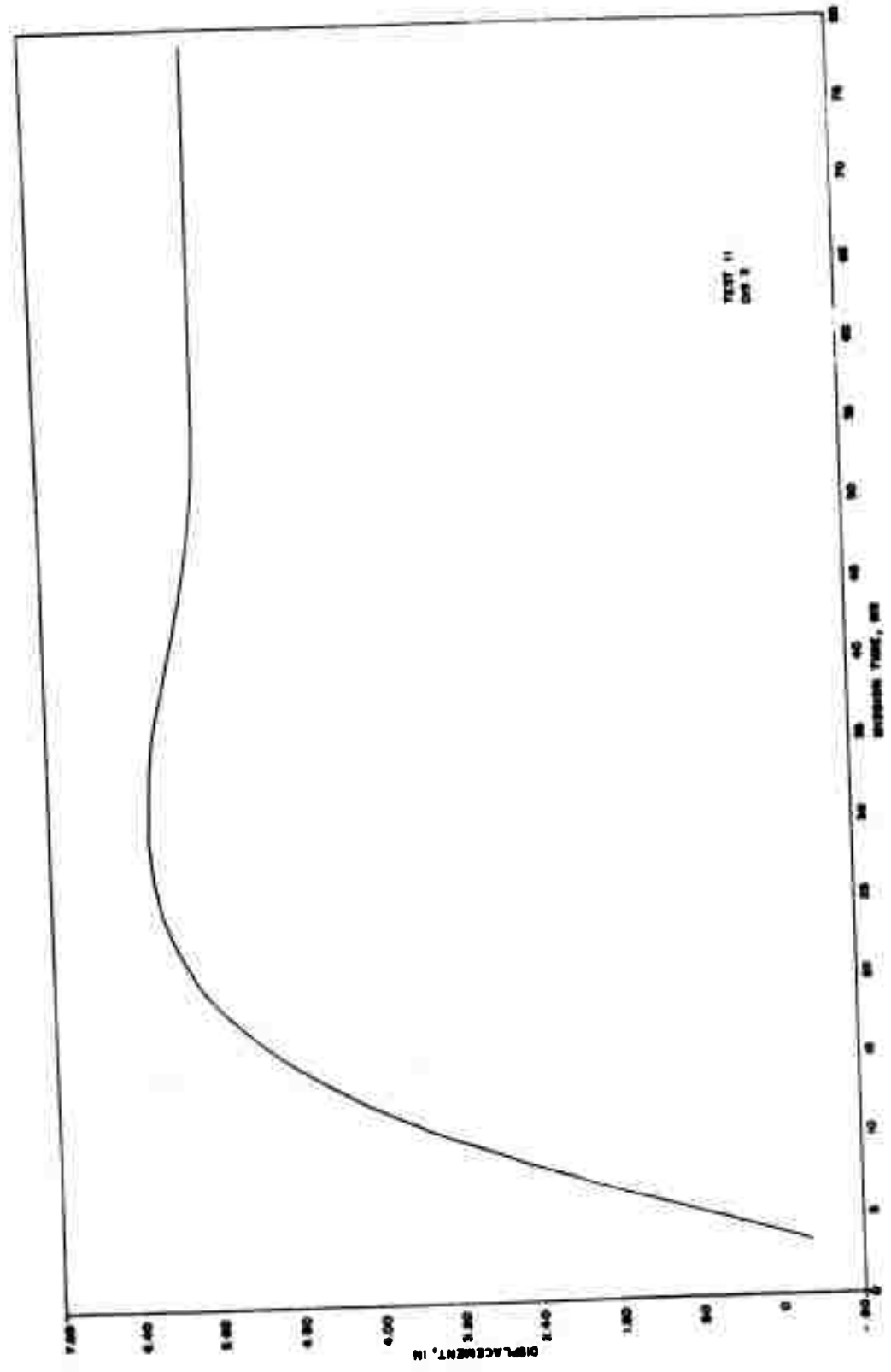

Figure 36. Calculated Center Displacement From AC-2, Test No. 11

SECTION VII

REACTION MEASUREMENTS

Instrumentation was provided for reaction measurement, primarily to supply more complete documentation of the phenomenological performance of test specimens. Based on reactions predicted by computer program IMPBC, a group of three load cells with a combined capacity of 30,000 lbs was placed at each end of the specimen. These load cells were placed between the reinforced concrete test frame and the beam support devices. The centroid of the load pattern was centered beneath the connection of the beam with the reaction device.

An objective of this program was to provide experimental data for the verification of computer program IMPBC, and the reaction forces, as a function of time, are calculated by the program. However, the flexibility of the beam end support structure could not be modeled by IMPBC and contributed to a difference between measured and experimental values. The resulting motion of the support structure produced inertia forces which were sensed by the load cells. It was noted in Section VI that it was not possible to determine the acceleration of the beam end support; consequently, it was not possible to separate support inertia forces from beam end reactions.

7.1 DISCUSSION OF DATA

The load cell measurements did not provide a reliable means for the measurement of the beam end forces. In addition to sensing the beam end forces, the load cells acted as accelerometers. Vibration of the load reaction device produced inertia forces which were superposed on beam end forces.

Although the maximum end reaction was estimated to be less than 25,000 pounds, measured reactions often exceeded 40,000 pounds. Furthermore, following tests No. 10 and No. 11 a load cell exhibited permanent strains which indicated it was subjected to loads which exceeded 15,000 pounds.

To illustrate reaction measurements, Figures 37 and 38 are included. The response of a typical load cell is shown in Figure 37. The combined output from load cells 1, 2 and 3, for test No. 10, is shown in Figure 38. The characteristics exhibited in Figure 38 are typical for all tests.

Additional analysis was performed in order to examine behavior of the measured reaction. The oscillation noted in Figure 37 was assumed to be related to flexibility of the support mechanism. To examine this assumption, several lumped parameter models were formulated. Stiffness and mass properties used in the models were determined by idealizing the support structure

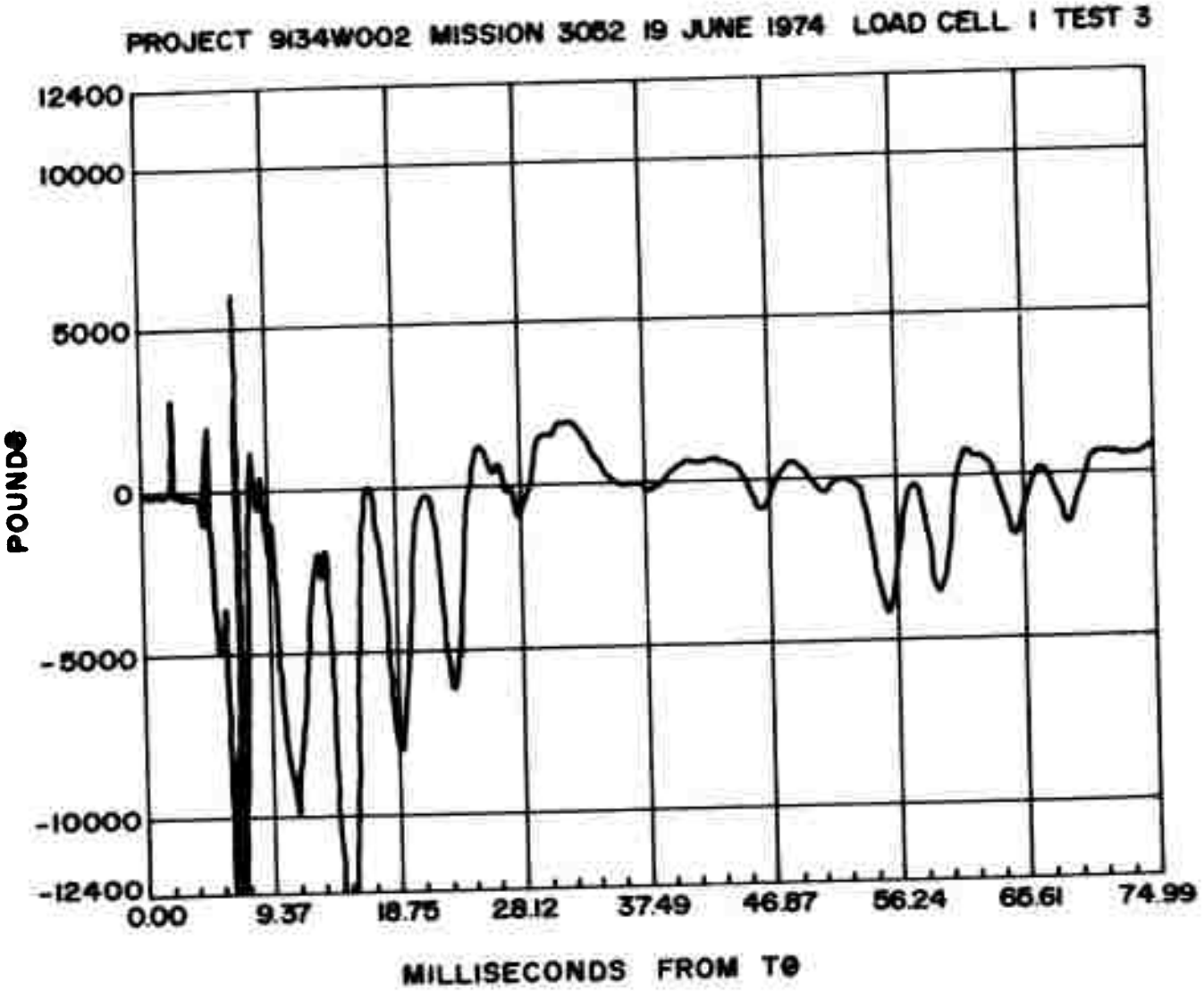

Figure 37. Typical Load Cell Data From Test No. 3

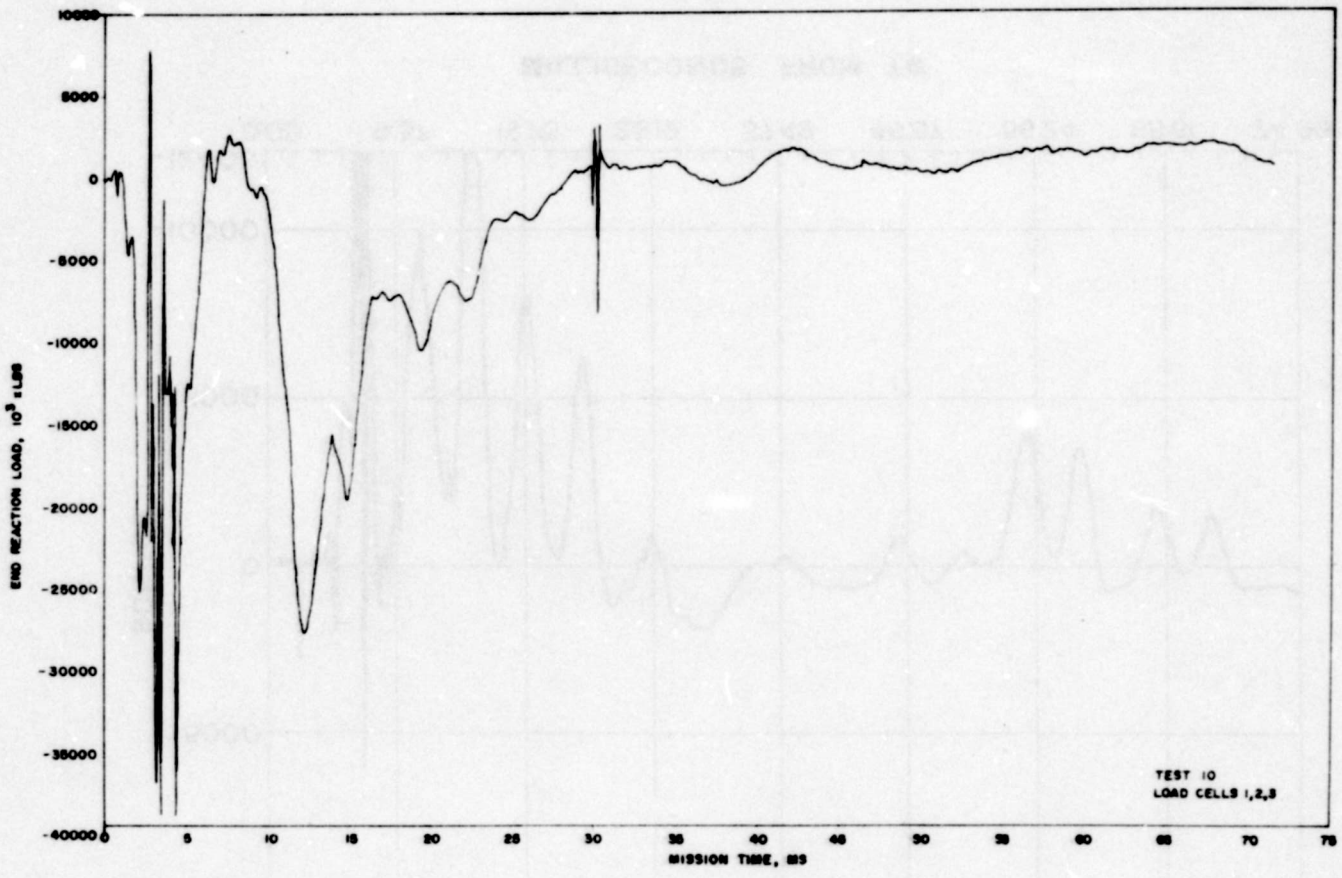

Figure 38. End Reaction Load From Beam 9, Test No. 10

as simple bars, beams, and plates. While some of the calculated frequencies compared favorably with measured frequencies, it was not possible to verify values of flexibility used in the model or represent the very high frequency response noted in the measured data. A physical test of the impulse response of the load reaction system was performed by striking the beam with a sledge hammer over a support. The output of the three load cells was measured to assess the transmissibility of the system. The result of this test is shown in Figure 39. The period of vibration noted in this figure is also shown in Figure 37.

7.2 CALCULATED REACTIONS--IMPBC

In this section the results from digital computer program IMPBC (Reference 2) will be presented. Since details of the program do not permit the description of flexible supports, the oscillation noted in the experimental data cannot be reproduced.

The nonlinear response of the impulse loaded beam was predicted by IMPBC for the material properties presented and discussed in Appendix B. Studies were performed for both typical beams and high strength concrete beams. These results are shown in Figures 40 and 41 as functions of applied impulse. Note that for an impulse of 700 psi-ms, failure was indicated for the typical beam. The response of the high strength concrete beam, shown in Figure 41, is similar to that of the typical beam. Furthermore, the calculated results indicate small changes in response for large changes in the applied impulse. A 50 percent increase in the applied impulse produces a 10 percent increase in the measured reaction.

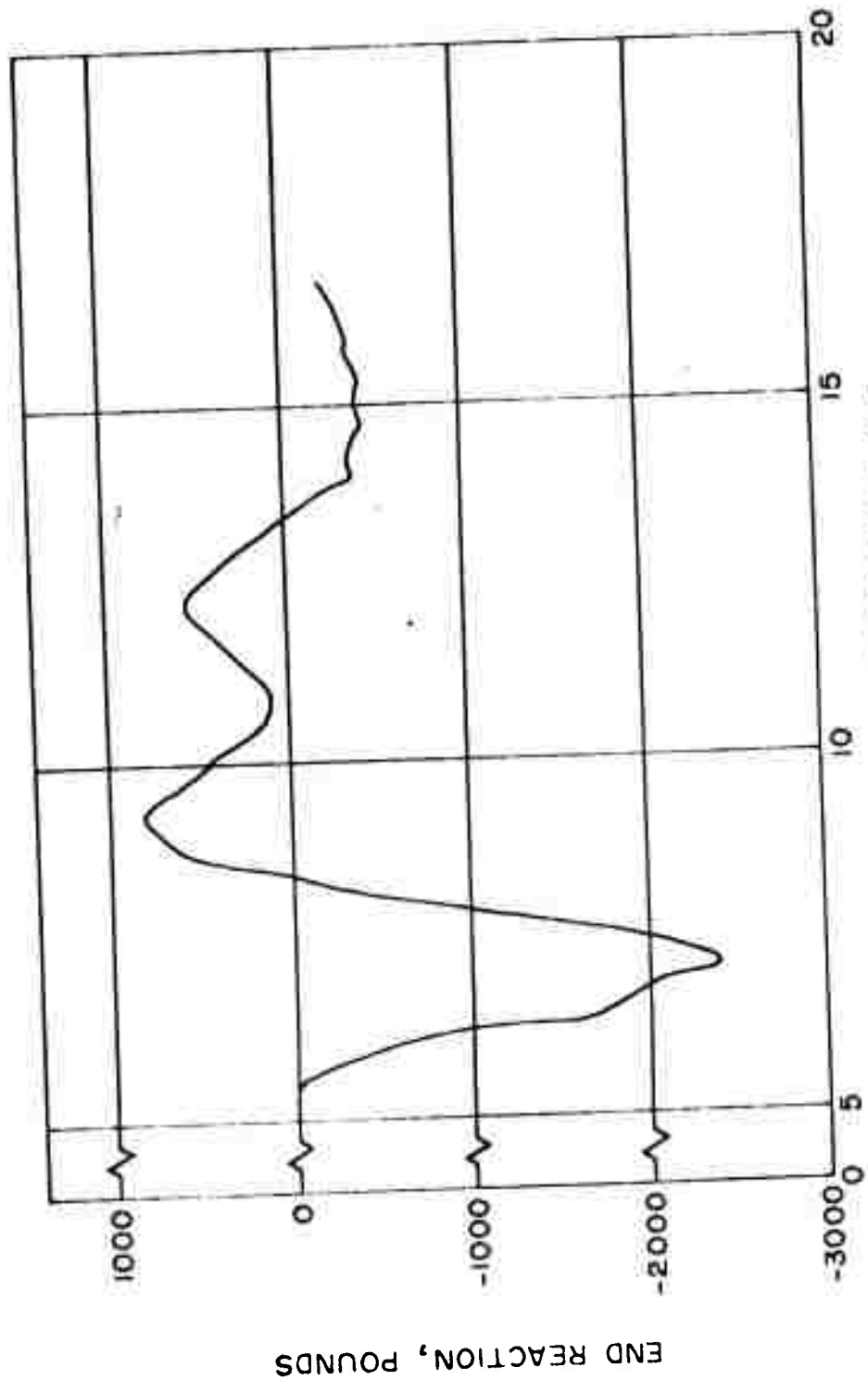

Figure 39. End Support Response for Hammer Blow at Axle Station

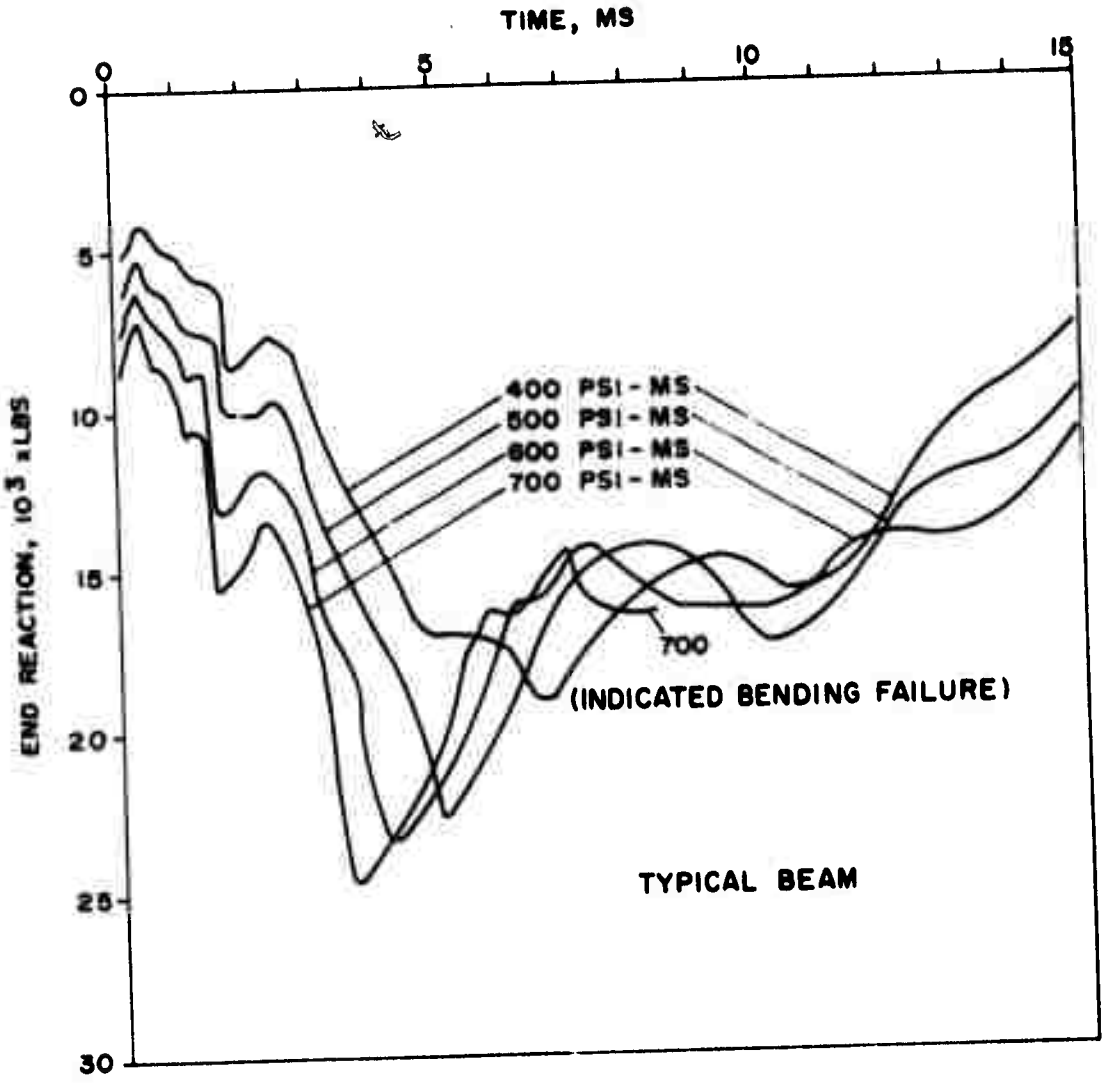

Figure 40. IMPBC Simulated End Reaction, Force for Typical Beam

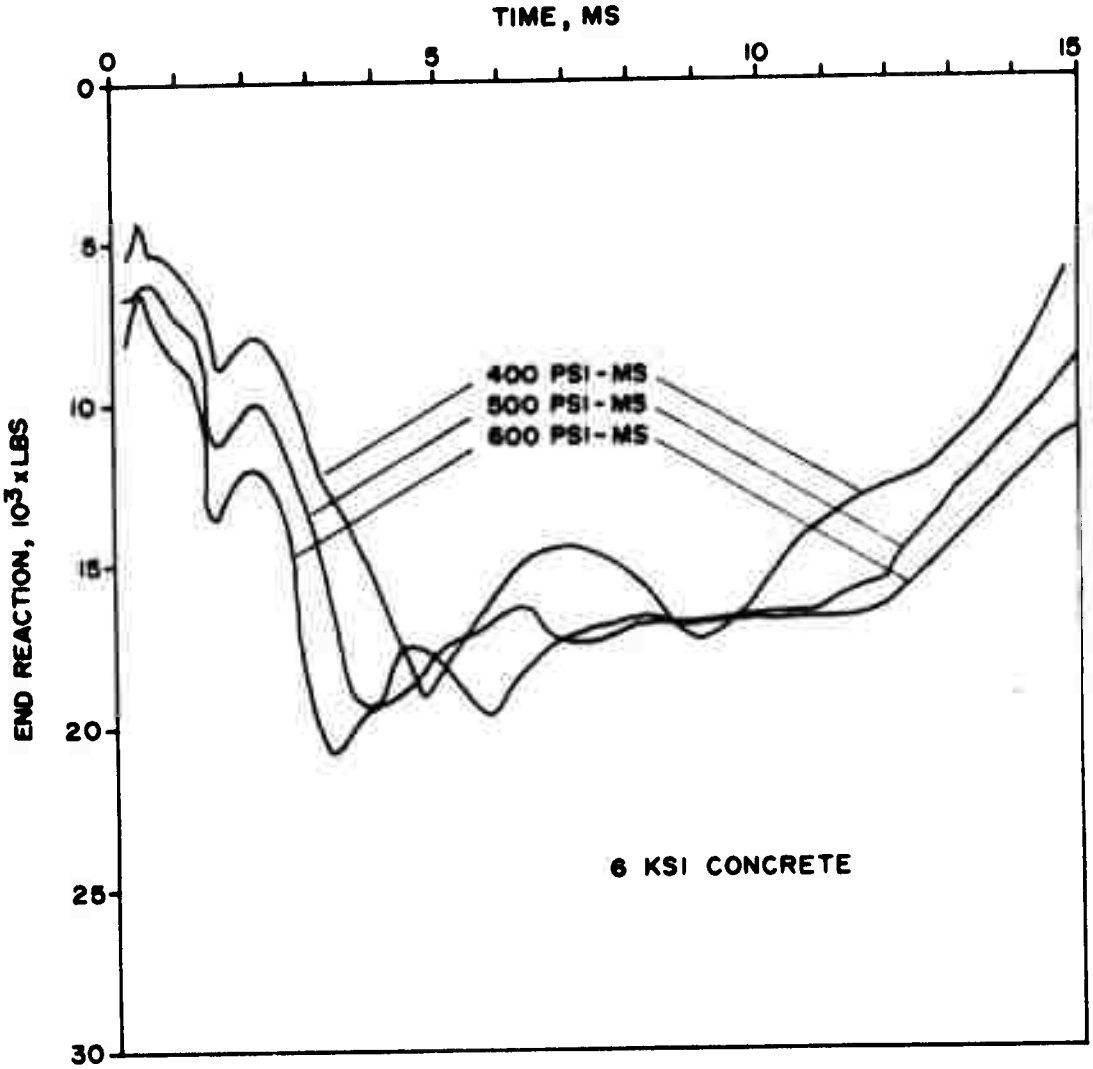

Figure 41. IMPBC Simulated End Reaction for 6 KSI Concrete Beam

SECTION VIII

BEAM STRAIN MEASUREMENT

Strain gages were placed at the midpoint and the two quarterpoints along the beams to monitor strains of the concrete and reinforcing steel during the impulse test. Strain data from the third test are shown to illustrate typical characteristics of the data. The method for the calculation of curvatures from measured strains is presented along with data from Test No. 11 to illustrate the curvature characteristics. General agreement was found between curvatures from Tests No. 10, No. 11, and No. 12 and with those calculated from the IMPBC simulations. A variety of experimental problems associated by testing, data requisition, and data reduction make similar comparisons with other tests pointless.

8.1 STRAIN DATA CHARACTERISTICS

One pair of quarterpoint and center strain gages are presented in Figures 42 and 43 to illustrate typical test data. These figures are reproductions of computer plots produced by the Computer Sciences Laboratory of Eglin AFB, Florida. The identification of data channels is presented in Figure A-2, Appendix A. The steel gage data channels were calibrated to 7500 μ in/in, several times the expected yield strain, while the concrete gage data channels were calibrated to 3000 μ in/in, the order of the magnitude of the static crushing strain. Since the concrete gages were located between the elastic neutral axis and the top surface, the measured concrete strains were approximately 50 percent of the top surface strain, provided simple beam theory is applicable.

Throughout the test series, continuous data records were available from the quarterpoint strain gages; the center gages, on the other hand, performed as shown in Figure 43. Inspection following the tests showed the center concrete gages to be broken in tension, presumably the result of beam rebound from the maximum displacement, or spalled off as the result of compression failure. The broken circuits were evident from the very high frequency, large amplitude signals which covered the latter part of the plots, as shown in Figure 43. Post-test continuity checks of steel gages indicated open circuits, although visual confirmation was not possible. The failure may have been due to gage distress or broken lead wires.

8.2 MEASURED BEAM CURVATURE

The strain gage data provided a measure of both the steel and concrete response to the impulse load. However, to determine the flexural response it

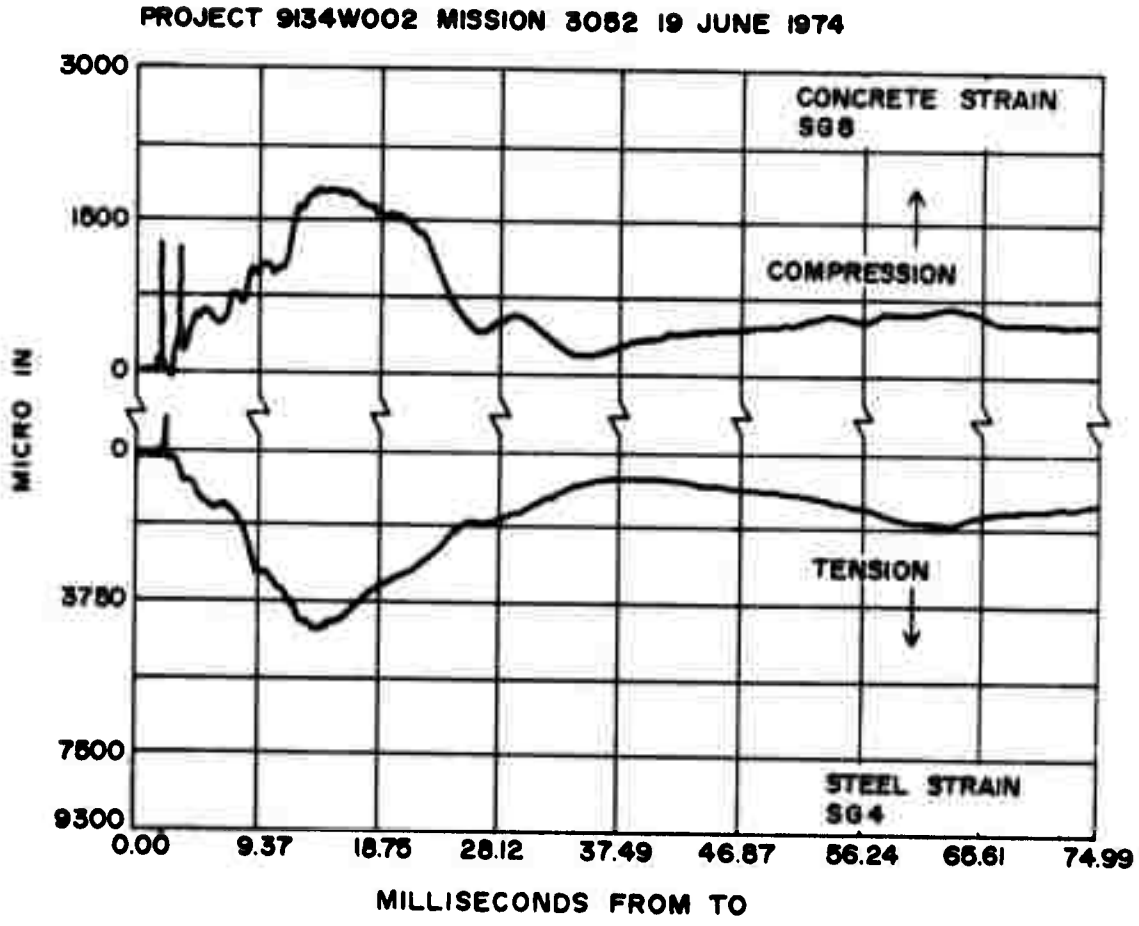

Figure 42. Typical Quarter Station Strain Data, Test No. 3

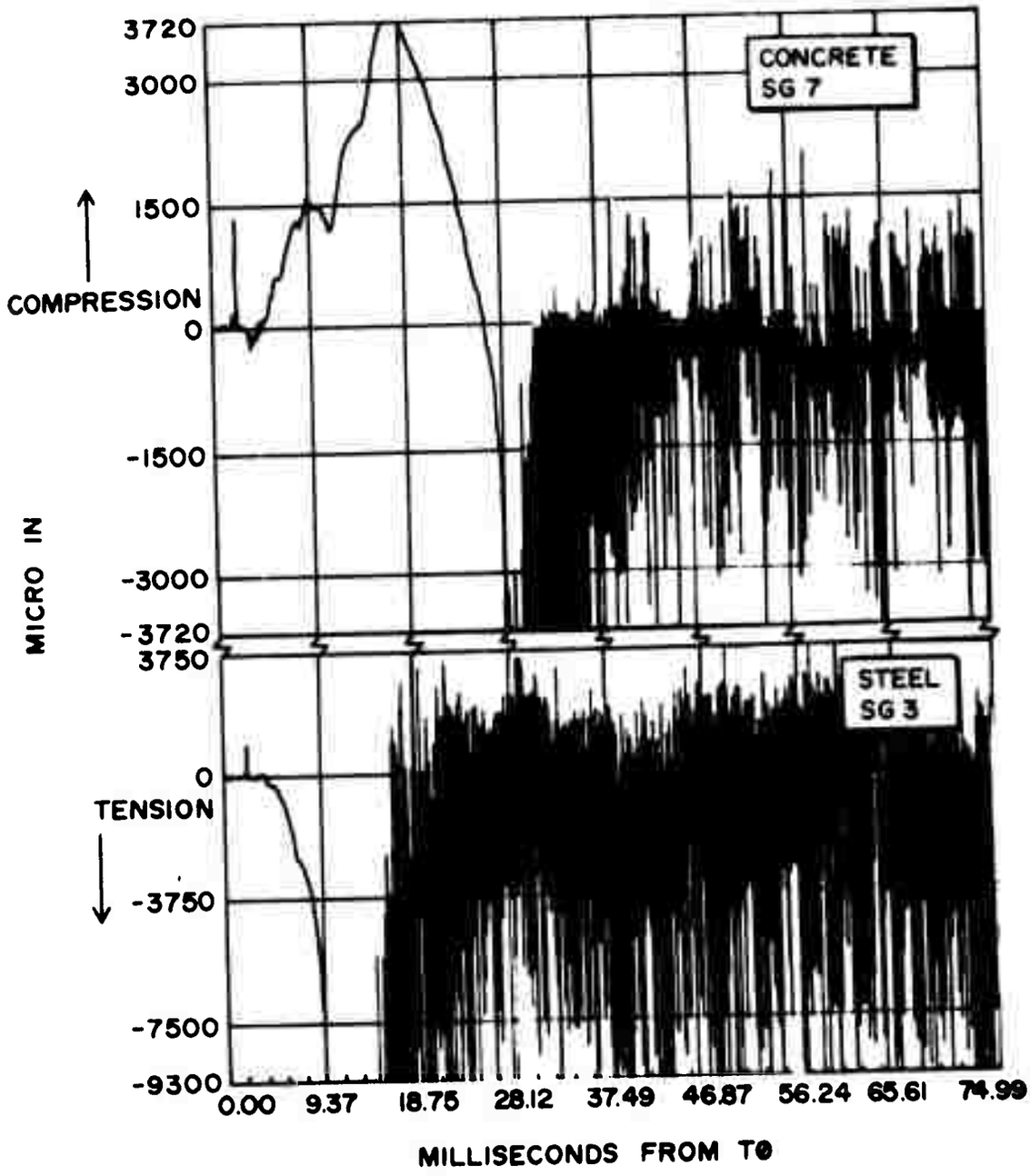

Figure 43. Typical Center Station Strain Data, Test No. 3

was necessary to estimate beam curvature at the mid- and quarterpoints by assuming planes remain plane. From the measured strain values the curvatures were calculated by:

$$\phi = \frac{(\epsilon_c - \epsilon_s)}{X_G} \tag{7}$$

where

ϕ = curvature, rad/in.;

ϵ_c = concrete strain, in/in, compressive strains positive;

ϵ_s = steel strain, in/in; and

X_G = vertical distance between steel gage and concrete gage, in., where X_G = 9.8 in. for No. 6 bars, and X_G = 9.6 for No. 9 bars.

Calculated curvatures are shown for Test No. 11 in Figure 44. The calculated quarterpoint curvature, ϕ_1, was the average of the two quarterpoint curvatures. Likewise, the center curvature, ϕ_2, is calculated from the average steel and concrete strains at the center station. However, strain gage signals which were missing or appeared to malfunction were omitted from the calculations.

The curvature-time history shown in Figure 44 is typical of the observed flexural response. Curvatures are indicated prior to shock wave arrival, probably the result of the electrical interference caused by detonation. The average rate of change of the center curvature for the first 3 ms after shock wave arrival was greater than that of the quarterpoint curvatures. The quarter curvature reached and oscillated about a constant value with small amplitude for about 12 ms. Finally, a discontinuity is noted in the center curvature at 500 μ/in., after which the curvature rate increased substantially. This is approximately the yield curvature predicted for the high strength concrete beam by the IMPBC simulations, as shown in Figure B-4, Appendix B.

8.3 CORRELATION WITH CALCULATED IMPBC CURVATURE

Curvatures for a typical beam from Tests No. 10 and No. 12 are compared with IMPBC results in Figure 45. Results for the high strength concrete beam of Test No. 11 are shown in Figure 46. The computer simulations were run with three impulse loads, 400, 500 and 600 psi-ms, to encompass the estimated test impulses. Although values predicted by Goodman (Reference 1) were 648 and 610 psi-ms for Tests No. 10 and No. 12, respectively (Figure 32), measured values were lower. It is probable that the actual impulse is between the two values. Curvatures which correspond to selected points on the idealized material stress-strain curves are identified in the figures. These curvatures designate transition points on the curve of moment variation with

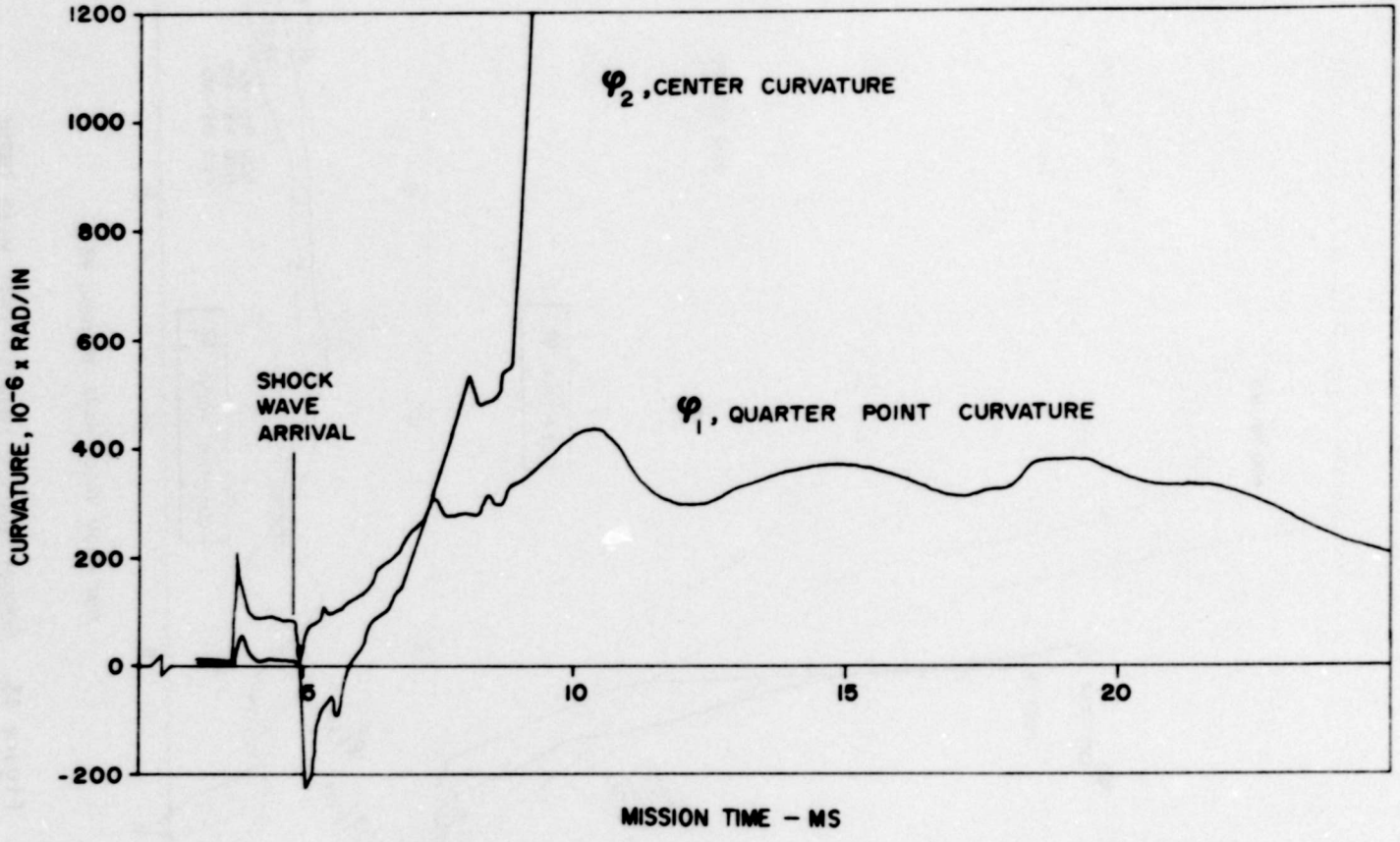

Figure 44. Curvatures Calculated From Center and Quarter Point Strain Data, Beam 3, Test No. 11

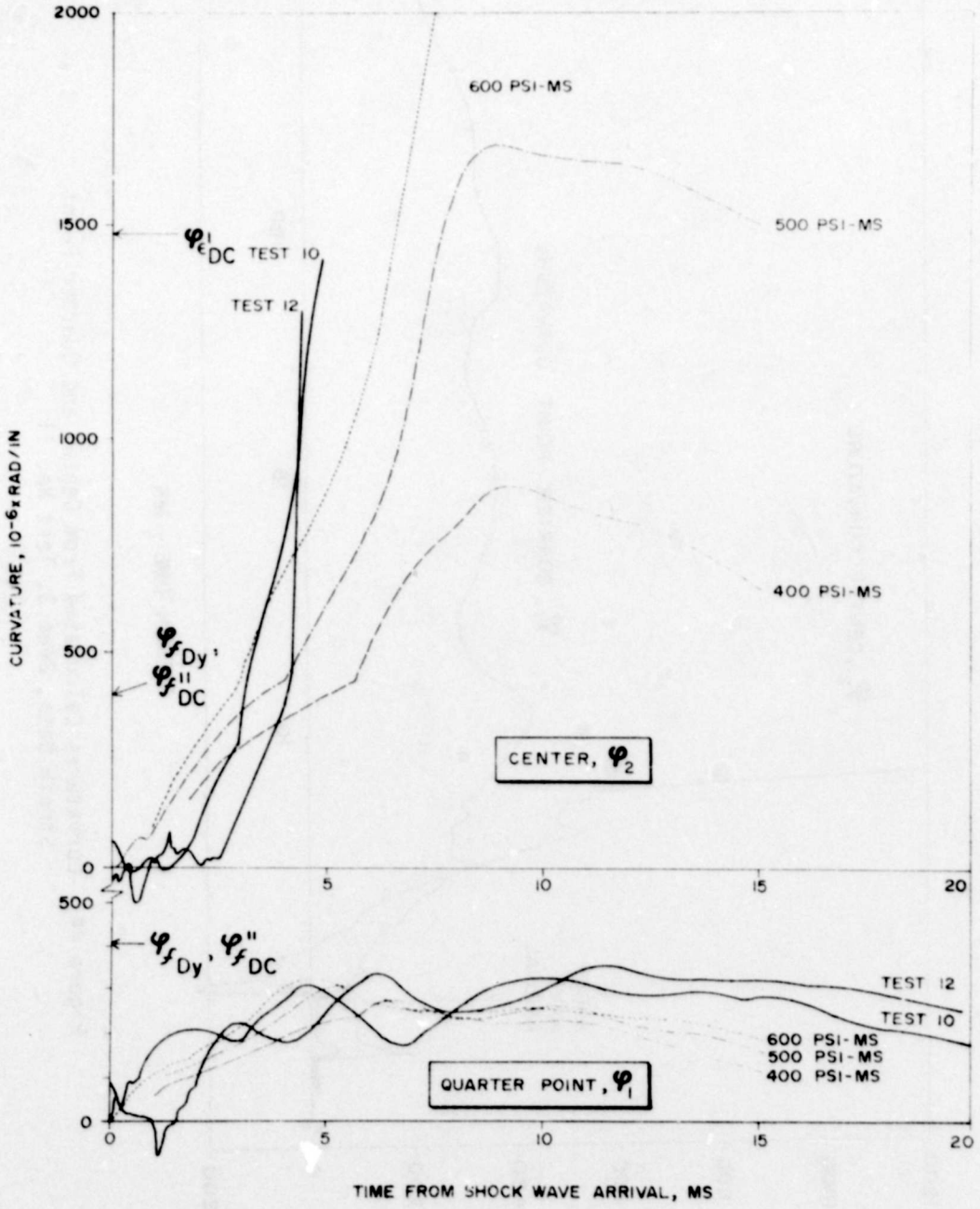

Figure 45. Comparison of Impulse Test With IMPBC Calculated Curvature, Typical Beams

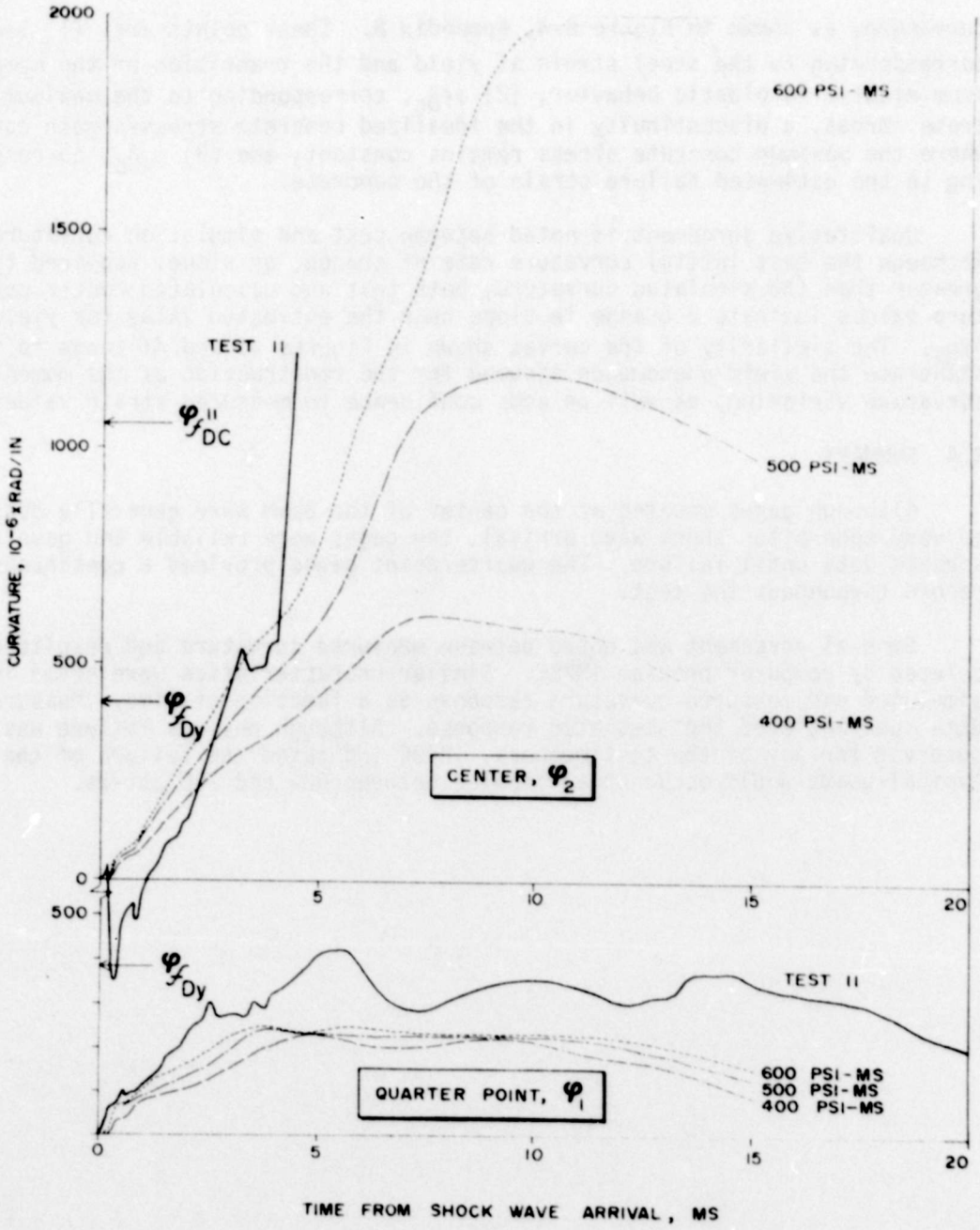

Figure 46. Comparison of Impulse Test With IMPBC Calculated Curvature, High Strength Concrete Beam

curvature, as shown in Figure B-4, Appendix B. These points are: (1) ϕf_{Dy}, corresponding to the steel strain at yield and the transition of the member from elastic to plastic behavior; (2) $\phi f''_{Dc}$, corresponding to the maximum concrete stress, a discontinuity in the idealized concrete stress-strain curve where the maximum concrete stress remains constant; and (3) $\phi_{\varepsilon} f'_{Dc}$, corresponding to the estimated failure strain of the concrete.

Qualitative agreement is noted between test and simulation curvatures. Although the test initial curvature rate of change, or slope, appeared to be greater than the simulated curvature, both test and calculated center curvature values indicate a change in slope near the estimated value for yield, ϕf_{Dy}. The similarity of the curves shown in Figures 45 and 46 tends to substantiate the yield phenomenon assumed for the construction of the moment-curvature variation, as well as adds confidence to measured strain values.

8.4 SUMMARY

Although gages mounted at the center of the beam were generally destroyed very soon after shock wave arrival, the gages were reliable and gave reasonable data until failure. The quarterpoint gages provided a continuous record throughout the test.

General agreement was noted between measured curvature and results calculated by computer program IMPBC. Similar characteristics were noted in the simulated and measured curvature response as a function of time. Measured data substantiated the simulated response. Although obvious failure was not observed for any of the test members, IMPBC indicated the failure of the typical beams would occur at an impulse between 600 and 700 psi-ms.

SECTION IX

BEAM DAMAGE ASSESSMENT

The visual inspection which followed the blast tests provided a qualitative assessment of blast damage. For several tests, the damage appeared slight to nonexistent. Therefore, it was necessary to develop a more precise evaluation of the damage caused by the impulse loading. The beams were returned to the Oklahoma State University, Stillwater, for final inspection and tests. The beams were loaded statically to failure and results of these tests were presented in Section IV. In this section a method, similar to one presented by Biggs (Reference 3), is proposed and evaluated for predicting damage caused by impulse loads. Although the study is limited to typical beams, it is proposed that the method may be extended to the other beams of this program as well as other members, such as plate and slab structures.

9.1 FINAL STATIC TEST RESULTS

The data from the final static tests are summarized in Table IX. In this chapter the properties of the damaged beams are presented as a function of charge standoff distance and include residual plastic work capacity and the ratio of measured to theoretical ultimate moment. These data are shown in Figures 47 and 48. Also shown in the figures are the results obtained from beam 13, which was not subjected to impulse loading prior to the static test.

Although scatter is apparent in the data for residual plastic work, shown in Figure 47, several trends are apparent. First, the beams with increased reinforcing steel, the high strength beams, exhibit little residual work capacity. Second is the relation between charge standoff distance and residual work capacity: as the charge standoff distance decreases, residual plastic work is decreased. Finally, the high strength concrete beams exhibited the largest residual work capacity, although they had been subjected to the greatest impulses.

Measured and theoretical moments are compared in Figure 48. It can be noted that the change in the maximum moment with impulse is less significant than the change noted in residual plastic work. Furthermore, the measured ultimate moment of the undamaged typical beam, beam 11, is approximately equal to the theoretical ultimate moment. The difference between the experimental and theoretical strength may have resulted from end restraint produced by test apparatus; if so, similar influences are probably involved in other strengths shown.

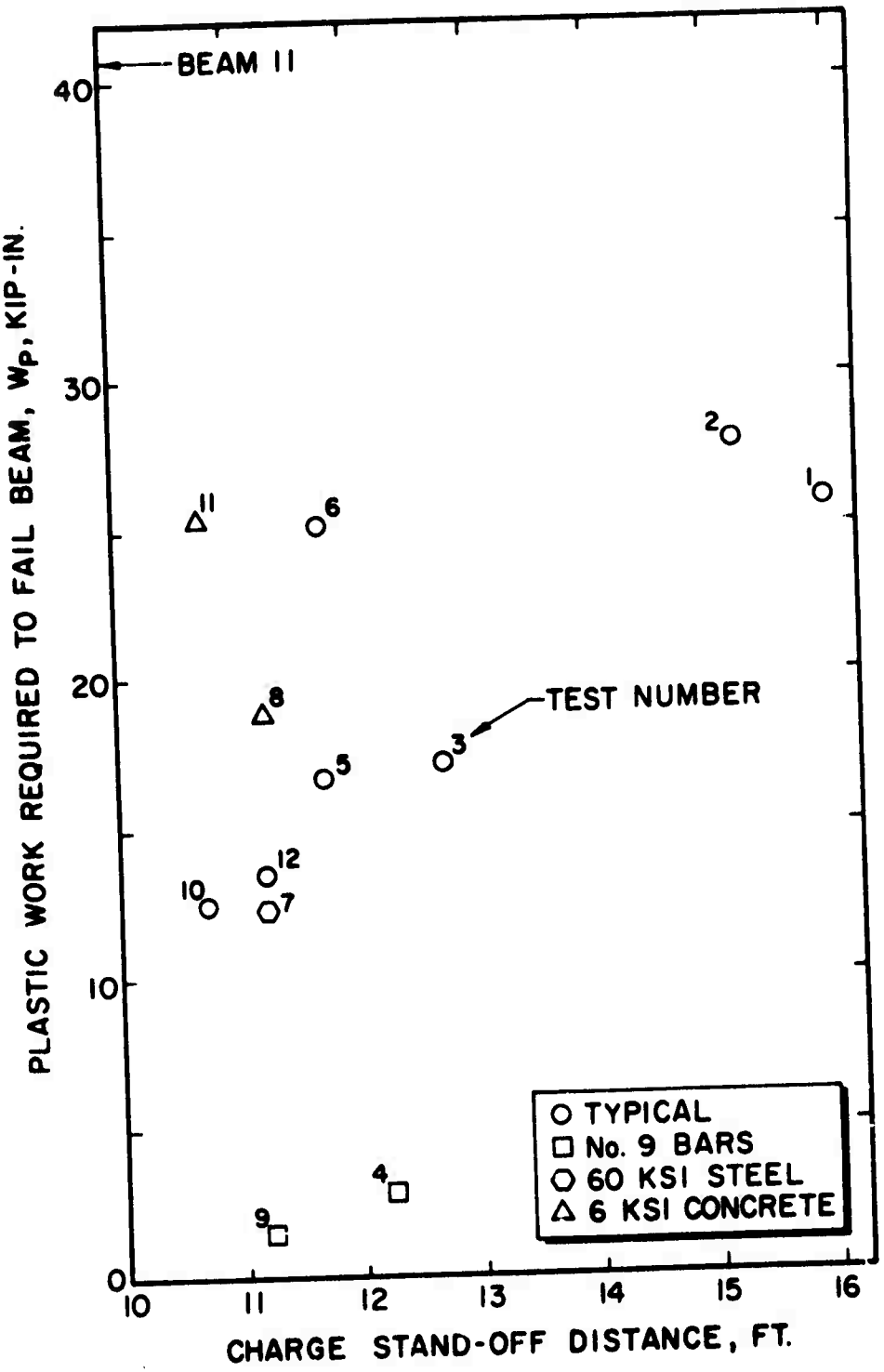

Figure 47. Variation of Residual Plastic Work With Charge Standoff Distance

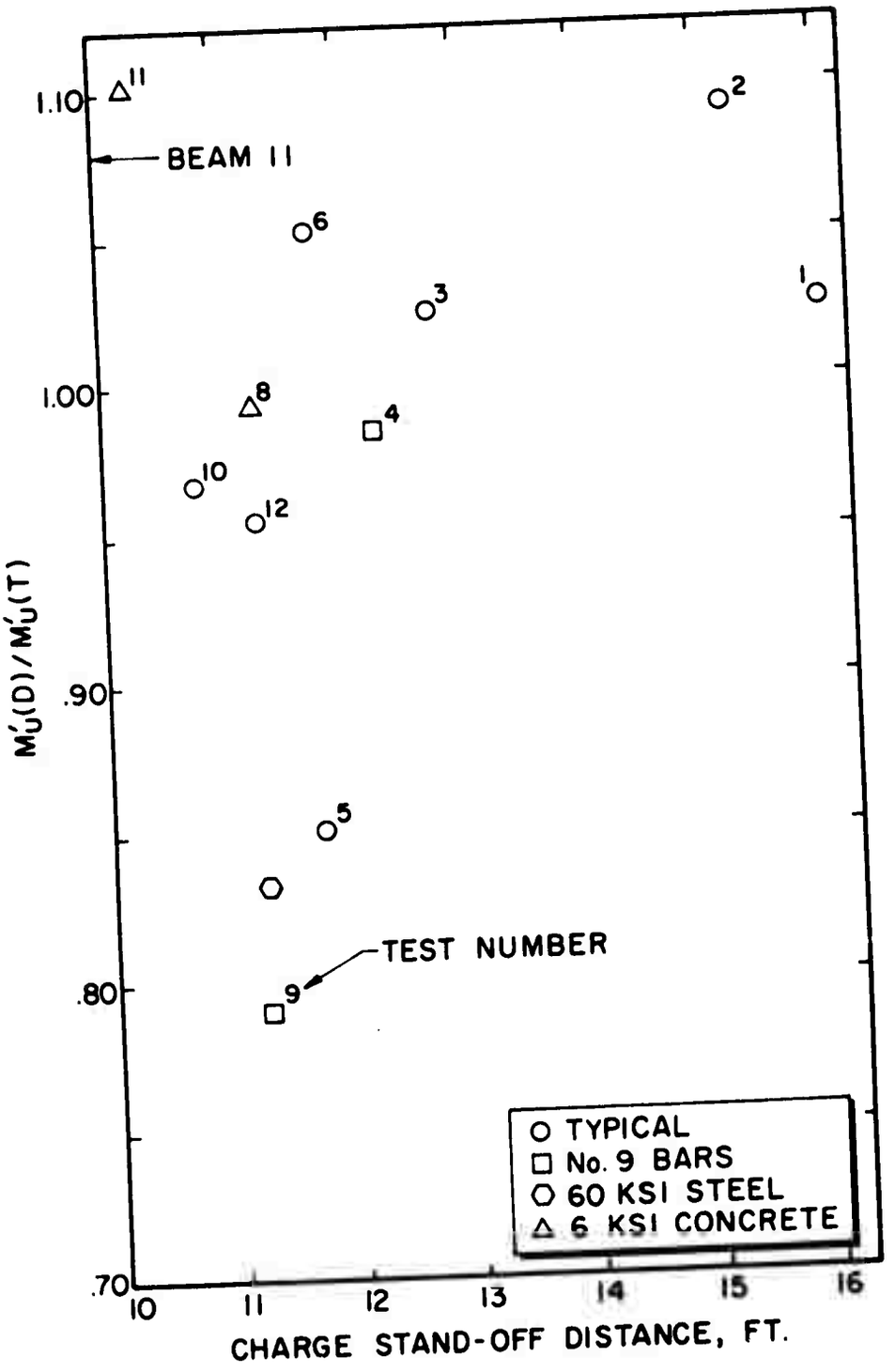

Figure 48. Variation of Measured to Theoretical Ultimate Moment Ratio With Change of Standoff Distance

Figures 47 and 48 show effects of impulse loads on the reinforced concrete beams. The standoff distance of the pentolite charge was assumed to be a quantitative measure of the level of impulse delivered to the beam. The reduction of residual plastic work may be interpreted as a measure of damaged caused by the blast loading. Although only limited data are available for high strength concrete and high steel ratio beams, a trend is apparent for these members.

The static response of damaged and undamaged typical beams is compared in Figure 29. Except for the reduced ductility of the damaged beams, the two curves exhibit similar characteristics. Little difference is noted in either the ultimate moment or the initial slope of the curves. In this section the damage due to the blast loading will be studied. Differences between the static tests will be related to damage produced by the kinetic energy imparted to the beam during the impulse loading.

In Figure 49 the residual plastic work of damaged beams is compared with the total work capacity of an undamaged member. Except for Test No. 6, excellent agreement is noted between standoff distance and the plastic work ratio. These data, along with the characteristics noted in Figure 29, will be the basis for the damage criterion developed in the next section.

9.2 IMPULSE DAMAGE PHENOMENON

The effect of the high intensity impulse loading is to transfer energy from the blast pressure wave to kinetic energy in the beam. Since the duration of the positive pressure is less than 2 ms, it may be assumed that the transfer is instantaneous, imparting to the beam a lateral velocity which is consistent with the support constraints. The kinetic energy related to the initial velocity must be dissipated by plastic deformation of the beam or stored in the beam as elastic strain energy. The static plastic work, or toughness, will be used to determine the capacity of the beam to dissipate kinetic energy. However, the moment due to static loading should approximate the shape of the dynamic bending moment. In the laboratory this was accomplished by a trapezoidal moment distribution where the center 48 inches of the beam was subjected to constant moment. The work related to this loading was recorded and will be used to estimate beam impulse capacity.

9.3 PREDICTION OF IMPULSE DAMAGE

A correlation between residual plastic work and charge standoff distance shown in Figure 49 for typical beams. As the charge standoff distance is decreased, the residual plastic work decreases. The work was determined from the laboratory resistance-displacement curves, shown in Figure 29. However, these data may be arranged as shown in Figure 50. Instead of a common initial point, failure is selected as the point common to both damaged and undamaged beam resistance-deflection curves. The proposed method for damage

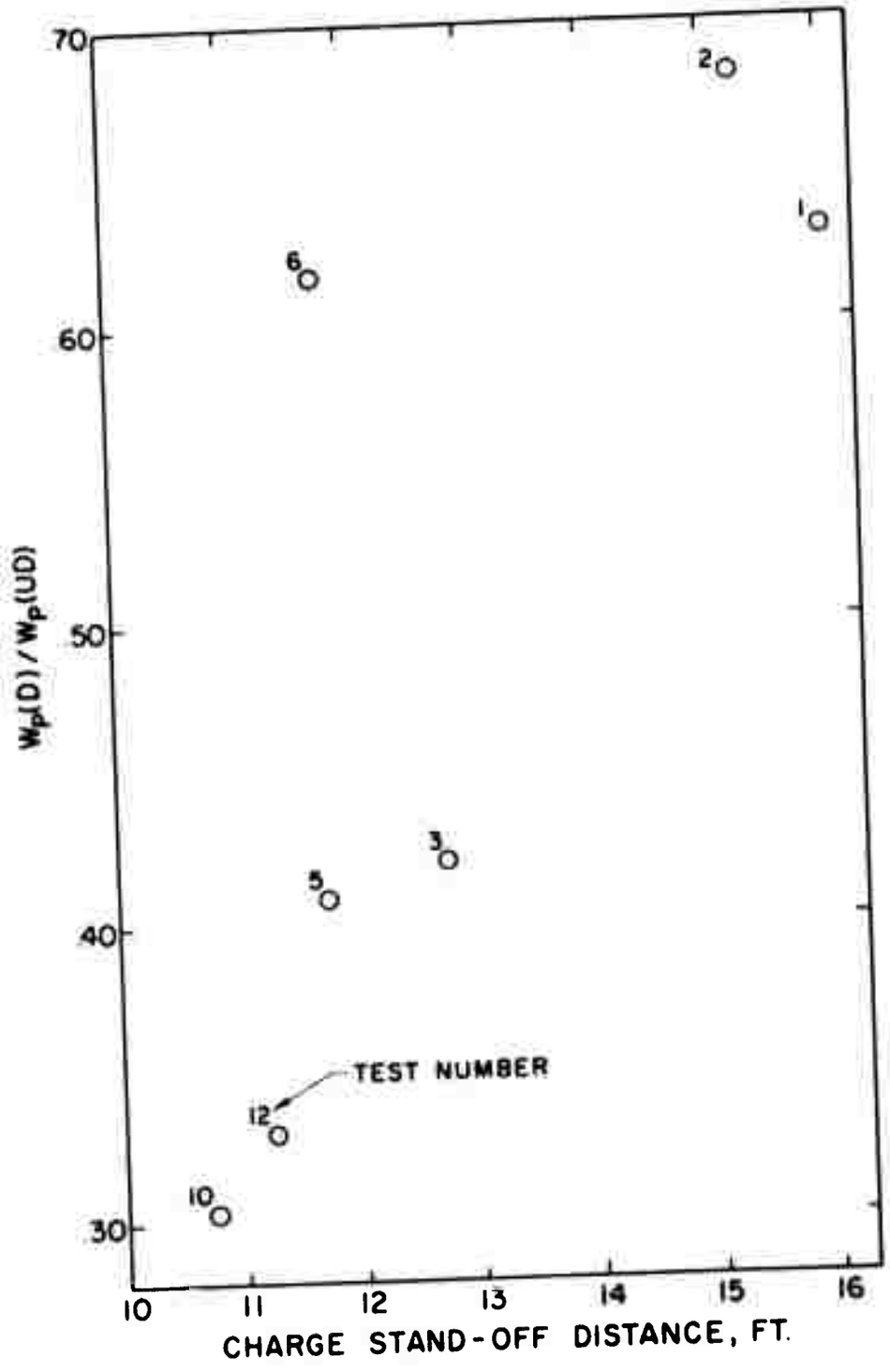

Figure 49. Variation of Residual Plastic Work Ratio for Typical Beams

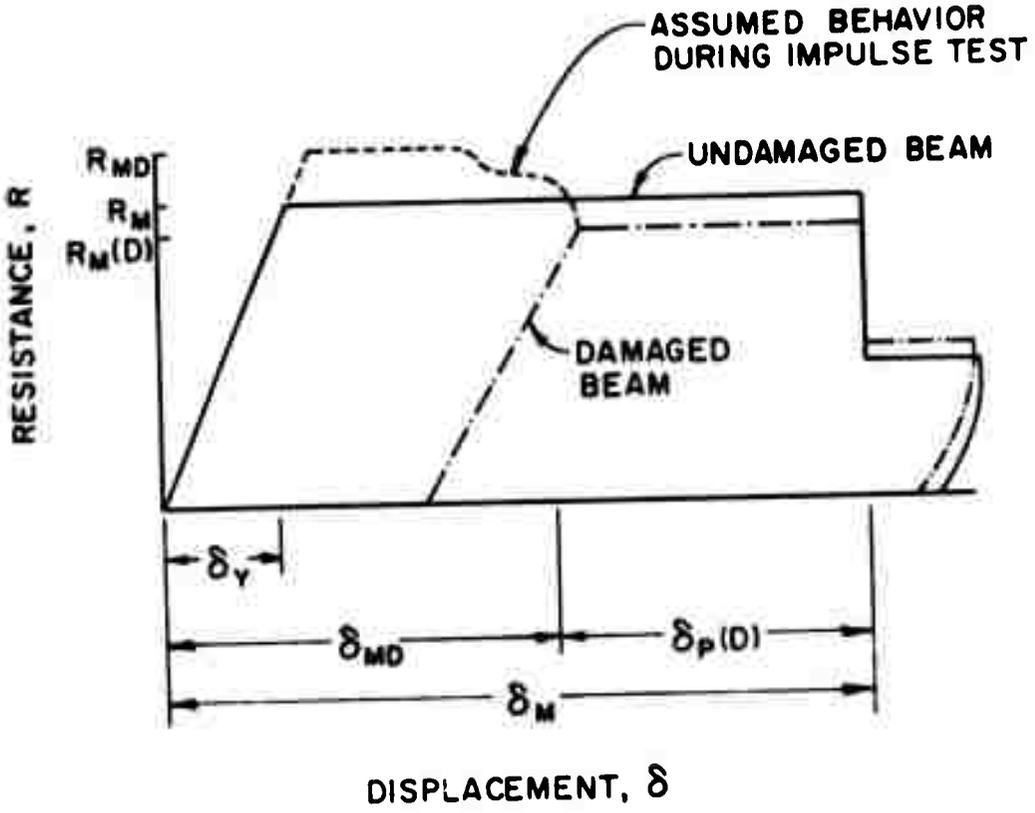

Figure 50. Idealized Resistance-Displacement Curves for Damaged and Undamaged Beams

analysis is shown by this figure. The reinforced concrete member has a predictable capacity for plastic work. If a portion of this capacity is expended, the remaining capacity can be determined by a static test. The reduction in work capacity may then be related to kinetic energy which had been dissipated.

Thus, the primary assumption of this technique is that the kinetic energy imparted to the beam by the impulse loading is transformed partially into elastic strain energy stored in the beam and energy dissipated by plastic deformation. For these tests it was assumed that the beam initial velocity distribution is sinusoidal with a maximum center velocity V_{max}.

$$V_{max} = \frac{Ib}{m} \tag{8}$$

where

I = impulse, psi-ms;

b = beam width, inches; and

m = beam mass per length, lb-sec^2/in^2.

The total kinetic energy of the beam is given by

$$KE = \frac{I^2 b^2 L}{4m} \tag{9}$$

where L is the length of the member.

It is assumed that the kinetic energy required to produce failure must be greater than or equal to the total static work capacity of an undamaged beam. For the beam of Figure 50 the total work capacity W is taken as the area under the curve to δ_m, where a substantial drop in load capacity occurs:

$$W = R_m \delta_y (\gamma - \frac{1}{2}) \tag{10}$$

where γ is ductility, the ratio of the maximum deflection δ_m to the elastic deflection δ_y. The total work may also be related to the total plastic work capacity of an undamaged beam, $W_p(UD)$:

$$W = W_p(UD) \frac{(\gamma - 1/2)}{(\gamma - 1)} \tag{11}$$

Equating kinetic energy [Equation (9)] to the total work capacity [Equation (11)], the minimum impulse required to produce failure in an undamaged beam is,

$$I = \left[\frac{4m}{b^2 L} \frac{W_p(UD)(\gamma - 1/2)}{(\gamma - 1)}\right]^{1/2} \tag{12}$$

This is also the value of impulse predicted by Biggs (Reference 3).

If a resistance-deflection curve is available for an undamaged member, it will be possible to estimate the impulse to which a beam was subjected. The residual plastic work, $W_p(D)$, as shown in Figure 50. This represents the work capacity which was not expended by the blast loading. However, the sum of the residual plastic work and the work requried to dissipate the kinetic energy of the blast must be equal to or greater than the total static work capacity of the beam. This may be represented mathematically as

$$KE + W_p(D) \geq W \tag{13}$$

where KE is the kinetic energy of the impulse loading. Substituting for W and KE [Equations (9) and (11)],

$$I \geq \frac{2}{b} \left(\frac{m}{L}\right)^{1/2} \left[\frac{W_p(UD)(\gamma - 1/2)}{(\gamma - 1)} - W_p(D)\right]^{1/2} \tag{14}$$

where I is an estimate of the minimum impulse to which the beam was subjected.

For the test data of Table IX, it is possible to predict the minimum impulse to which the typical beams were subjected by Equation (14). The results are shown in Table XI, along with the predicted impulse of Goodman (Reference 1). From undamaged beam data, it is estimated that an impulse of at least 708 psi-ms would be required to produce failure. It should be noted that there is agreement between this estimate and the calculated results of digital computer program IMPBC.

9.4 SUMMARY

Post-test visual inspection of the beams indicated moderate to slight damage. However, the final static tests indicated significant losses in plastic work capacity which were related to the dissipation of kinetic energy.

A method for predicting damage based on work of Biggs (Reference 3) was proposed. Although reliable measured values of impulse were unavailable, excellent agreement was noted between impulse predicted by Goodman and Equation (14). It is reasonable to assume that the method presented in this report may be extended to other concrete members.

TABLE XI. ESTIMATE OF TEST IMPULSE FROM RESIDUAL PLASTIC WORK AND REFERENCE 1

Test No.	Minimum Kinetic Energy Imparted to Beam (kip-in) Equation (13)	Impulse I (psi-ms)	
		Equation (14)	Goodman[a]
1	18.9	460	375
2	16.8	434	410
3	27.5	555	520
5	28.0	560	560
6	19.5	468	560
10	32.3	602	650
12	31.2	595	620
Beam 13	44.6[b]	708	---[c]

[a]From Figure 32.

[b]Maximum work available for kinetic energy.

[c]Static test beam.

SECTION X

SUMMARY AND RECOMMENDATIONS

These tests provided both qualitative and quantitative data of the blast-respone phenomenon for reinforced concrete beams. The major results are summarized and recommendations are proposed for additional studies.

Three general conclusions of this study are:

1. Although the threshold impulse for beam failure was not defined, the impulse tests provided valuable information concerning the coupling of the blast pressure wave with the beam.

2. The technique of statically testing the impulse-damaged beams was a valuable method for obtaining quantitative assessment of beam damage.

3. Beams with high strength concrete exhibited the greatest resistance to damage due to impulse loading. On the other hand, the beams with a large steel ratio were the least resistant to impulse loading.

10.1 TEST EVALUATION

10.1.1 Test Equipment

The test beams were suitable for the test program. The beams were neither model sized nor too large to handle in the laboratory or field. The test fixture performed well during the blast tests. It sustained little damage and would be available for future test programs. A spherical pentolite charge suspended above the test specimen was effective in providing the required impulse loads.

The manner in which beams were supported should be improved if additional tests are performed. In this program sufficient accelerations were imparted to the test to result in measurements which were a combination of both reaction and inertial forces. It was also noted that in some tests, longitudinal forces were being resisted by the support devices in spite of precautions taken to eliminate such forces. From this study it seems probable that an ideal support condition is not achievable in a blast environment and it suggests that in future work, simpler but well-instrumented end conditions be provided.

Although pressure data were improved by changing pressure transducers, additional work is required to investigate the response of transducers to the very short duration, high pressure loading produced in these tests. The

PCB transducers appeared to give consistent results, but because the measured impulses found by integrating the pressure-time data were generally less than those predicted by Goodman (Reference 1), the accuracy of these measurements should be studied.

The accelerometer installation utilized for these tests did not prove to be suitable. A zero shift, which was of the order of magnitude of the data, was produced by large shock transients.

Data from strain gages attached to the test specimens were normally of acceptable quality but of limited usefulness because of gage failure during the early portion of response. It is recommended that in future work, efforts be made to develop reliable transducers which can directly monitor the deflection of beams.

10.1.3 Damage Assessment

An important development of this work was the assessment of damage from a comparison of static resistance-deflection characteristics of damaged and undamaged beams. The variations noted in these curves were attributed to the impulse loading. It was found that: (1) for the range of standoff distances studied, there was not a large reduction in the ultimate moment capacity of the damaged beams; (2) there appeared to be substantial reductions in the ductility of the damaged beams; and (3) of the parameters studied, the residual plastic work, which includes items (1) and (2), exhibited the greatest change with the standoff distance.

The beam damage assessment method was used to predict test impulse. The impulse predicted by the damage criterion for the typical beams compared favorably with Goodman (Reference 1). Similar evaluations could have been made if undamaged samples of the other beam types had been available.

10.1.4 Comparison of Test Data With IMPBC Analysis

Results of program IMPBC were compared with experimental reactions and curvatures. Excellent agreement was noted between calculated and measured curvatures. Comparison of reactions must be qualified because of the vibration of the support mechanism. Measured reactions are a combination of beam end forces and support mechanism inertial forces. However, the IMPBC results are similar to the measured data when the effect of the change of impulse on the change in reaction is considered. Finally, the agreement between IMPBC and Biggs (Reference 3) for failure impulse should be noted.

It is concluded that the program becomes a versatile and valuable analytical tool for investigating the impulse-response characteristics of reinforced concrete beams. However, it is also recommended that the digital computer program be extended to include:

1. A criterion to represent loss of material from the top layers of concrete in the highest moment region, and account for the changed cross section by revising the moment-curvature curves at the affected nodes.

2. Automatic evaluation of strain rate effects within the program.

3. Damage assessment criterion developed in this work.

10.1.5 Beam Performance

Beam damage was evaluated on the basis of visual observations and static load tests to failure. On the basis of visual observations, the high strength steel beam appeared to sustain the most damage; however, the static tests showed the large steel area beams to have the least residual energy capacity. The high strength concrete beams appeared to have the greatest blast resistance on the basis of both visual observation and residual static capacity.

10.2 RECOMMENDATIONS FOR ADDITIONAL STUDIES

Limited studies should be performed to evaluate the damage criterion presented in this report for other structural members. The program should include static testing of undamaged members, to predict failure impulse, followed by blast tests. It is further recommended that the existing test fixture be utilized for these tests.

The members which should be investigated are:

1. Tee and double-tee beams, with attention to web shear failure and shear transfer from flange to web in high moment regions;

2. Composite beams, with attention to shear transfer from the concrete to the steel portion of the member;

3. Prismatic beams with compression reinforcement; and

4. Prestressed concrete beams.

REFERENCES

1. Goodman, H. J. "Compiled Free-Air Blast Data on Bare Spherical Pentolite." Aberdeen Proving Ground, Maryland: Ballistics Research Laboratories, Report No. 1092, July, 1956.

2. Dawkins, W. P. "A Method of Analysis for Reinforced Concrete Beam-Columns Subejcted to Impulse Loading." Report submitted to Oklahoma State University, March, 1971.

3. Biggs, John M. Introduction to Structural Dynamics. New York: McGraw-Hill Book Co., Inc., 1964, pp. 199-224.

4. Manjoine, M. J. "Influence of Rate of Strain and Temperature on Yield Stresses of Mild Steel." Transactions, Journal of Applied Mechanics, American Society of Mechanical Engineers, Vol. 66, No. 4 (December, 1944), pp. A.211-A.218.

5. Norris, Charles H., et al. Structural Design for Dynamic Loads. New York: McGraw-Hill Book Co., Inc., 1959, p. 27.

6. Allgood, J. R. and G. R. Swihart. Design of Flexural Members for Static and Blast Loading. ACI Monograph No. 5. Detroit: American Concrete Institute, 1970, pp. 23-25.

7. Perrone, Nicholas. "On a Simplified Method for Solving Impulsively Loaded Structures of Rate-Sensitive Materials." Transactions, Journal of Applied Mechanics, American Society of Mechanical Engineers, Vol. 87 (September, 1965), pp. 489-492.

8. Watstein, D. "Effect of Straining Rate on the Compressive Strength and Elastic Properties of Concrete." Proceedings, Journal of the American Concrete Institute, Vol. 49, No. 8 (April, 1953), pp. 729-744.

9. Atchley, B. L. and H. L. Furr. "Strength and Energy Absorption Capabilities of Plain Concrete Under Dynamic and Static Loadings." Proceedings, Journal of the American Concrete Institute, Vol. 64, No. 11 (November, 1967), pp. 745-746.

10. Keenan, William A. "Dynamic Shear Strength of Reinforced Concrete Beams--Part I." Port Hueneme, Calif.: Naval Civil Engineering Laboratory, Technical Report No. R-395 (AD627661), December, 1965.

REFERENCES (Continued)

11. Fox, E. N. "Some Exploratory Tests on the Strength of Concrete Beams Under Pulse Loads." Mechanical Properties of Non-Metallic Brittle Materials. Ed. W. H. Walton. London: Butterworths Scientific Publications, 1958, pp. 283-299.

12. Galloway, J. W. and K. D. Rathby. "Effects of Rate of Loading on Flexural Strength and Fatigue Performance of Concrete." Crowthorne, Berkshire: Transport and Road Research Laboratory, Report No. LR 547, 1973.

13. Mylrea, T. E. "Effect of Impact on Reinforced Concrete Beams." Proceedings, Journal of the American Concrete Institute, Vol. 36, No. 6 (June, 1940), pp. 581-594.

14. Kluge, R. W. "Impact Resistance of Reinforced Concrete Slabs." Proceedings, Journal of the American Concrete Institute, Vol. 39, No. 5 (April, 1943), pp. 397-412.

15. Bate, S. C. C. "The Strength of Concrete Members Under Dynamic Loading." Proceedings of a Symposium on the Strength of Concrete Structures. London: Cement and Concrete Association, 1956, pp. 487-524.

16. Simms, L. G. "Actual and Estimated Resistance of Some Reinforced-Concrete Units Failing in Bending." Journal of the Institution of Civil Engineers, Vol. 23, No. 4 (February, 1945), pp. 163-179.

17. Hansen, Robert J. "Long Duration Impulsive Loading of Simple Beams." Journal of the Boston Society of Civil Engineers, Vol. 35, No. 3 (July, 1948), pp. 272-285.

18. Penzien, J. and R. J. Hansen. "Static and Dynamic Elastic Behavior of Reinforced Concrete Beams." Proceedings, Journal of the American Concrete Institute, Vol. 50, No. 7 (March, 1954), pp. 545-568.

19. Nordell, William J. "Hinging in Statically and Dynamically Loaded Reinforced Concrete Beams." Port Hueneme, Calif.: Naval Civil Engineering Laboratory, Technical Report No. R-489 (AD642108), October, 1966.

20. Nordell, William J. "Plastic Hinge Formation in Reinforced Concrete Beams." Port Hueneme, Calif.: Naval Civil Engineering Laboratory, Technical Report R-371 (AD617246), June, 1965.

REFERENCES (Continued)

21. Mavis, F. T. and E. A. Richards. "Impulsive Testing of Concrete Beams." Proceedings, Journal of the American Concrete Institute, Vol. 52, No. 1 (September, 1955), pp. 93-102.

22. Mavis, F. T. and M. J. Greaves. "Destructive Impulse Loading of Reinforced Concrete Beams." Proceedings, Journal of the American Concrete Institute, Vol. 54, No. 3 (September, 1957), pp. 233-252.

23. Balog, Louis et al. A discussion of "Destructive Impulse Loading of Reinforced Concrete Beams." Proceedings, Journal of the American Concrete Institute, Vol. 54, No. 9 (March, 1958), pp. 811-824.

24. Shaw, W. A. and J. R. Allgood. "Blast Resistance of Reinforced Concrete Beams Influenced by Grade of Steel." Proceedings, Journal of the American Concrete Institute, Vol. 55, No. 10 (March, 1959), pp. 935-946.

25. Mavis, F. T. and J. J. Stewart. "Further Tests of Dynamically Loaded Beams." Proceedings, Journal of the American Concrete Institute, Vol. 55, No. 11 (May, 1959), pp. 1215-1223.

26. Wadlin, G. K. and J. J. Stewart. "Comparison of Prestressed Concrete Beams and Conventionally Reinforced Concrete Beams Under Impulsive Loading." Proceedings, Journal of the American Concrete Institute, Vol. 50, No. 4 (October, 1961), pp. 407-422.

27. Hamilton, Wayne A. "Dynamic Response of Pretensioned Prestressed Concrete Beams." Proceedings, Journal of the American Concrete Institute, Vol. 65, No. 10 (October, 1968), pp. 851-855.

28. Cowles, Bruce C. and Wayne A. Hamilton. "Repetitive Dynamic Loading on Pretensioned Prestressed Beams." Proceedings, Journal of the American Concrete Institute, Vol. 66, No. 9 (September, 1969), pp. 745-747.

29. Reichstetter, F. G. "Blast Loaded Concrete Beam Test." Eglin Air Force Base, Florida: Armament Development and Test Center, Data Package 74-11, Project AFATWG02, November, 1974.

30. Armament Development and Test Center. "Vulnerability and Lethality Testing System." Technical Report No. ADTC-TR-72-127. Eglin Air Force Base, December, 1972.

REFERENCES (Concluded)

31. Gupchup, Vijay N. and Indravandan K. Shah. "Static and Dynamic Behavior of Reinforced Concrete Arches." Boston: Massachusetts Institute of Technology, Civil Engineering Dept., Report No. R63-5, March, 1963.

APPENDIX A

IMPULSE TEST DATA

All recorded test data are presented in this appendix. The following data are copies of plotted data provided by the Eglin AFB Computer Sciences Laboratory. The data are presented as recorded, and although it is recognized that much of the data shown in this section did not prove to be suitable for the analysis of the phenomenon under investigation, it was all utilized for the analysis of the beam response.

As many as 23 channels of pressure, load, strain, and accelerometer data were recorded during the impulse tests. These data were recorded as analog signals and later converted to discrete digital data. The data are available in three forms: (1) computer printout listings; (2) computer-generated plots; and (3) computer data tapes. The location and channel notations of the various instruments are shown schematically in Figure A-1. The figure is a top view of the beam and its two support mechanisms. It shows locations of: (1) the load cells; (2) accelerometers on the bottom surfaces of the beam and beam support axles; (3) steel strain gages; (4) concrete strain gages; and (5) pressure transducers at three locations on the top surface of the test fixture and at one location within the test frame cavity.

The data are stored on three tapes with the Oklahoma State University Computer Center, Serial Nos. T6528, T9090, and T6530 with 114, 180, and 10 files, respectively. The tapes are nine track, 1600 bpi in IBM 360 format.

The plotted data are presented in Figures A-2 through A-12. These are copies of figures which were produced by the Eglin AFB Computer Sciences Laboratory.

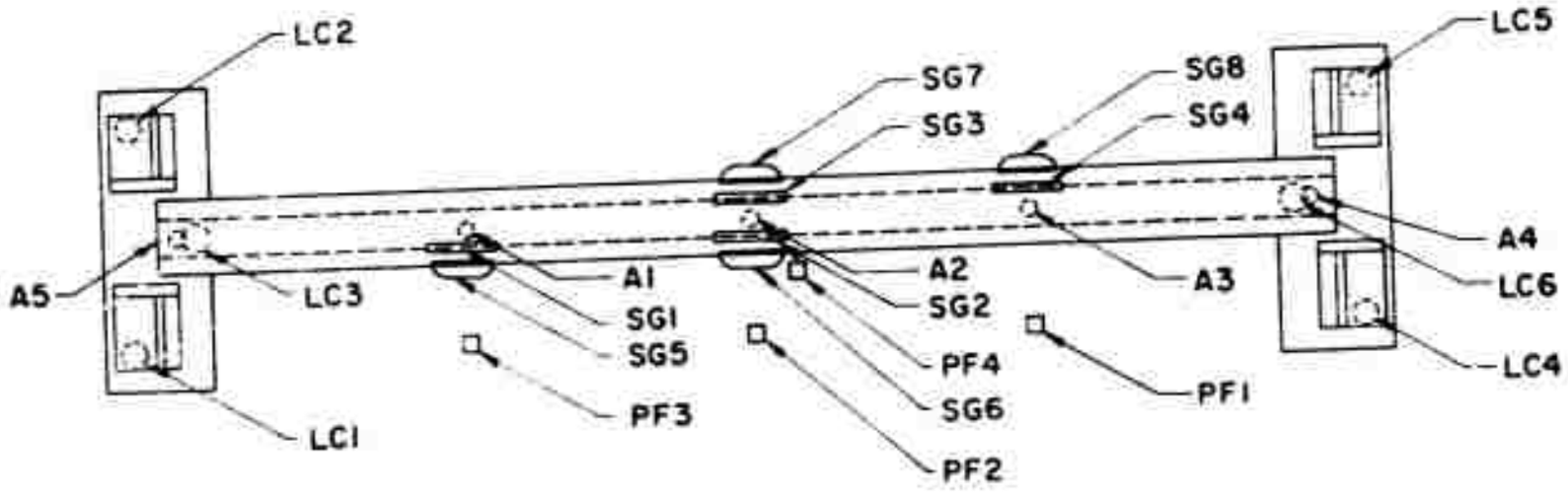

○ LOAD CELLS BENEATH BEAM SUPPORT MECHANISM, LC1 - LC6

o ACCELEROMETERS; A1, A2, A3 ON BEAM BOTTOM SURFACE; A4, A5 ON BEAM AXLES, A

⌓ CONCRETE STRAIN GAGE; ON BEAM SIDE, SG5 - SG8

▭ STEEL STRAIN GAGE; ON REINFORCING STEEL, SG1 - SG4

□ PRESSURE TRANSDUCER; PF1 - PF3 ON TOP STEEL COVER; PF4 IN TEST FIXTURE CAVITY

Figure A-1. Schematic of Instrumentation Location and Data Channel Notation

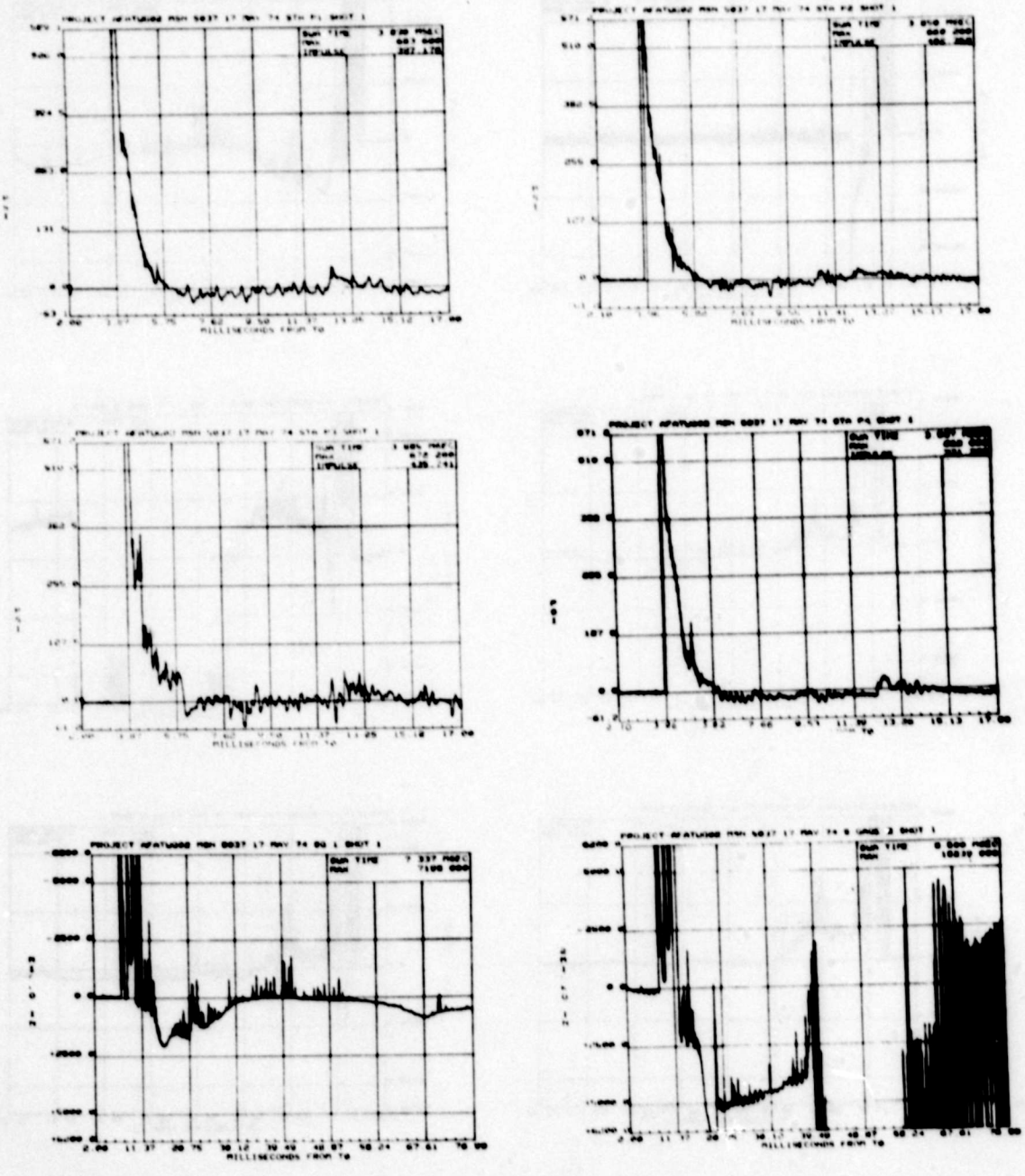

Figure A-2. Data From Impulse Test No. 1, Beam 15, 17 May 1974

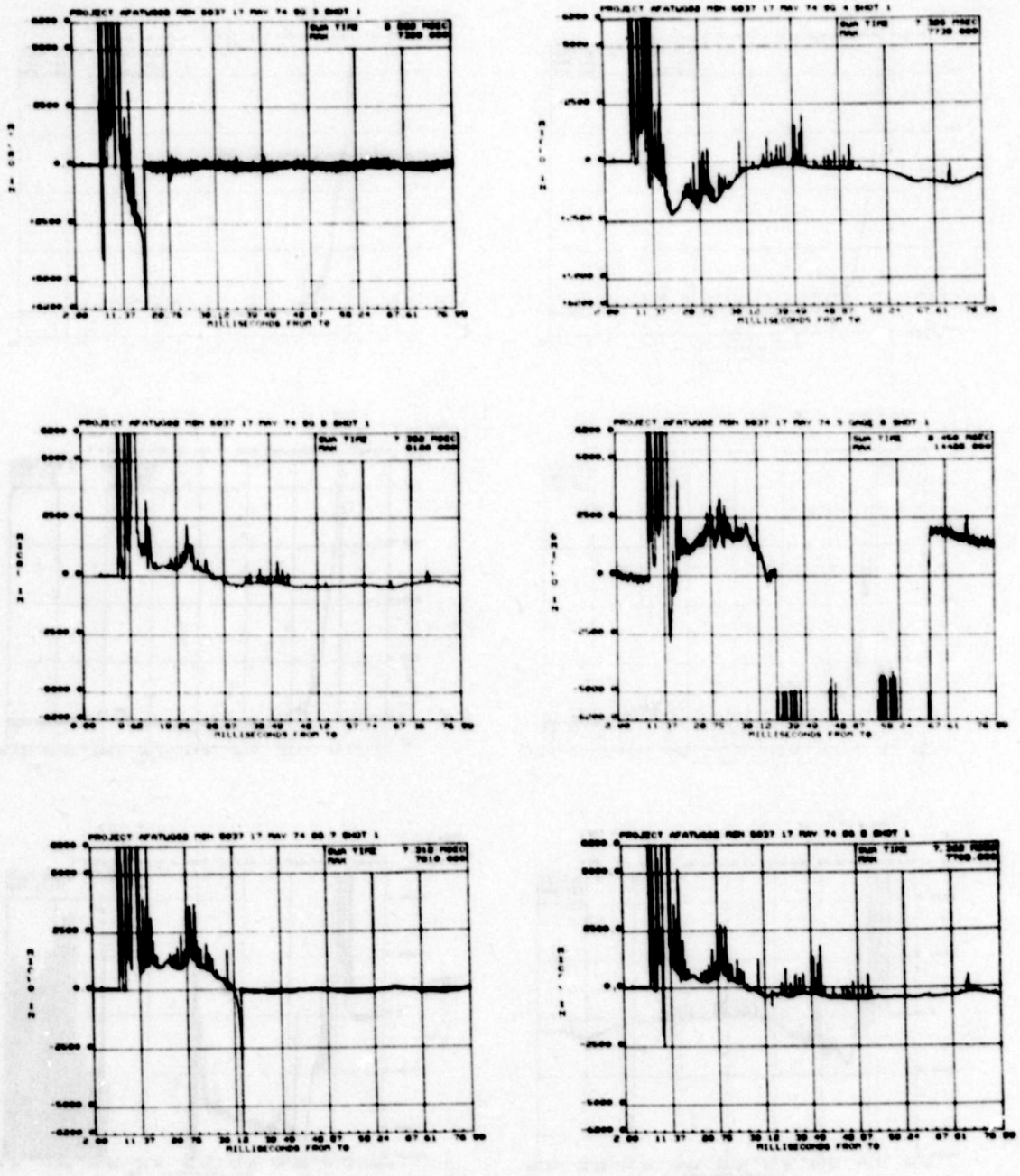

Figure A-2. Data From Impulse Test No. 1, Beam 15, 17 May 1974 (Continued)

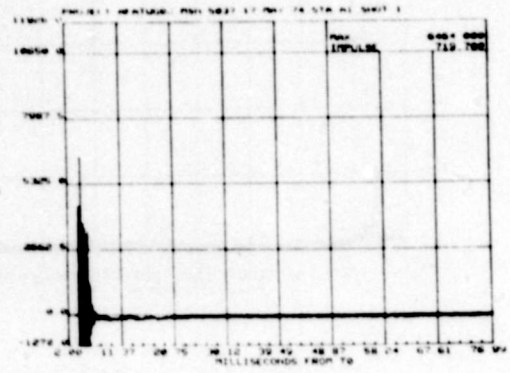

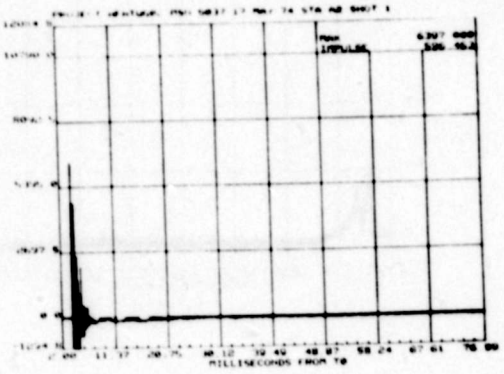

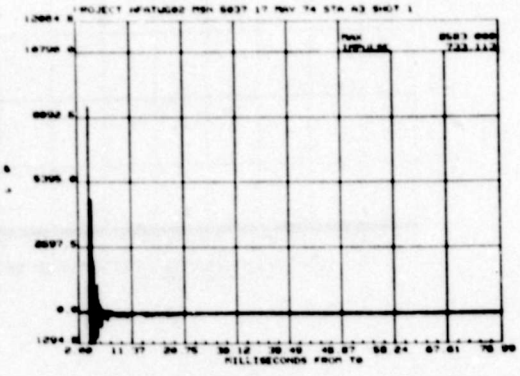

Figure A-2. Data From Impulse Test No. 1, Beam 15, 17 May 1974 (Concluded)

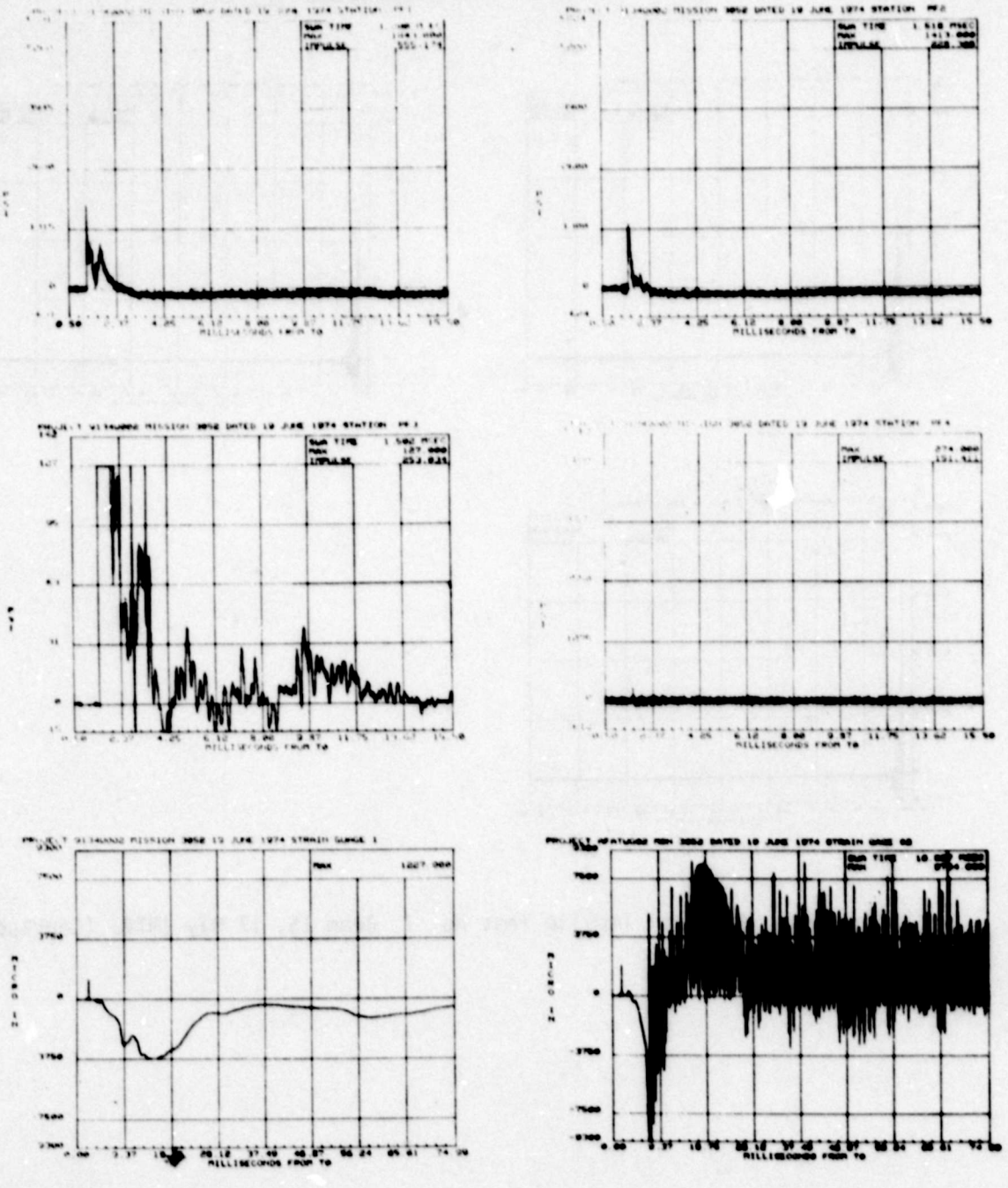

Figure A-3. Data From Impulse Test No. 3, Beam 12, 19 June 1974

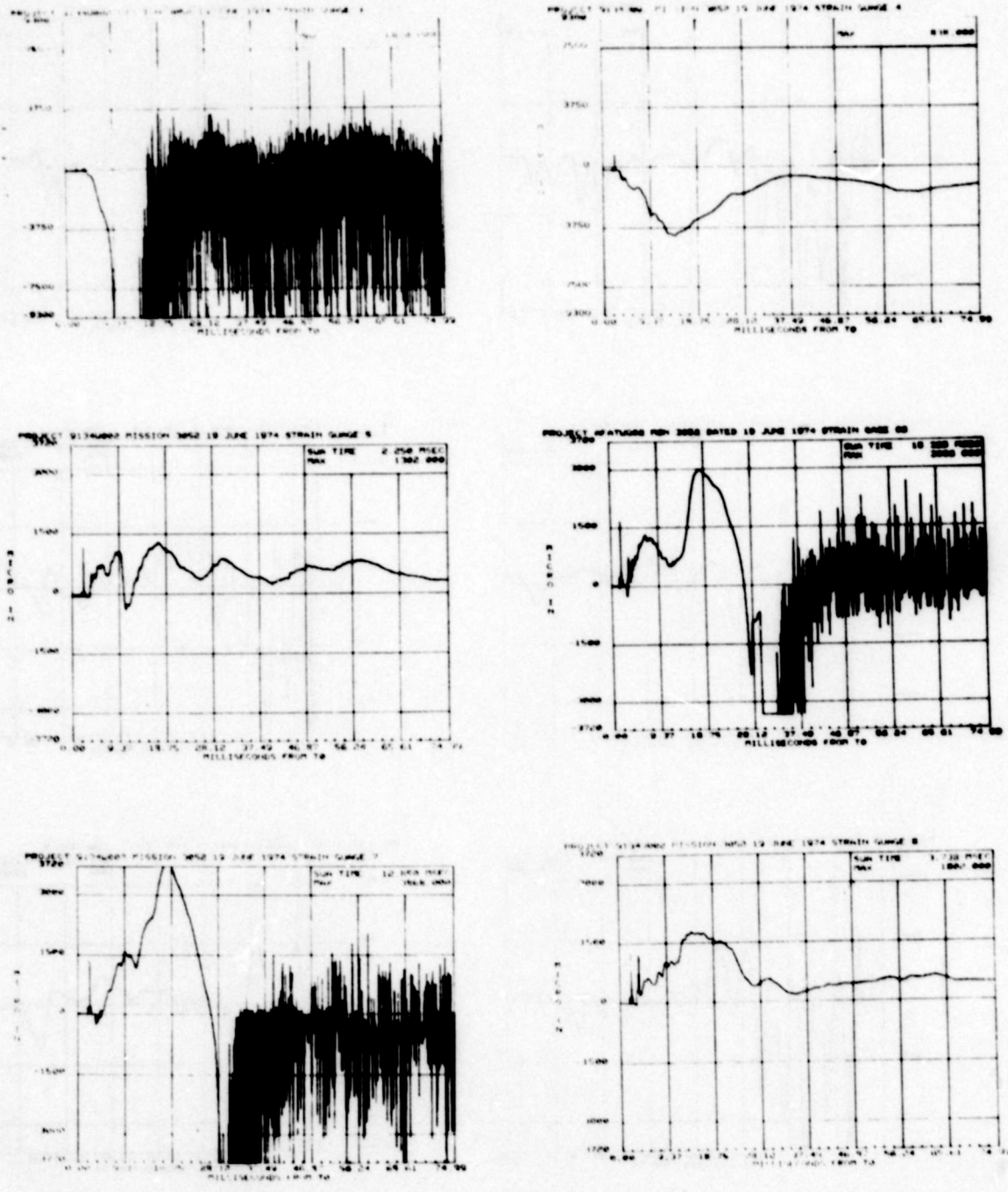

Figure A-3. Data From Impulse Test No. 3, Beam 12, 19 June 1974 (Continued)

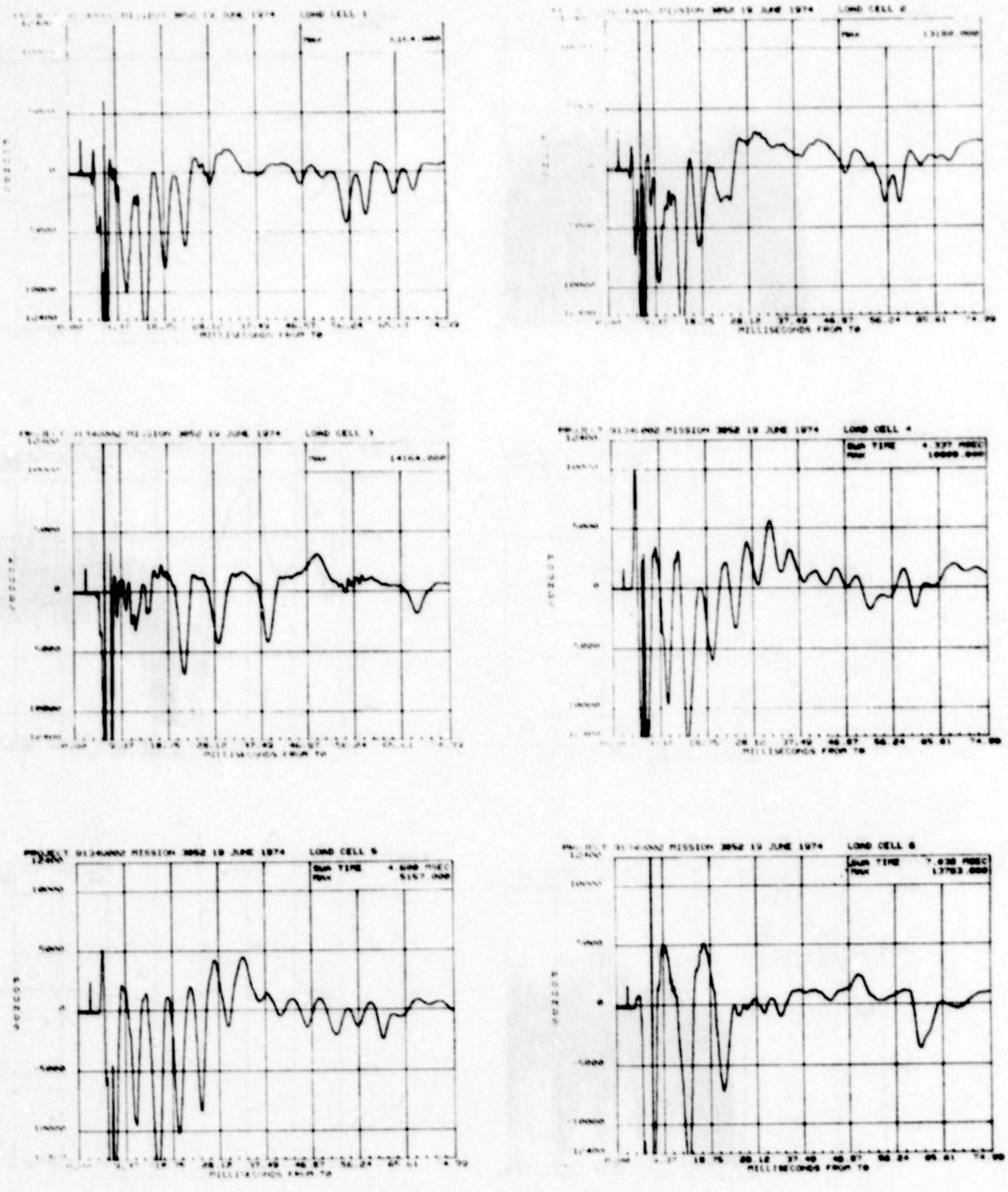

Figure A-3. Data From Impulse Test No. 3, Beam 12, 19 June 1974 (Continued)

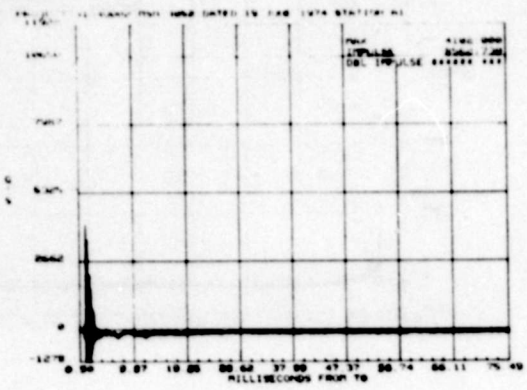

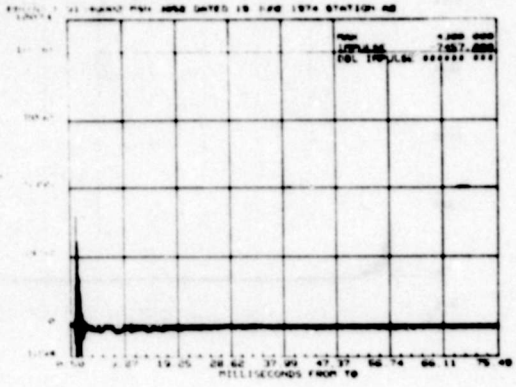

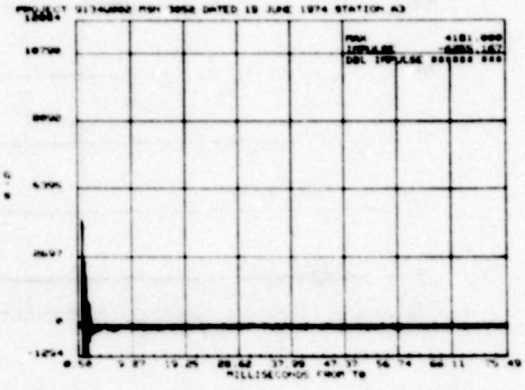

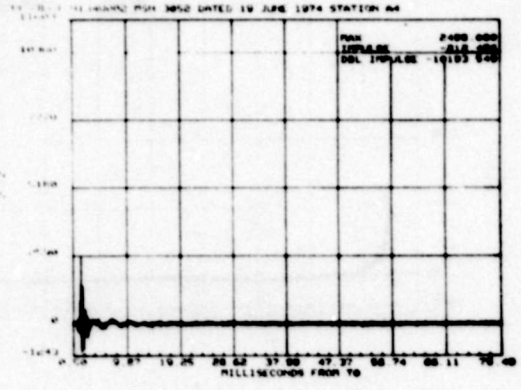

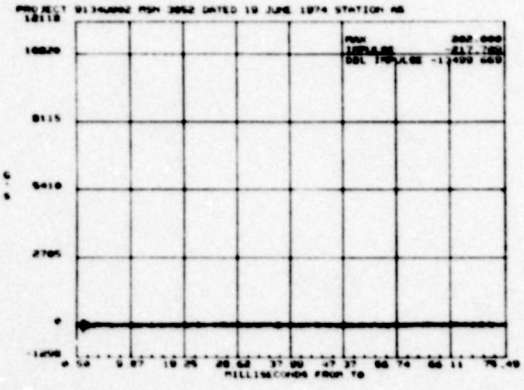

Figure A-3. Data From Impulse Test No. 3, Beam 12, 19 June 1974 (Concluded)

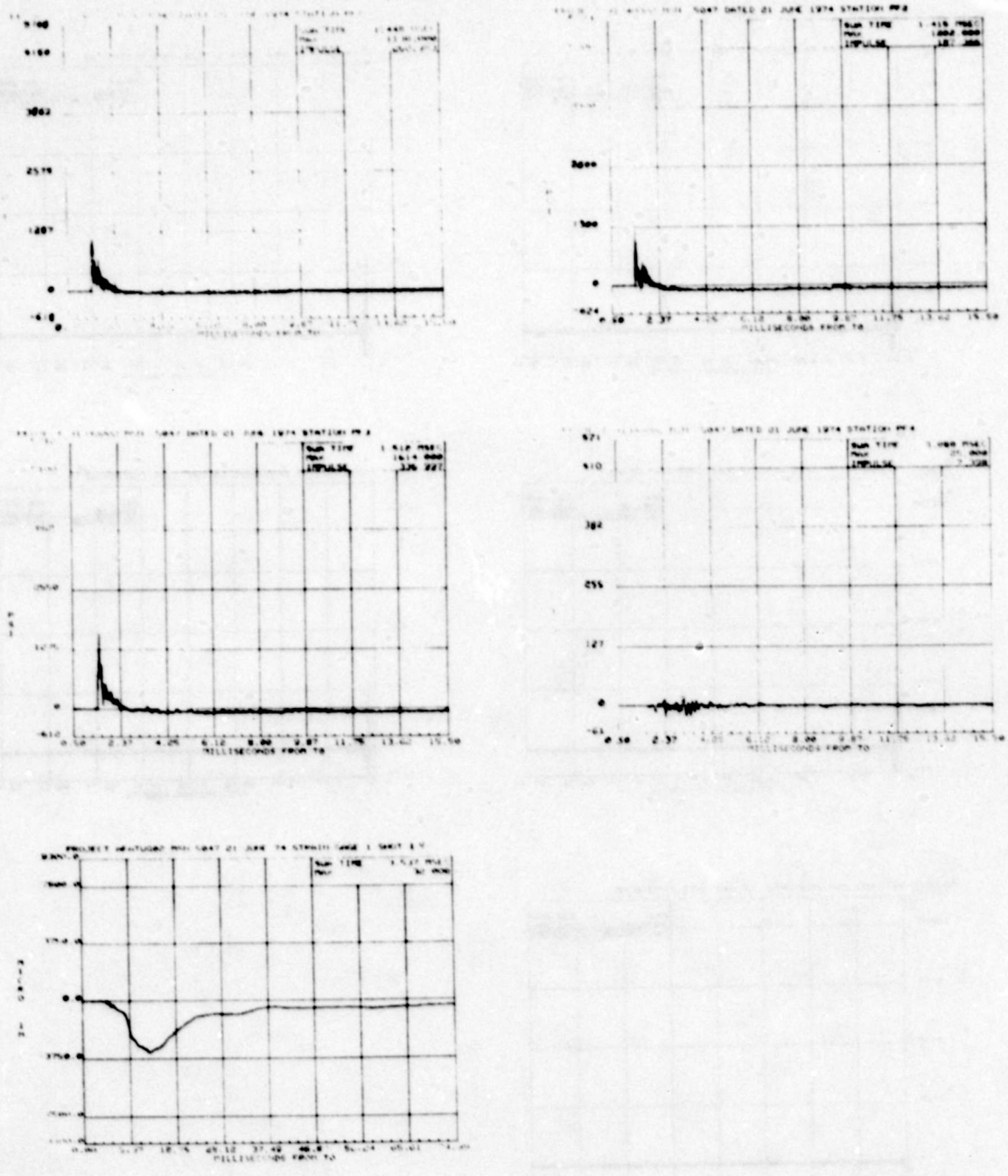

Figure A-4. Data From Impulse Test No. 4, Beam 4, 21 June 1974

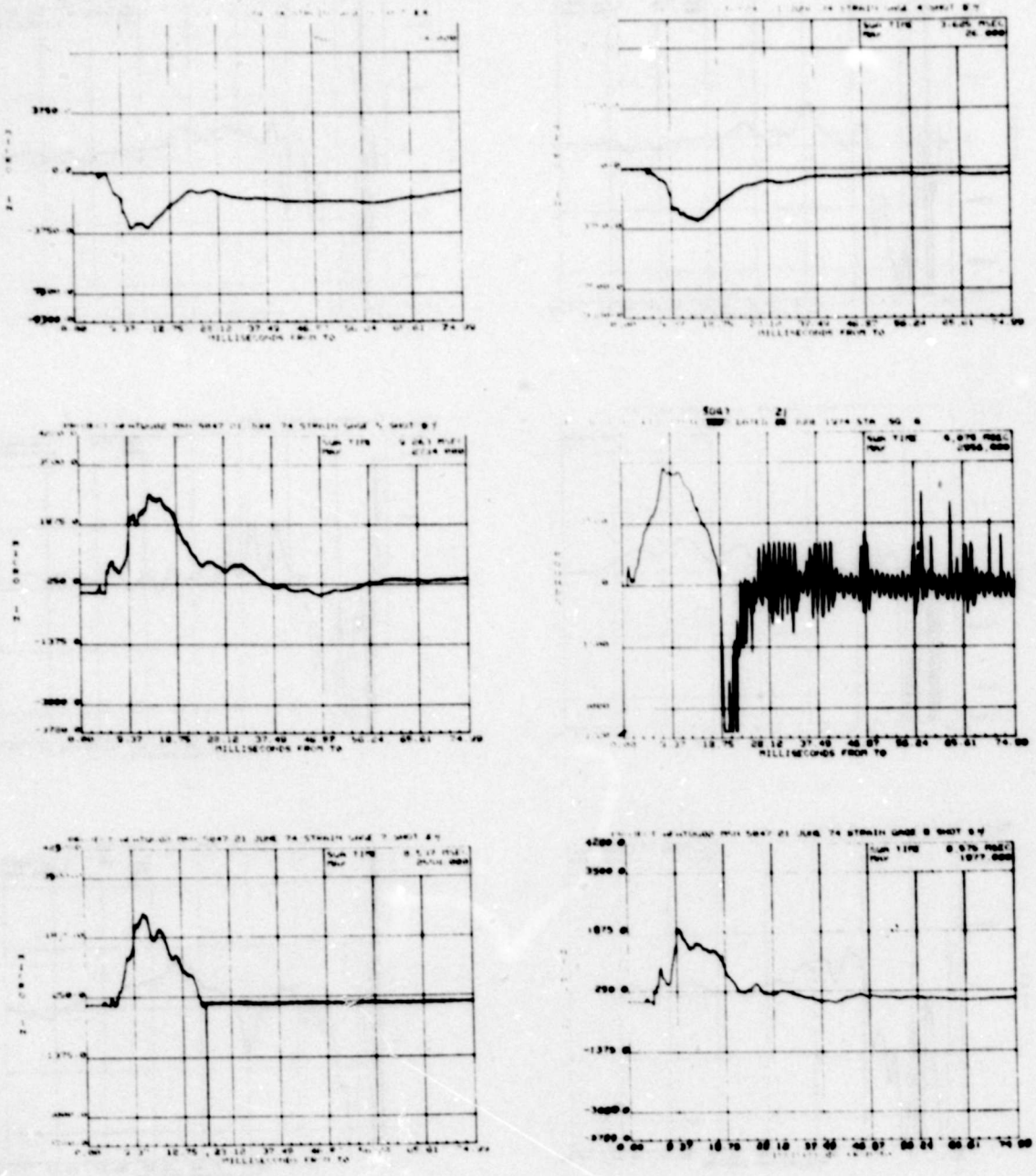

Figure A-4. Data From Impulse Test No. 4, Beam 4, 21 June 1974 (Continued)

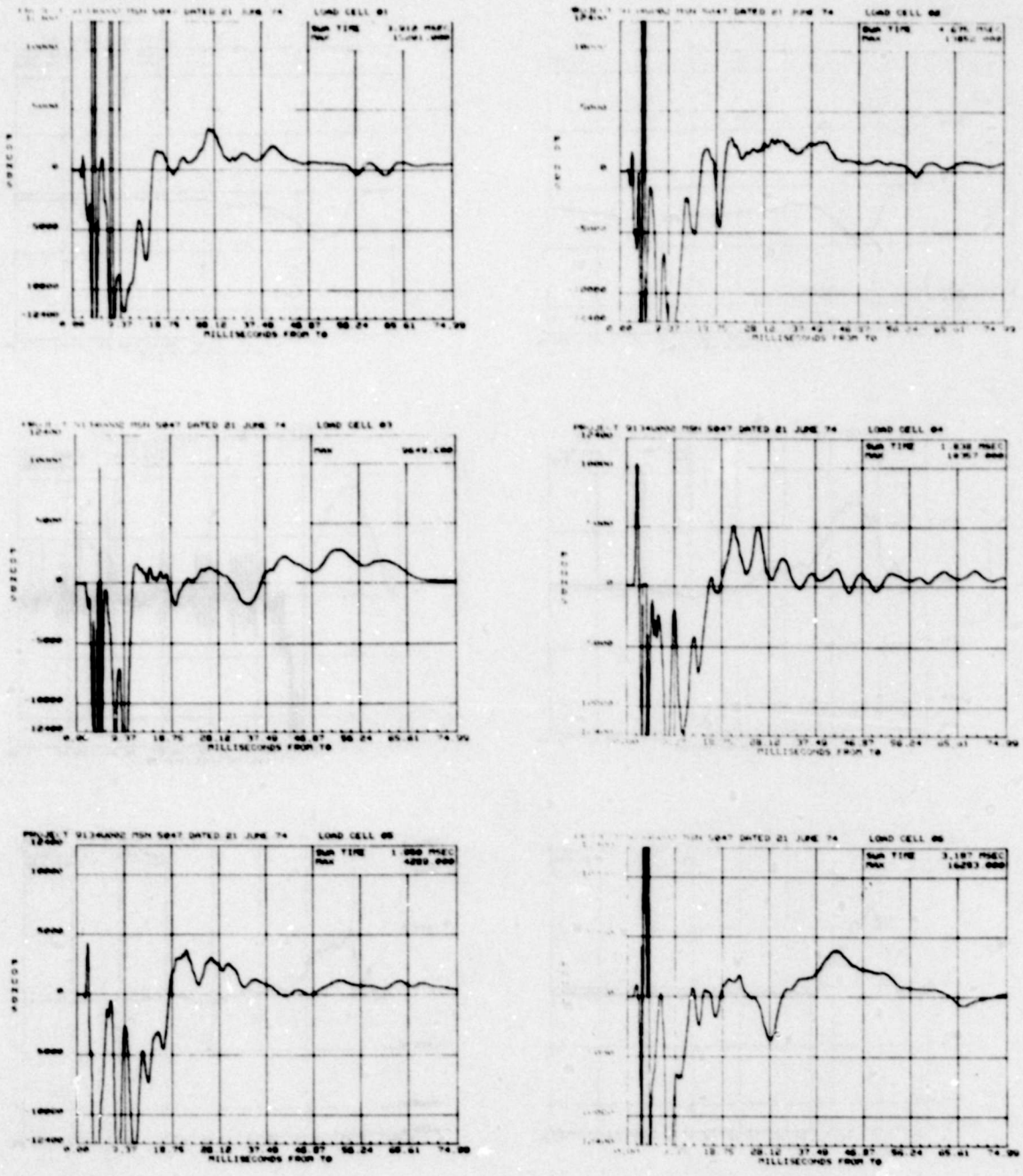

Figure A-4. Data From Impulse Test No. 4, Beam 4, 21 June 1974 (Continued)

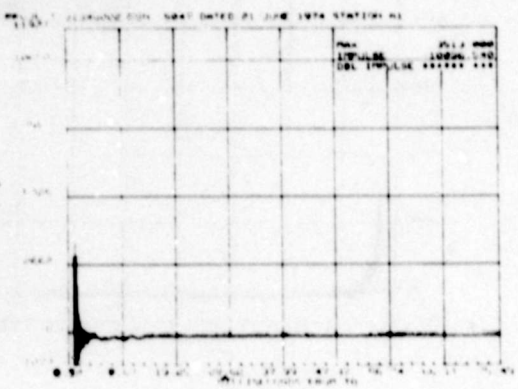

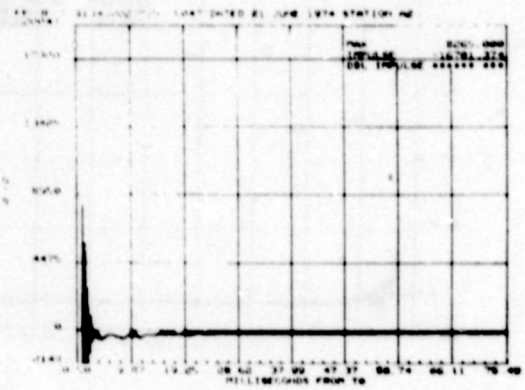

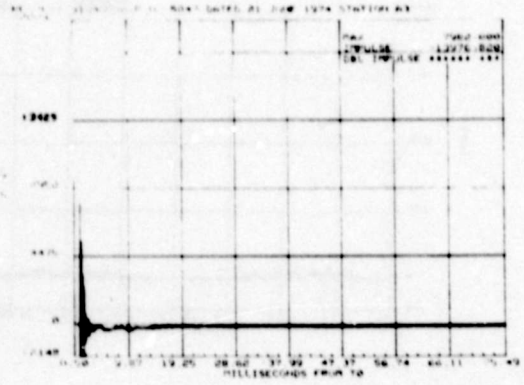

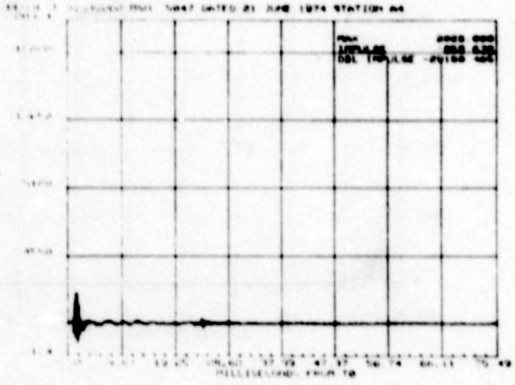

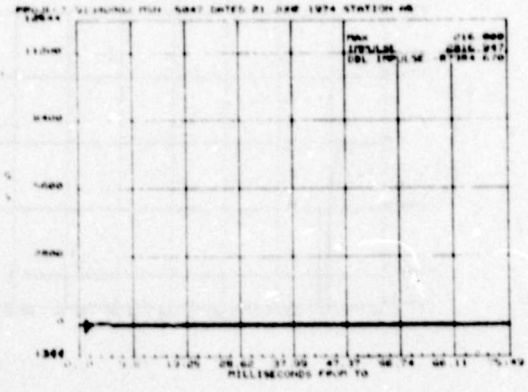

Figure A-4. Data From Impulse Test No. 4, Beam 4, 21 June 1974 (Concluded)

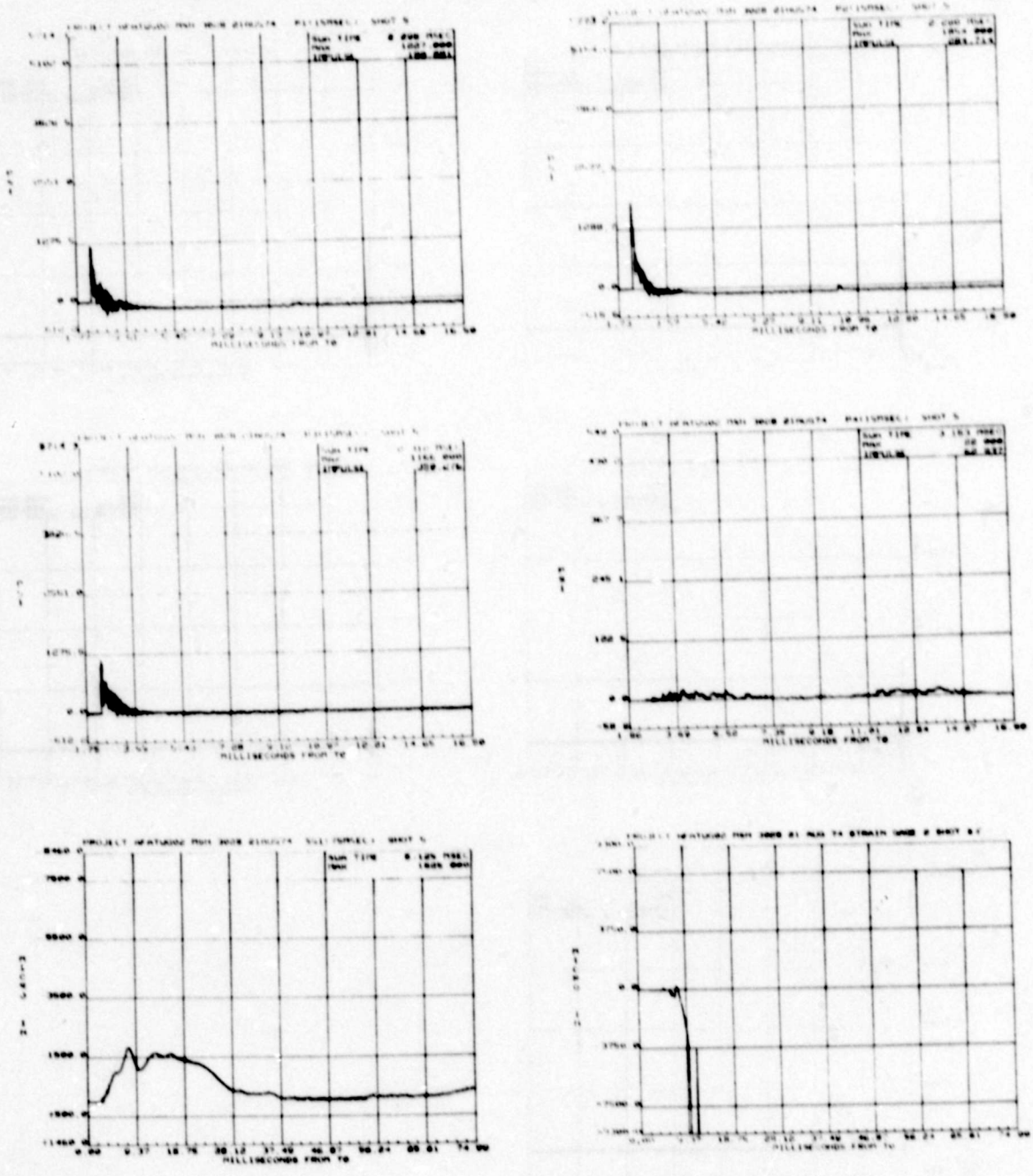

Figure A-5. Data From Impulse Test No. 5, Beam 10, 21 August 1974

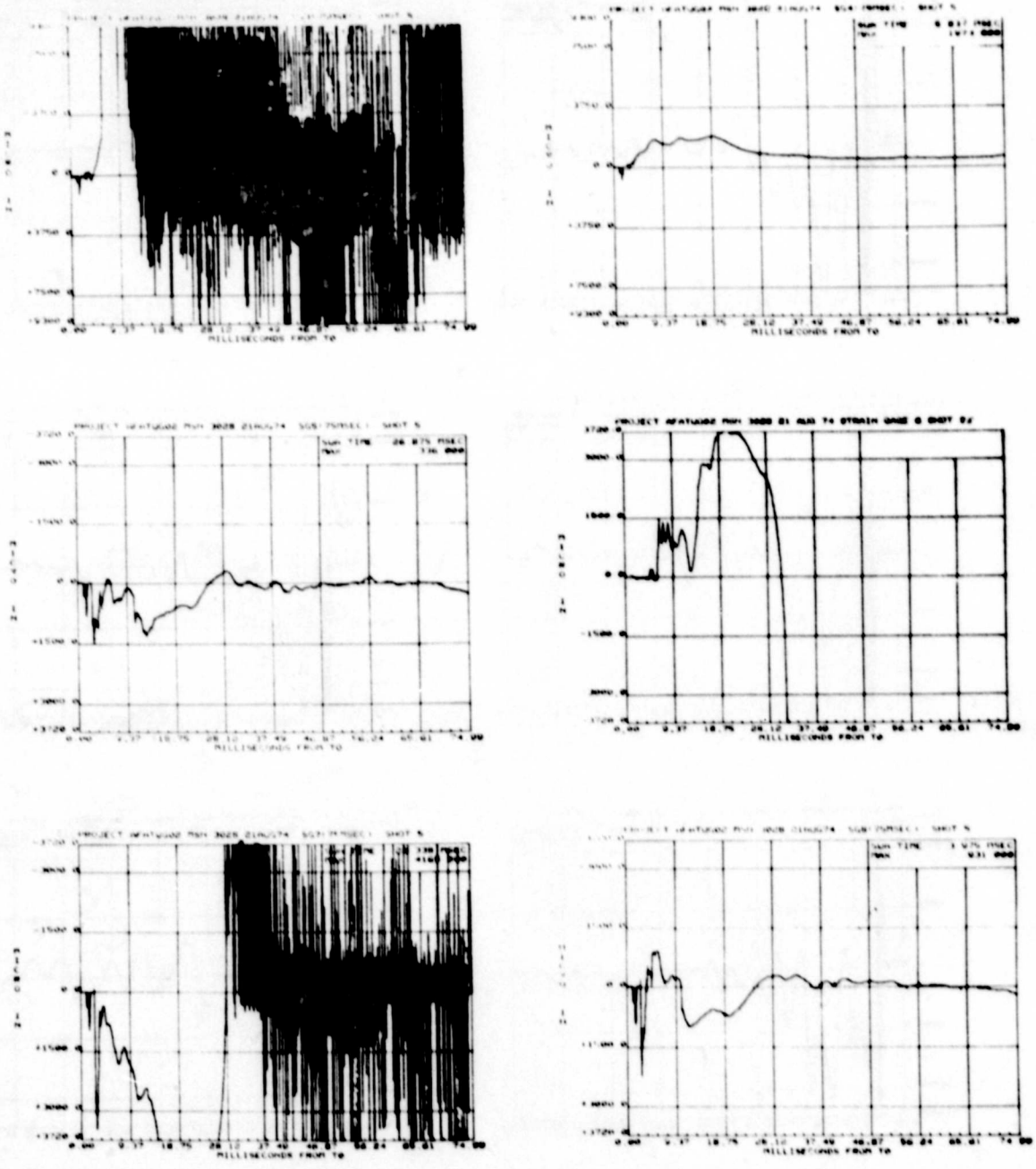

Figure A-5. Data From Impulse Test No. 5, Beam 10, 21 August 1974 (Continued)

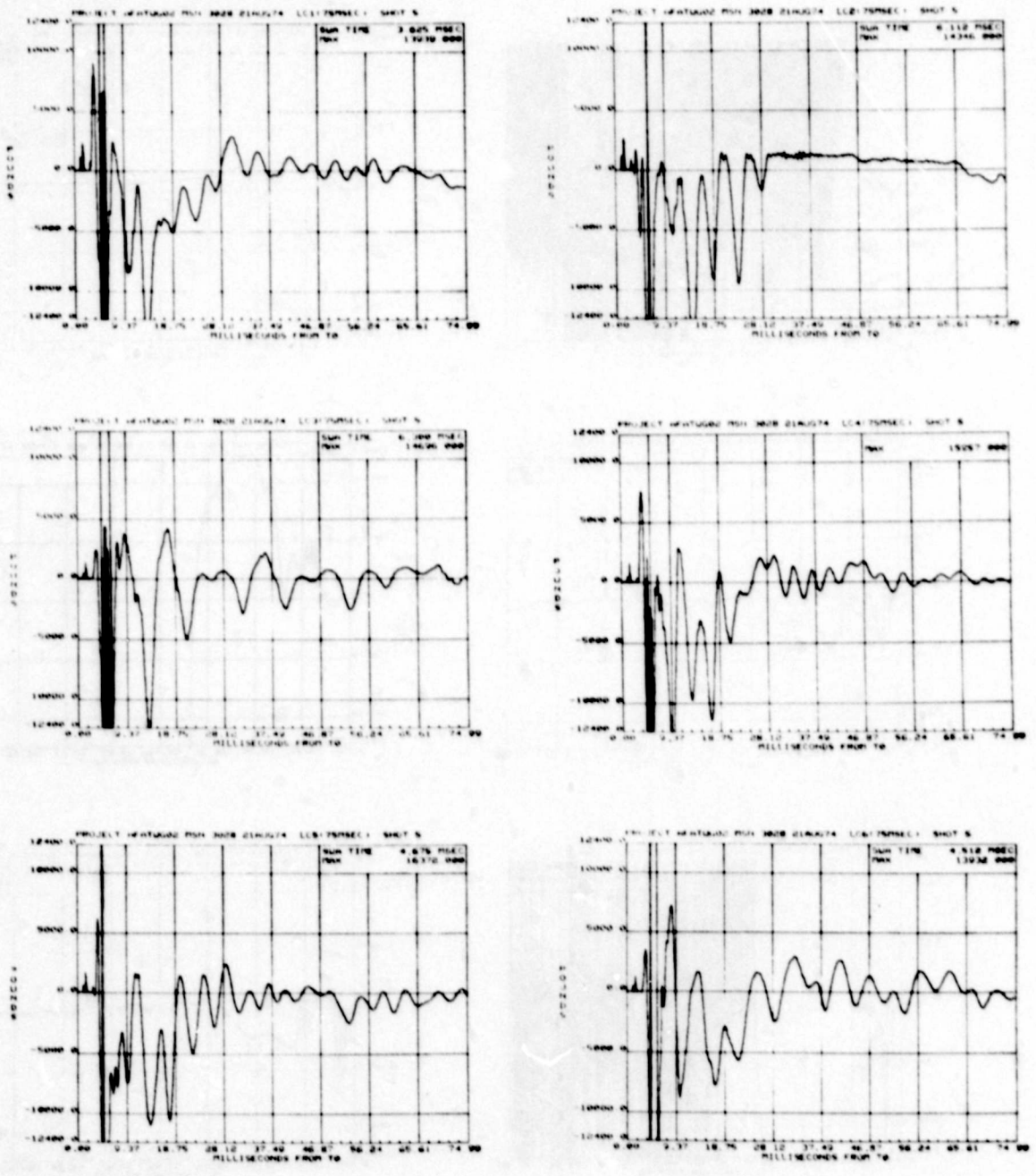

Figure A-5. Data From Impulse Test No. 5, Beam 10, 21 August 1974 (Continued)

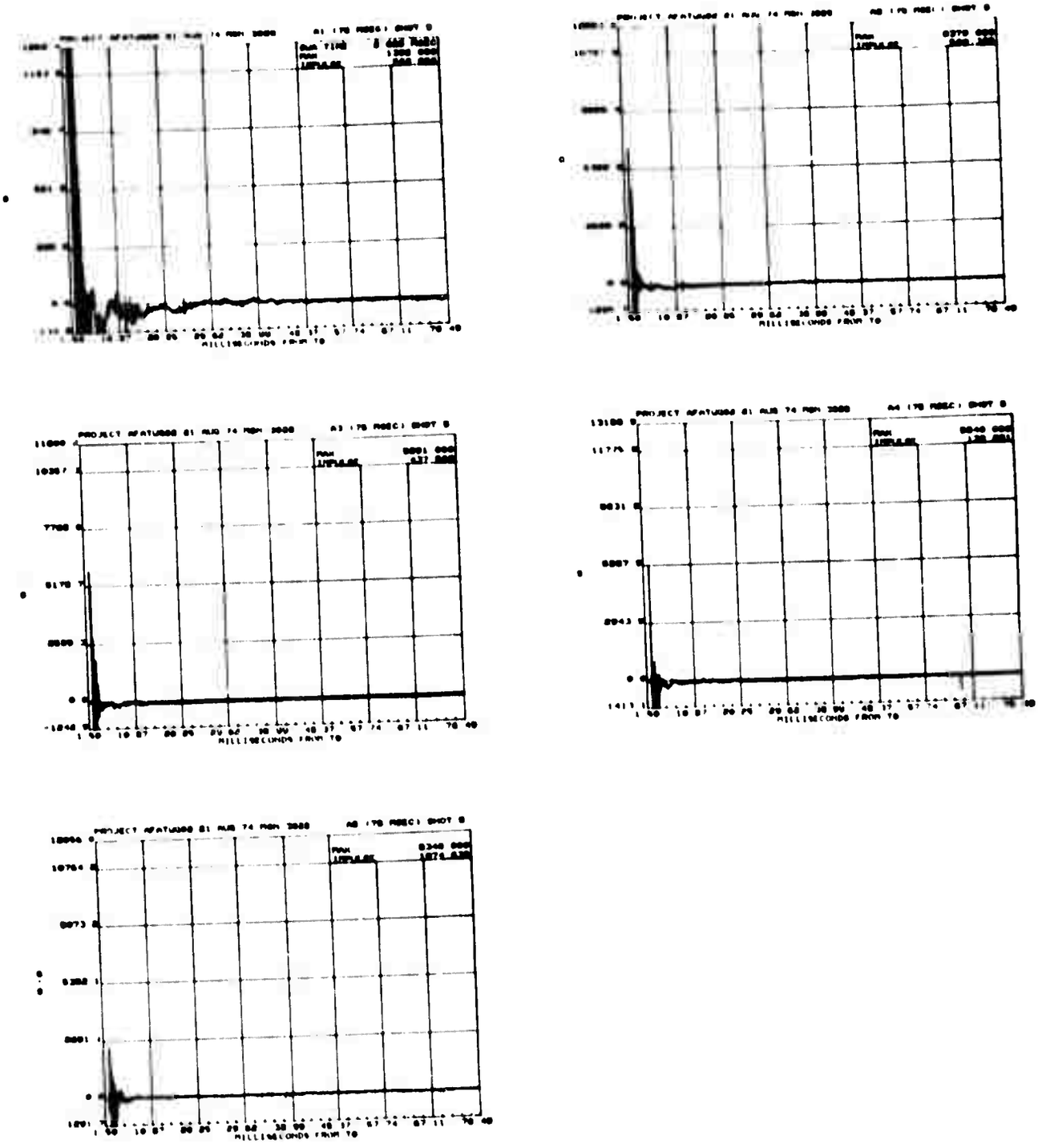

Figure A-5. Data From Impulse Test No. 5, Beam 10, 21 August 1974 (Concluded)

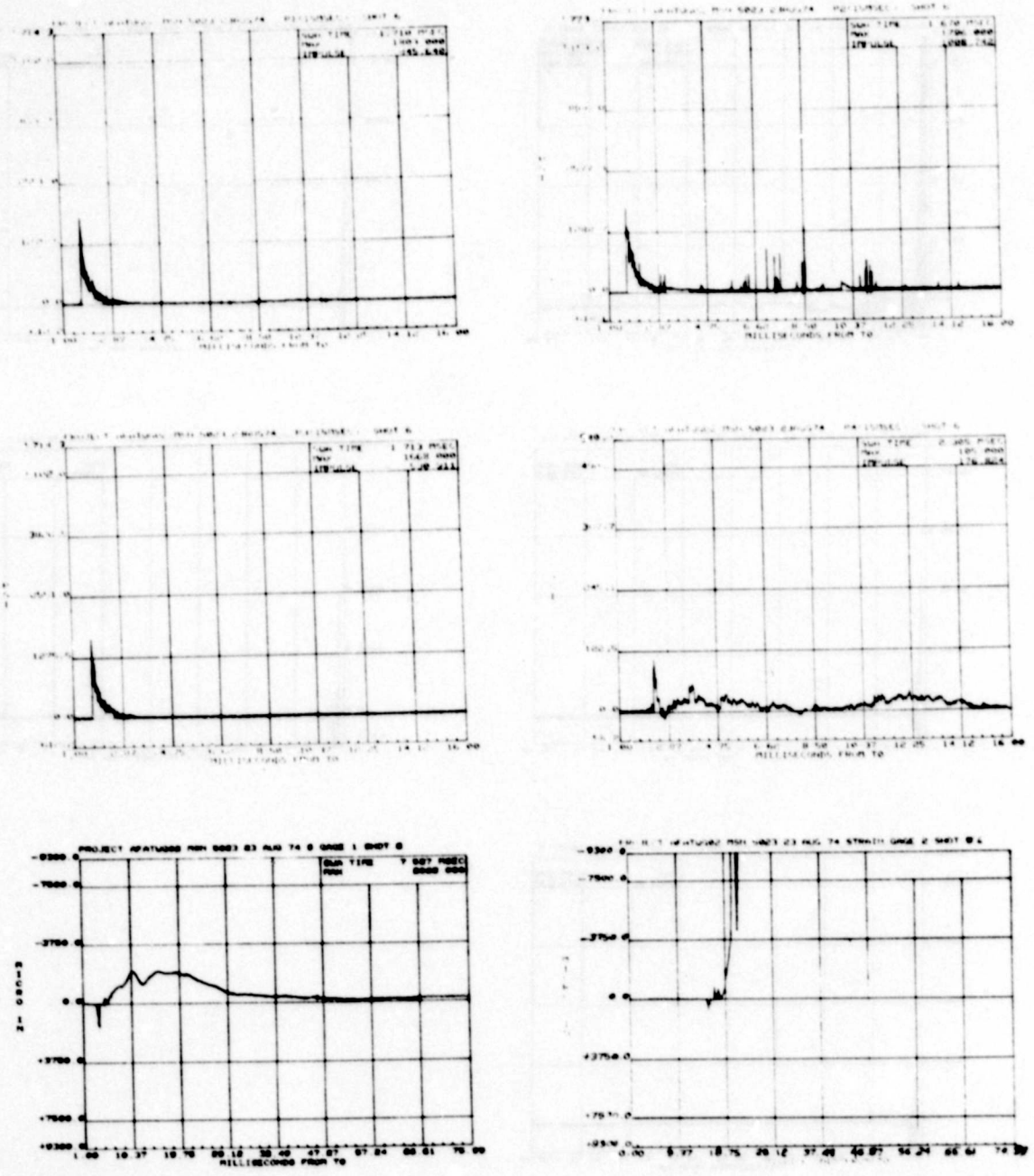

Figure A-6. Data From Impulse Test No. 6, Beam 8, 23 August 1974

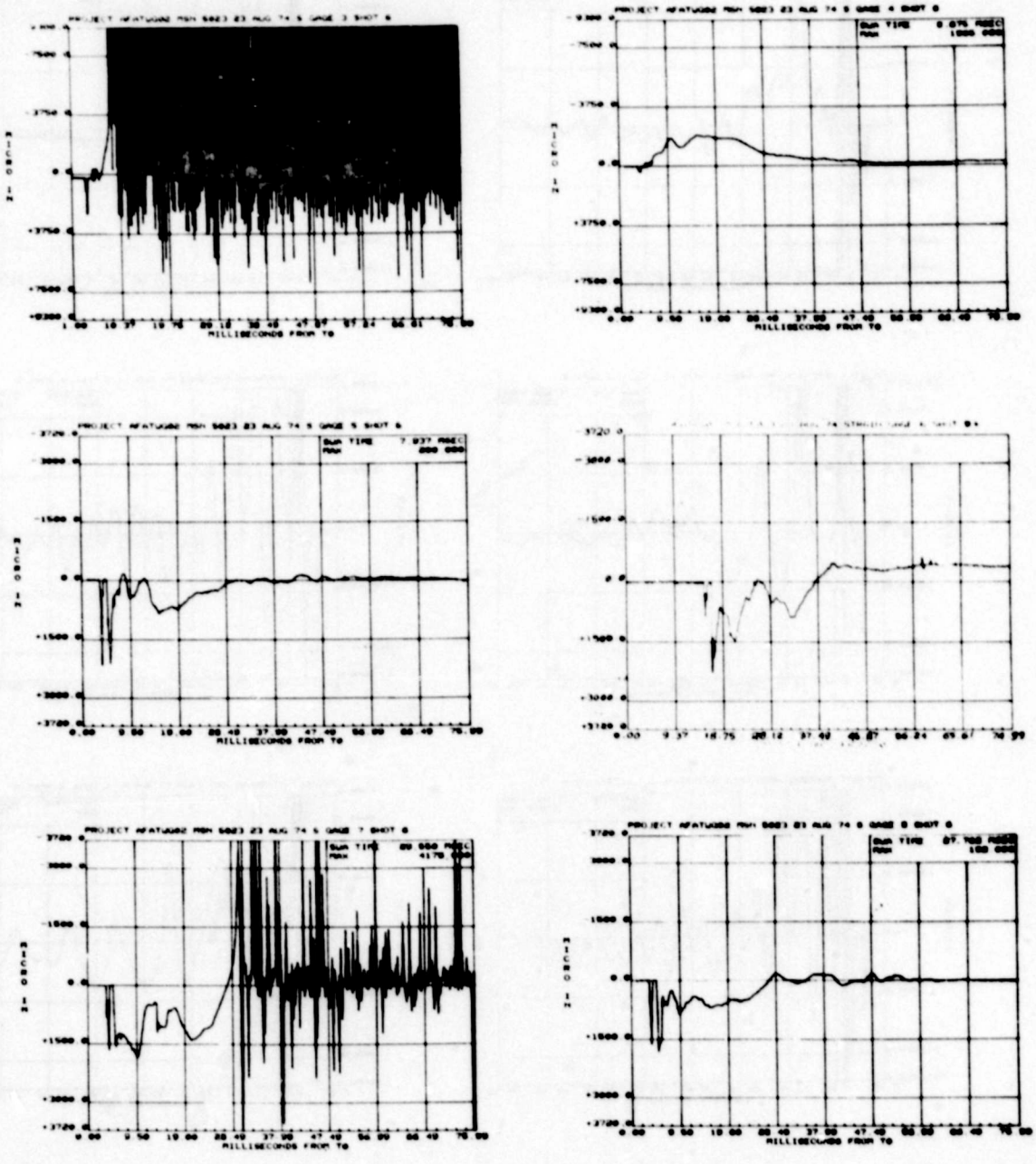

Figure A-6. Data From Impulse Test No. 6, Beam 8, 23 August 1974 (Continued)

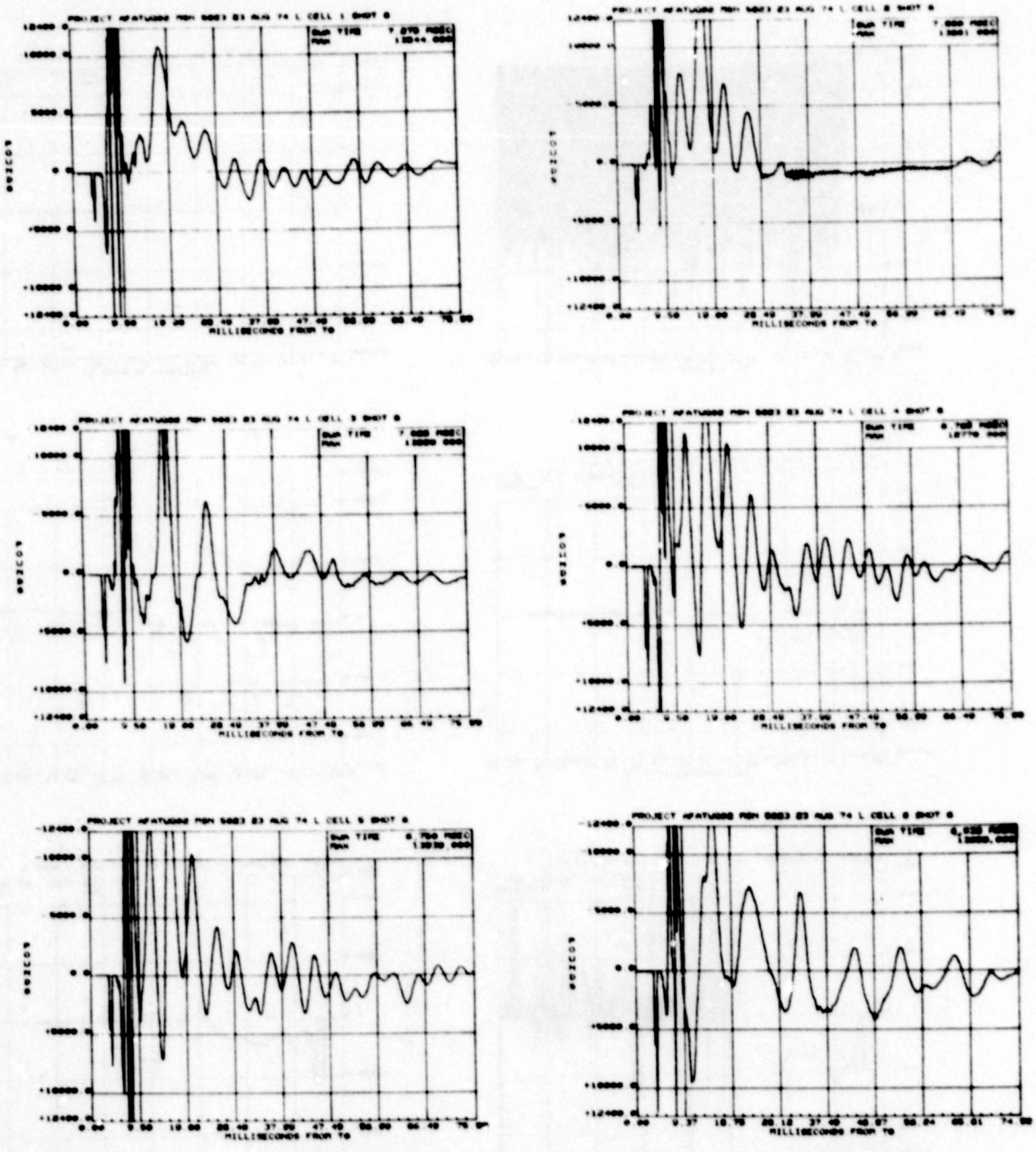

Figure A-6. Data From Impulse Test No. 6, Beam 8, 23 August 1974 (Continued)

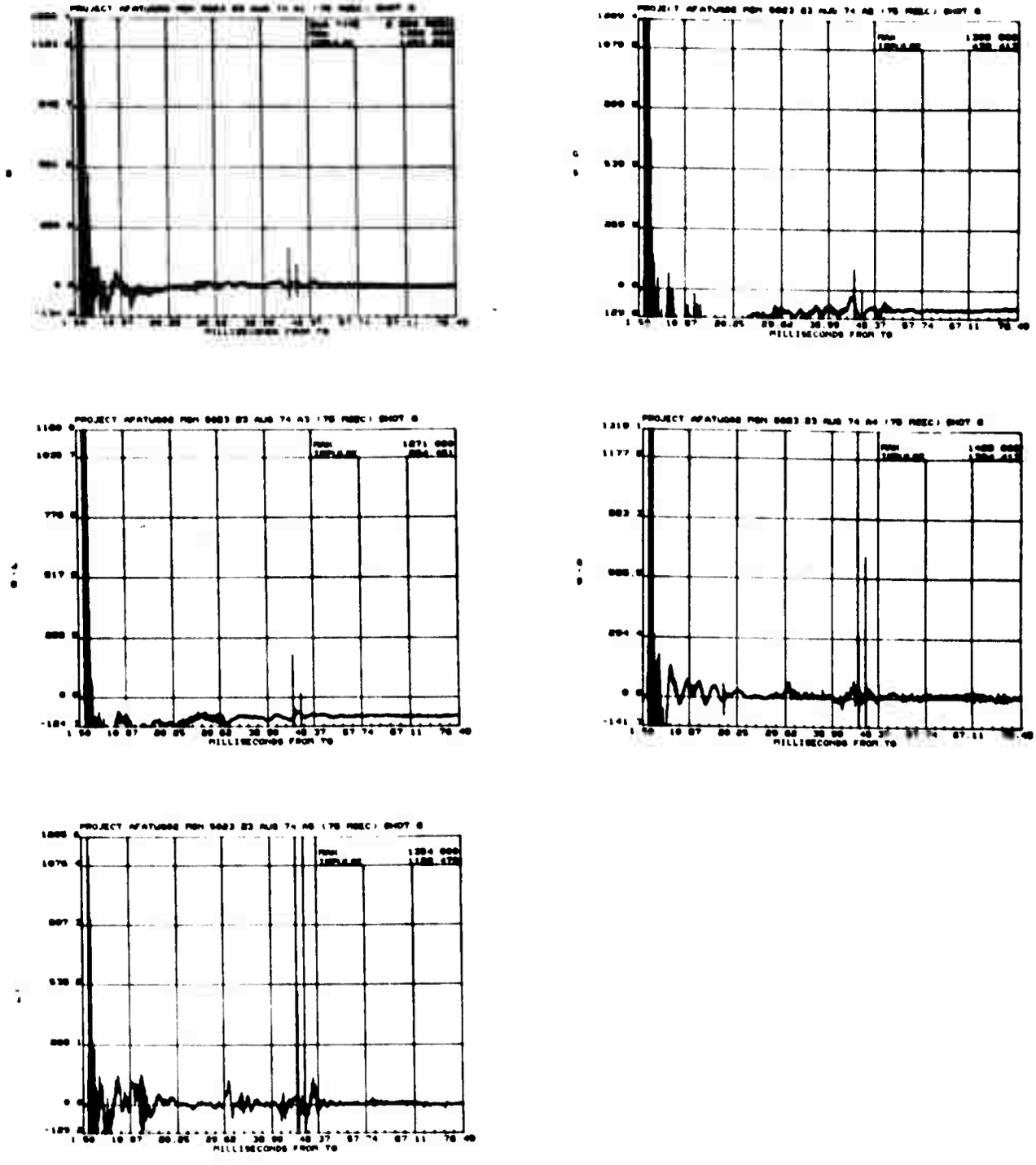

Figure A-6. Data From Impulse Test No. 6, Beam 8, 23 August 1974 (Concluded)

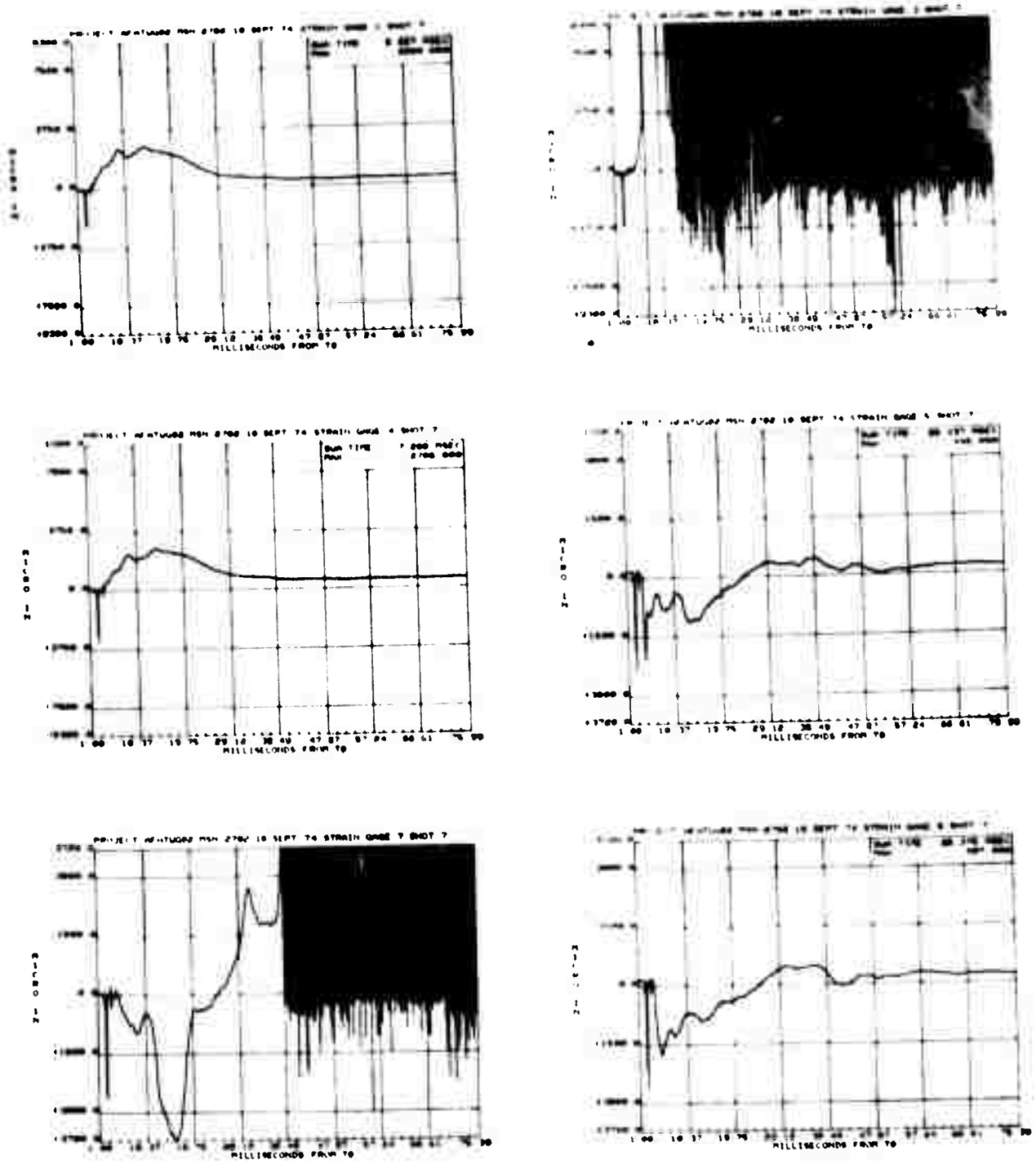

Figure A-7. Data From Impulse Test No. 7, Beam 3, 10 September 1974

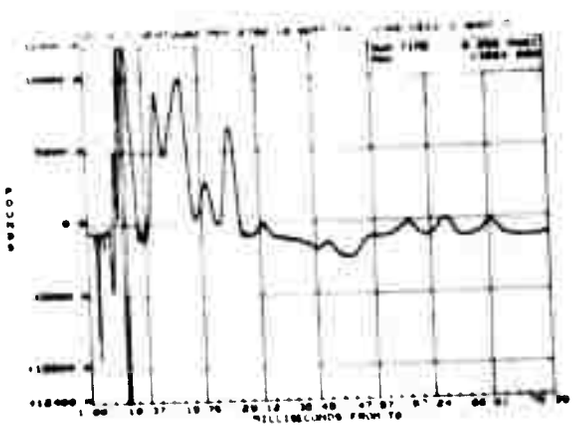

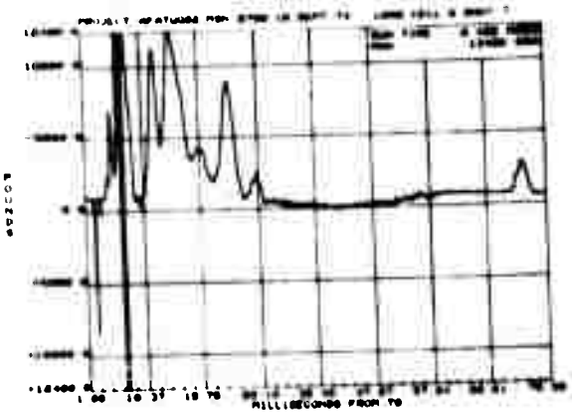

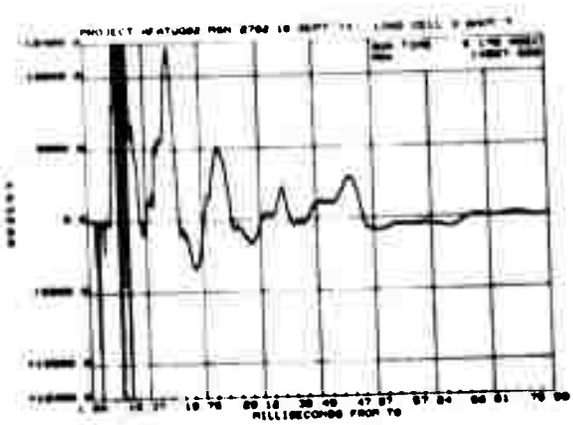

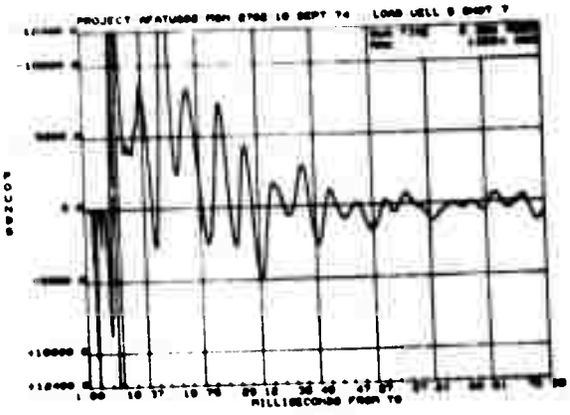

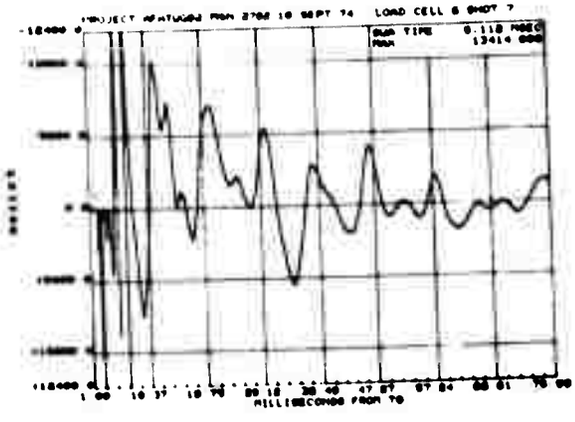

Figure A-7. Data From Impulse Test No. 7, Beam 3, 10 September 1974 (Concluded)

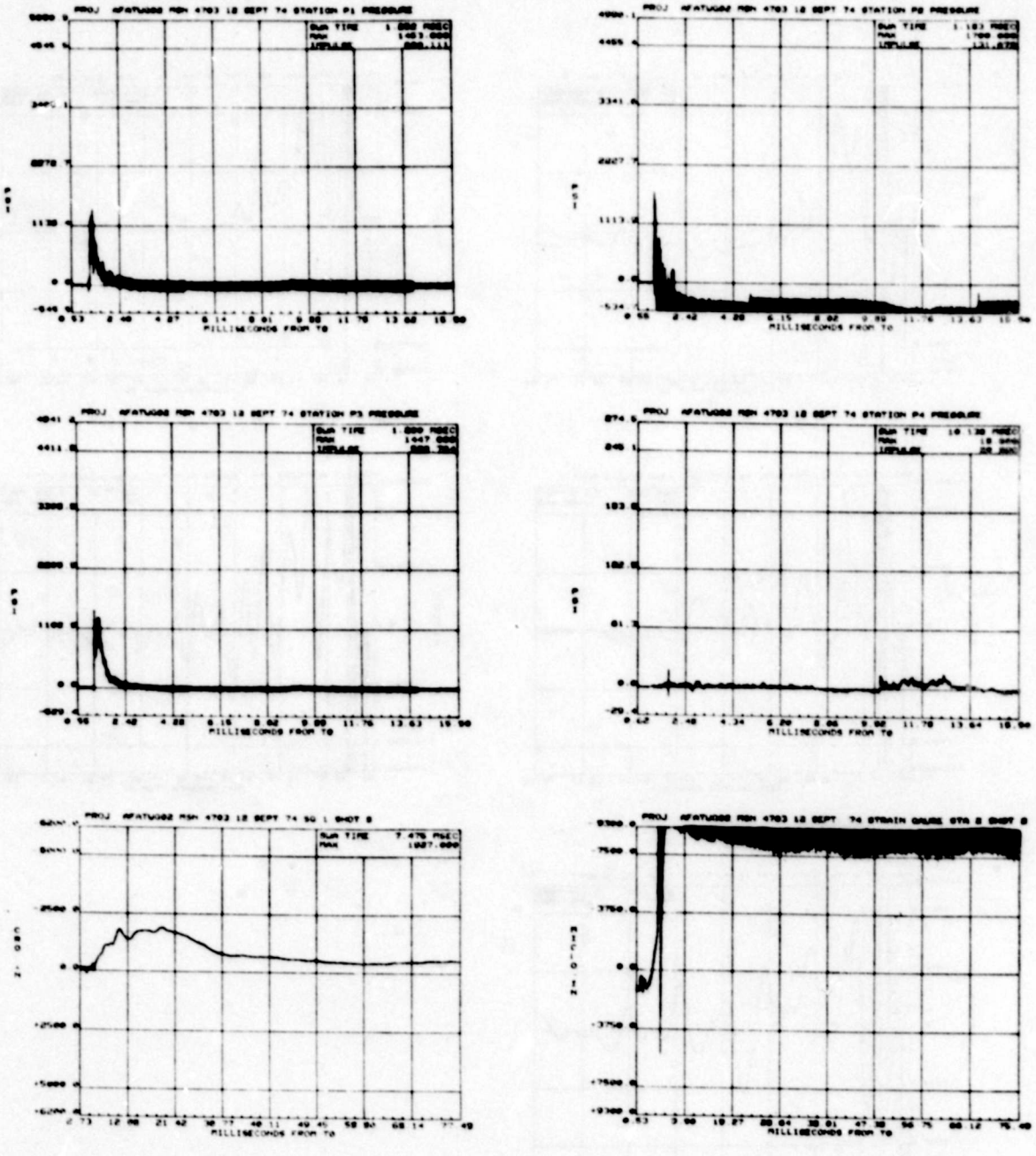

Figure A-8. Data From Impulse Test No. 8, Beam 2, 12 September 1974

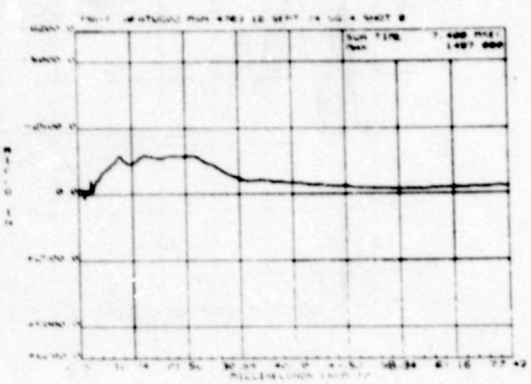

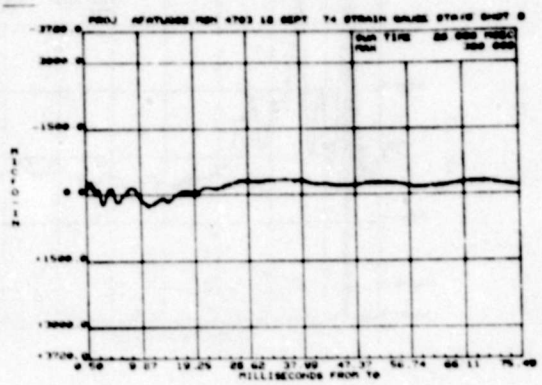

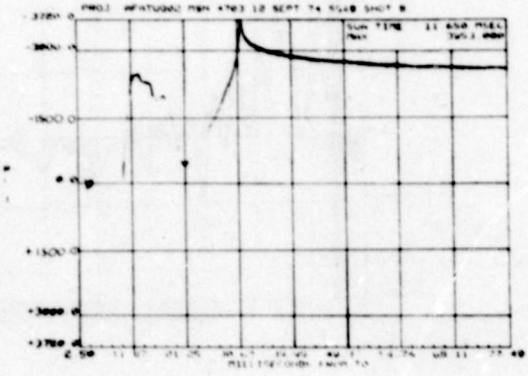

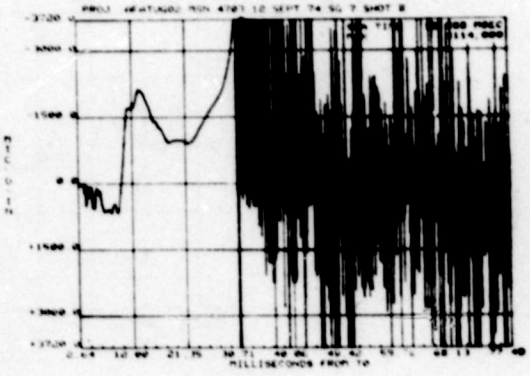

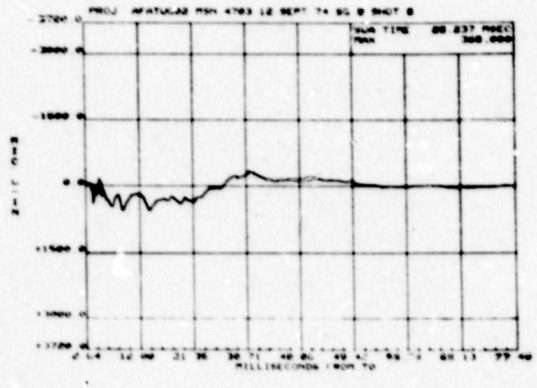

Figure A-8. Data From Impulse Test No. 8, Beam 2, 12 September 1974 (Continued)

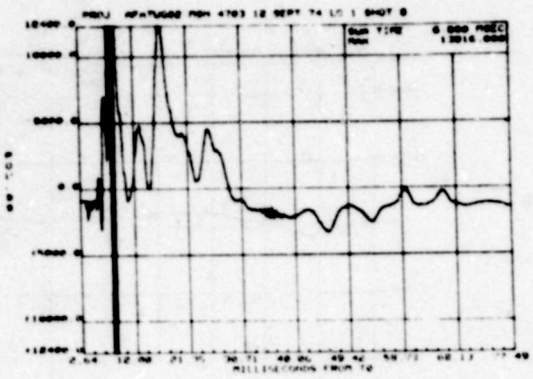

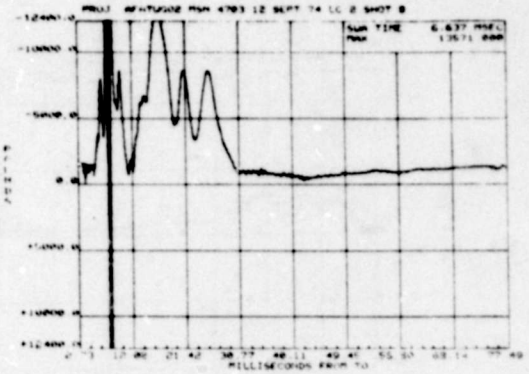

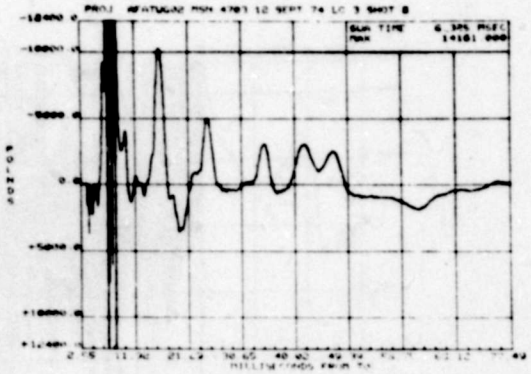

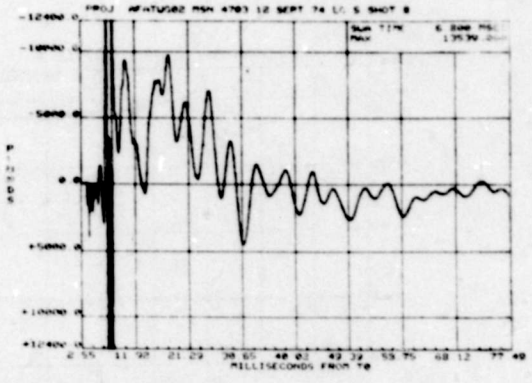

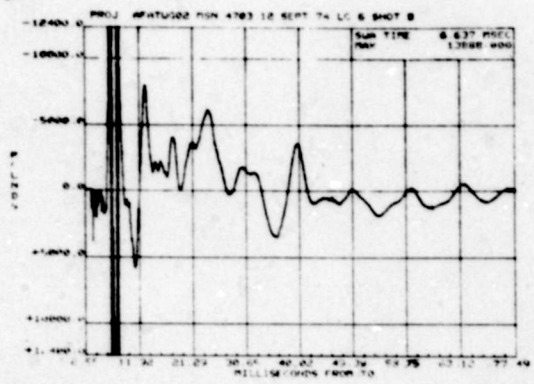

Figure A-8. Data From Impulse Test No. 8, Beam 2, 12 September 1974 (Continued)

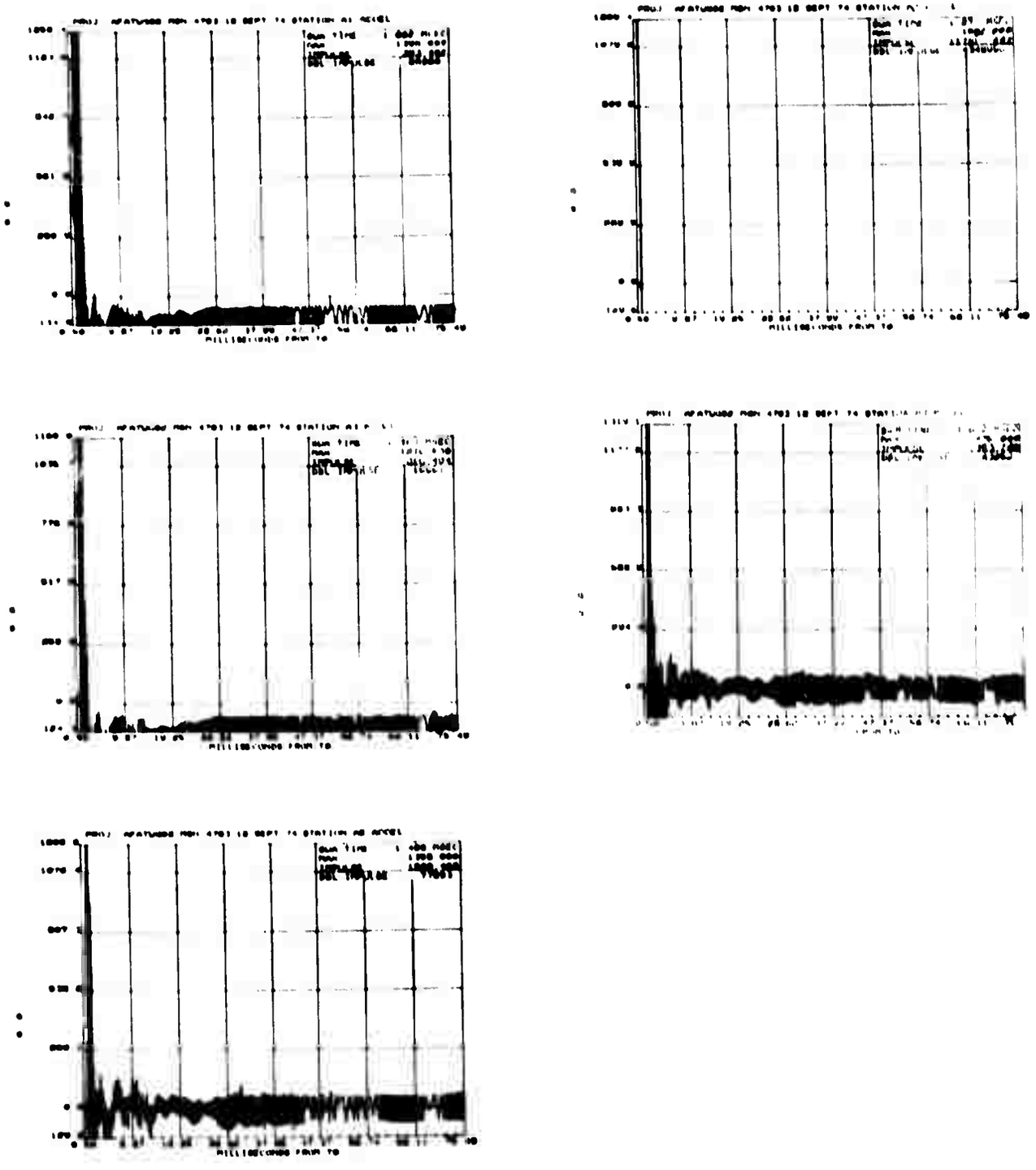

Figure A-8. Data From Impulse Test No. 8, Beam 2, 12 September 1974 (Concluded)

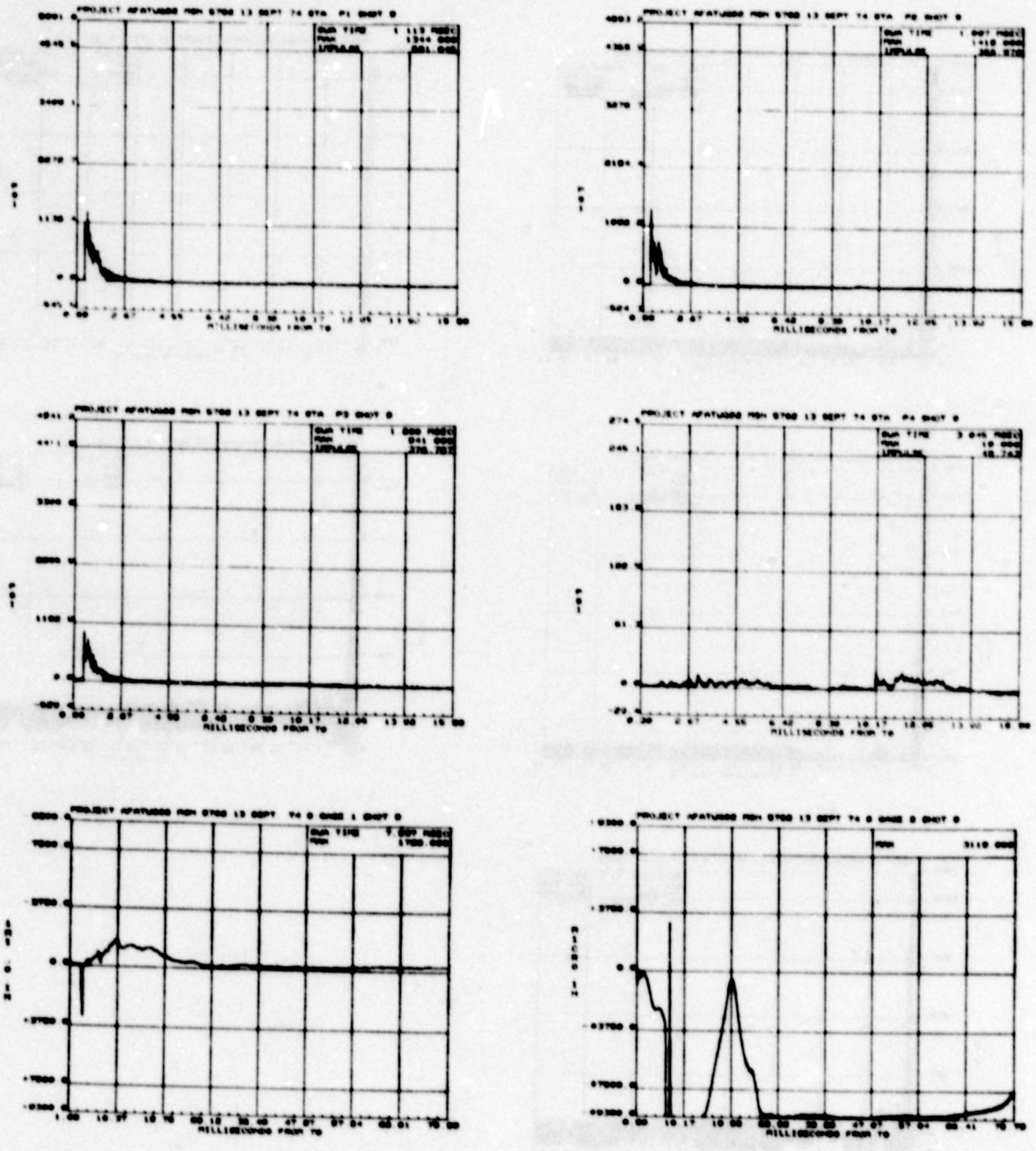

Figure A-9. Data From Impulse Test No. 9, Beam 5, 13 September 1974

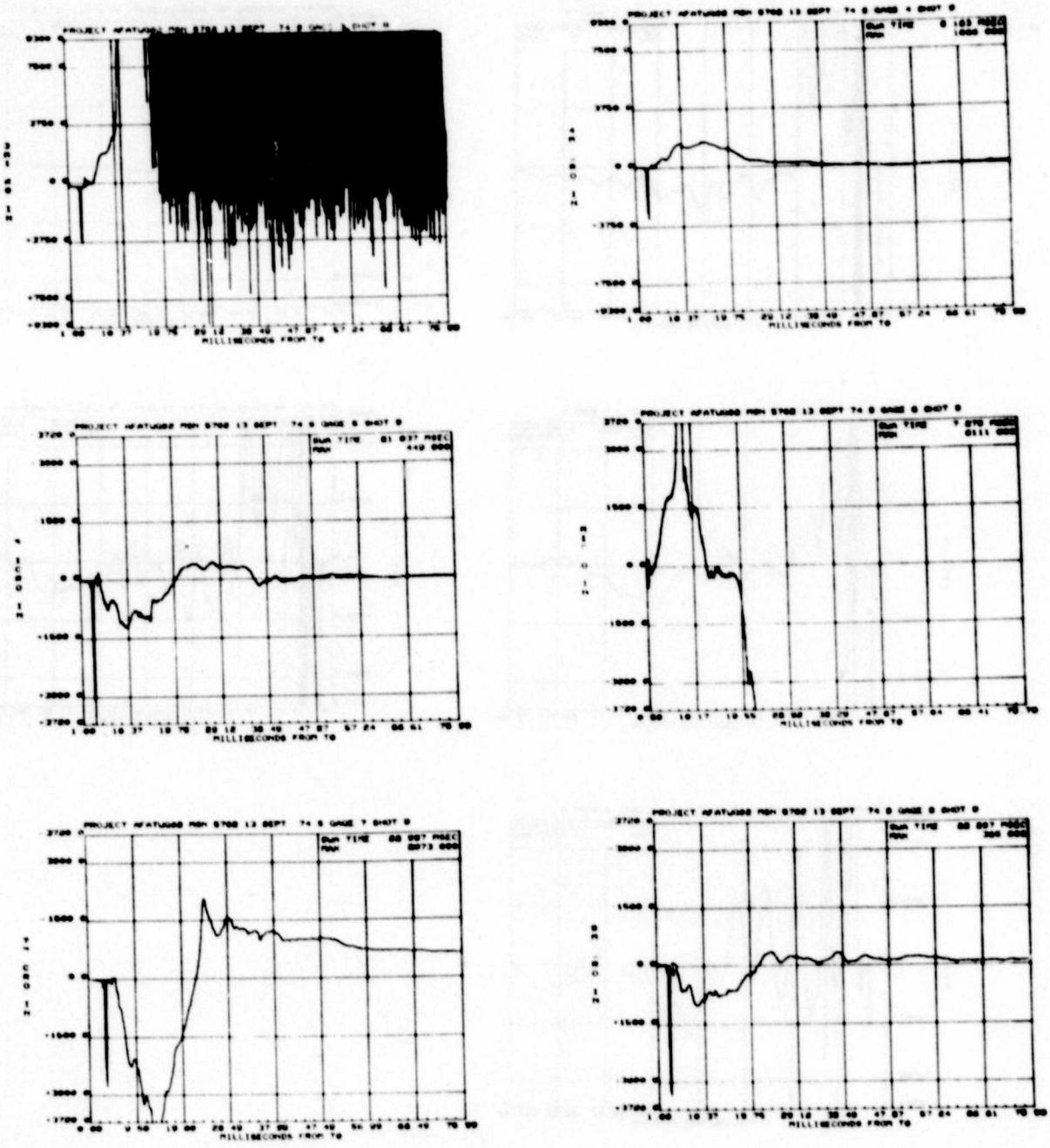

Figure A-9. Data From Impulse Test No. 9, Beam 5, 13 September 1974 (Continued)

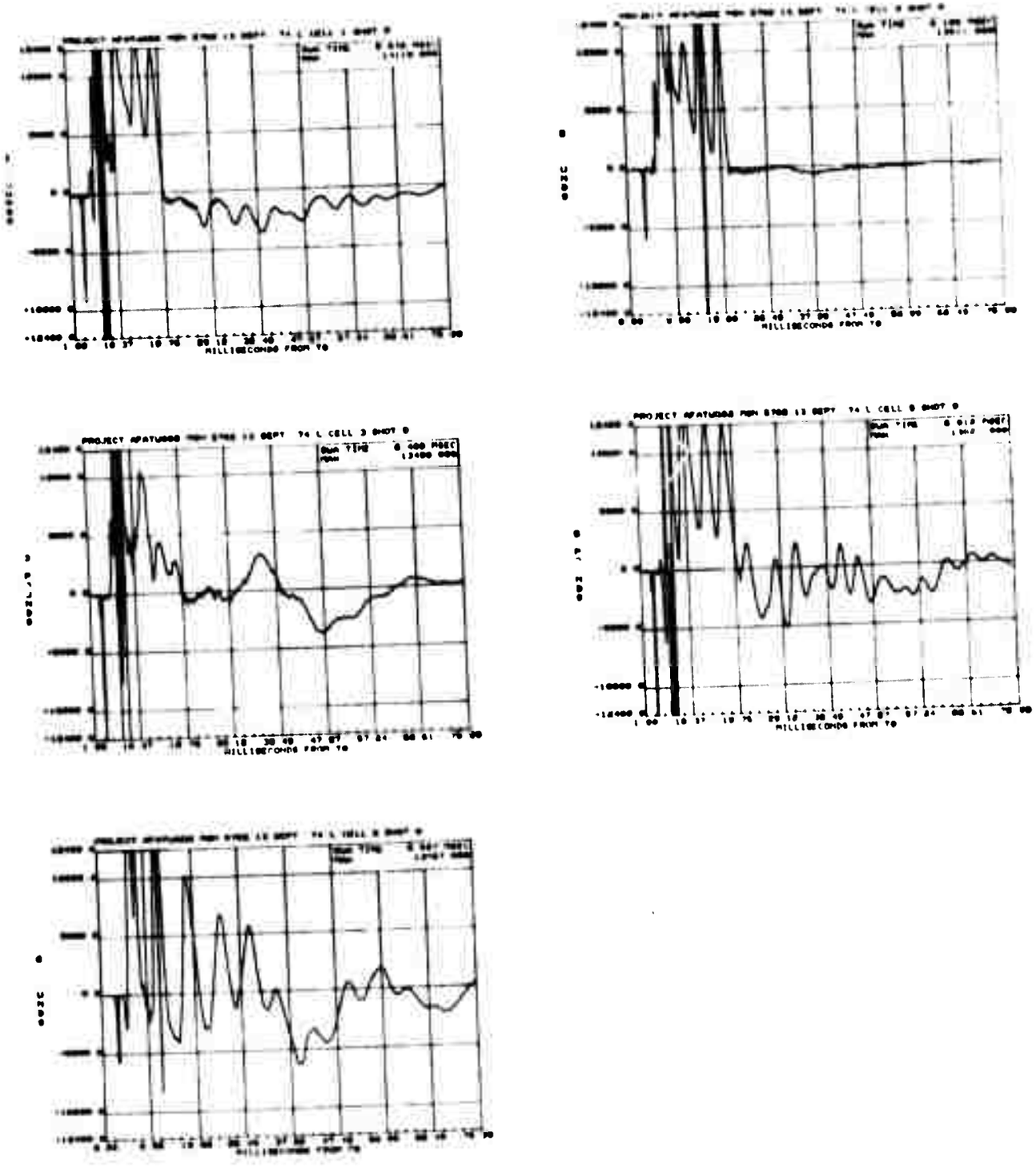

Figure A-9. Data From Impulse Test No. 9, Beam 5, 13 September 1974 (Continued)

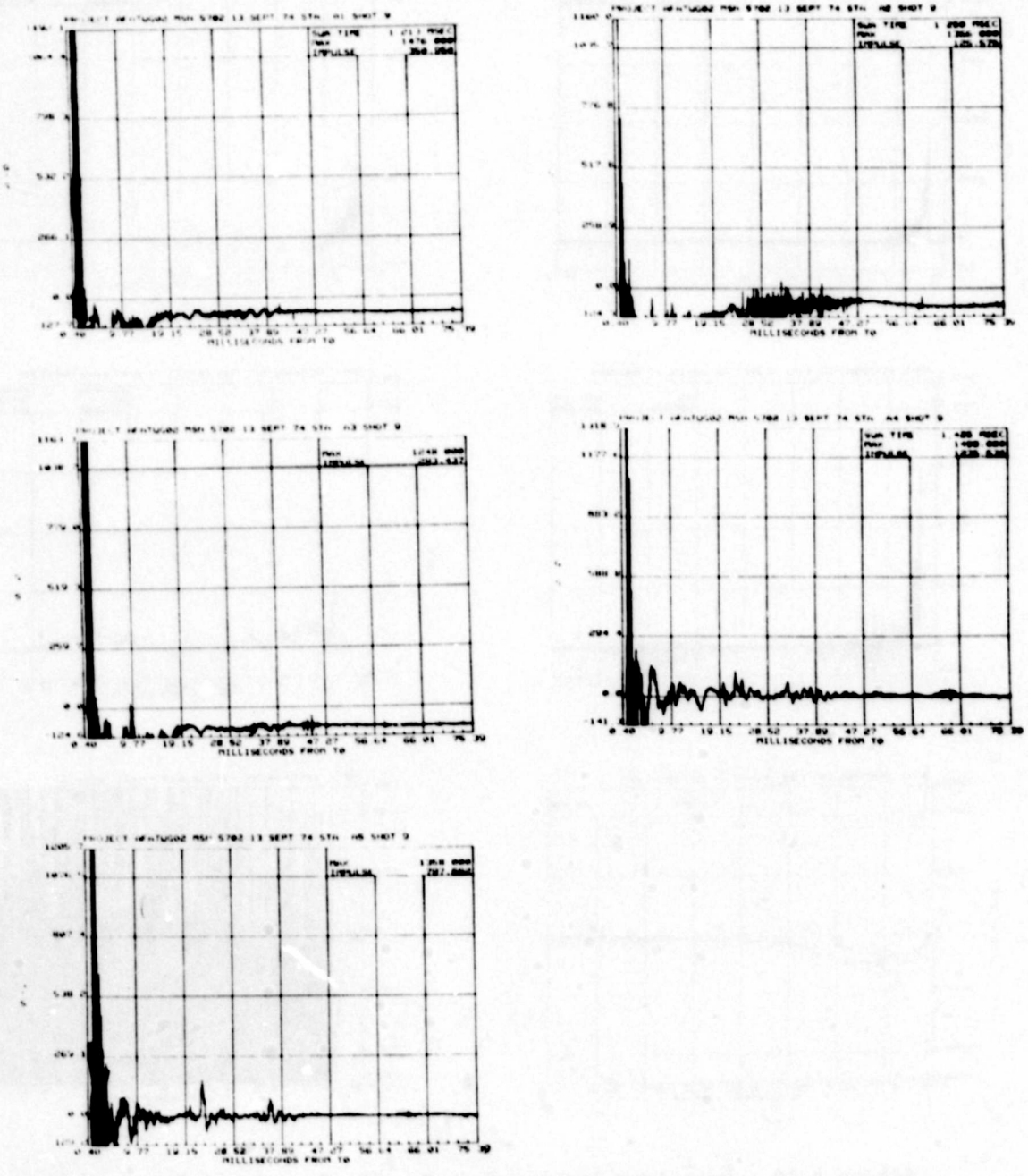

Figure A-9. Data From Impulse Test No. 9, Beam 5, 13 September 1974 (Concluded)

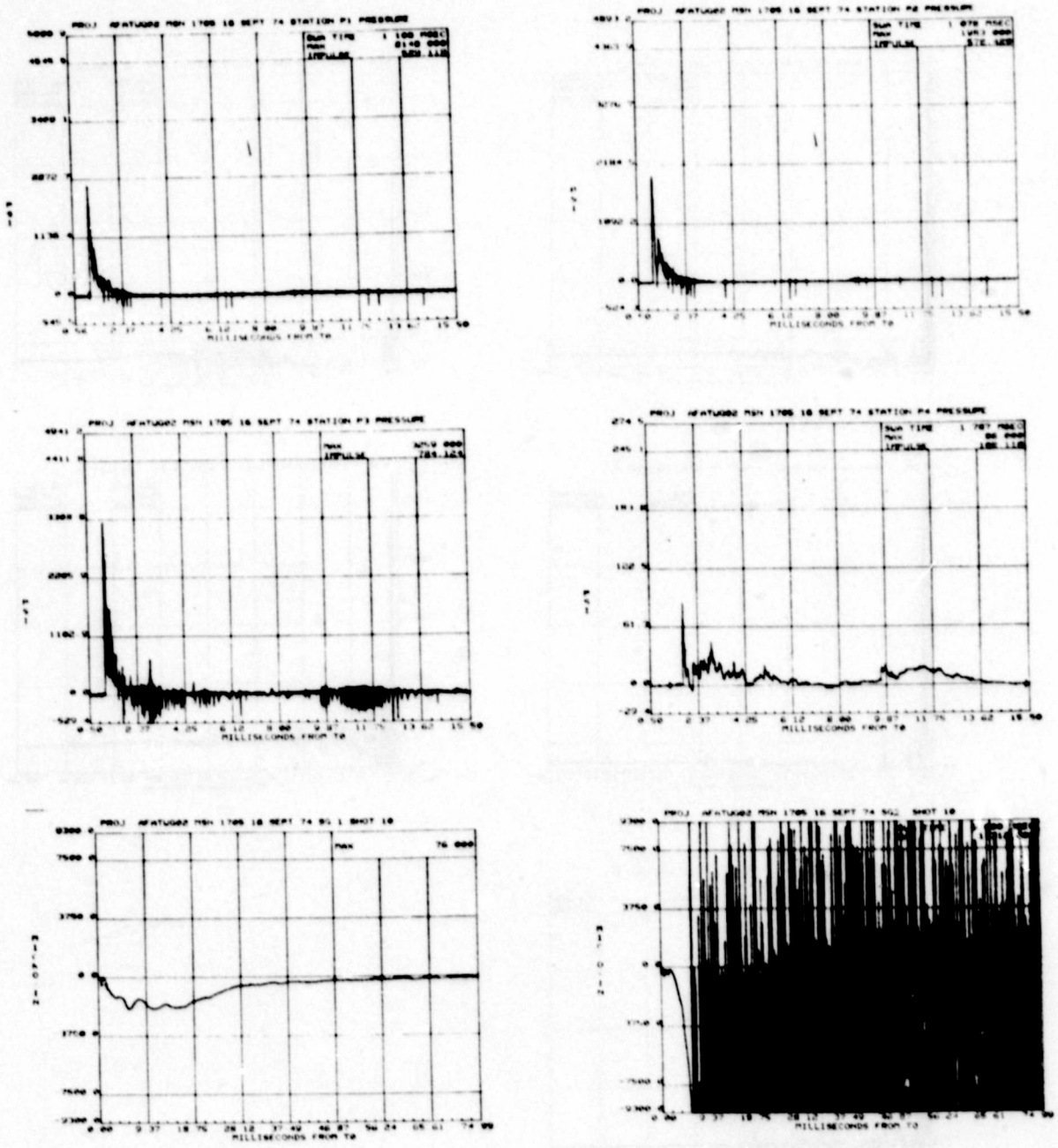

Figure A-10. Data From Impulse Test No. 10, Beam 9, 16 September 1974

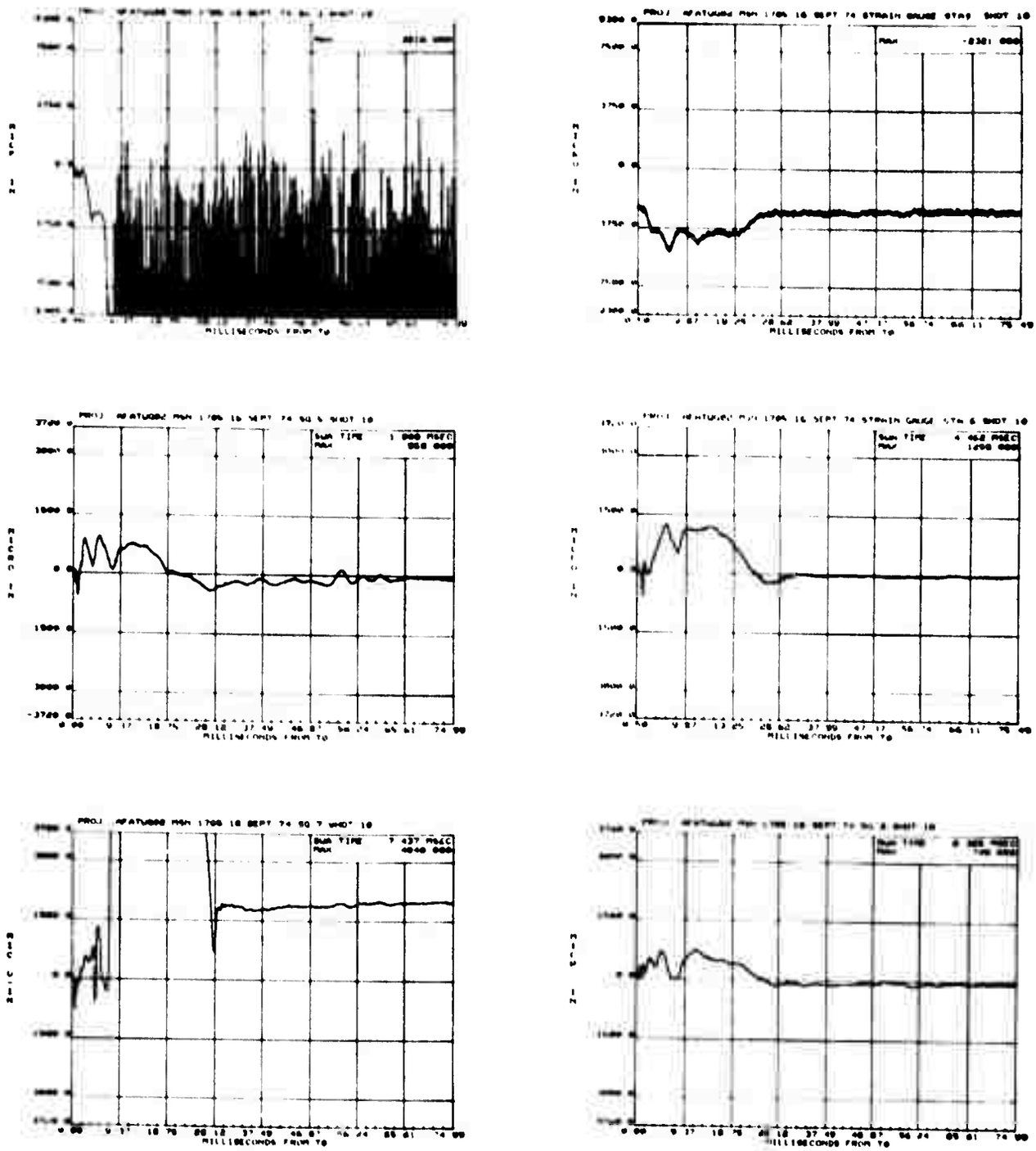

Figure A-10. Data From Impulse Test No. 10, Beam 9, 16 September 1974 (Continued)

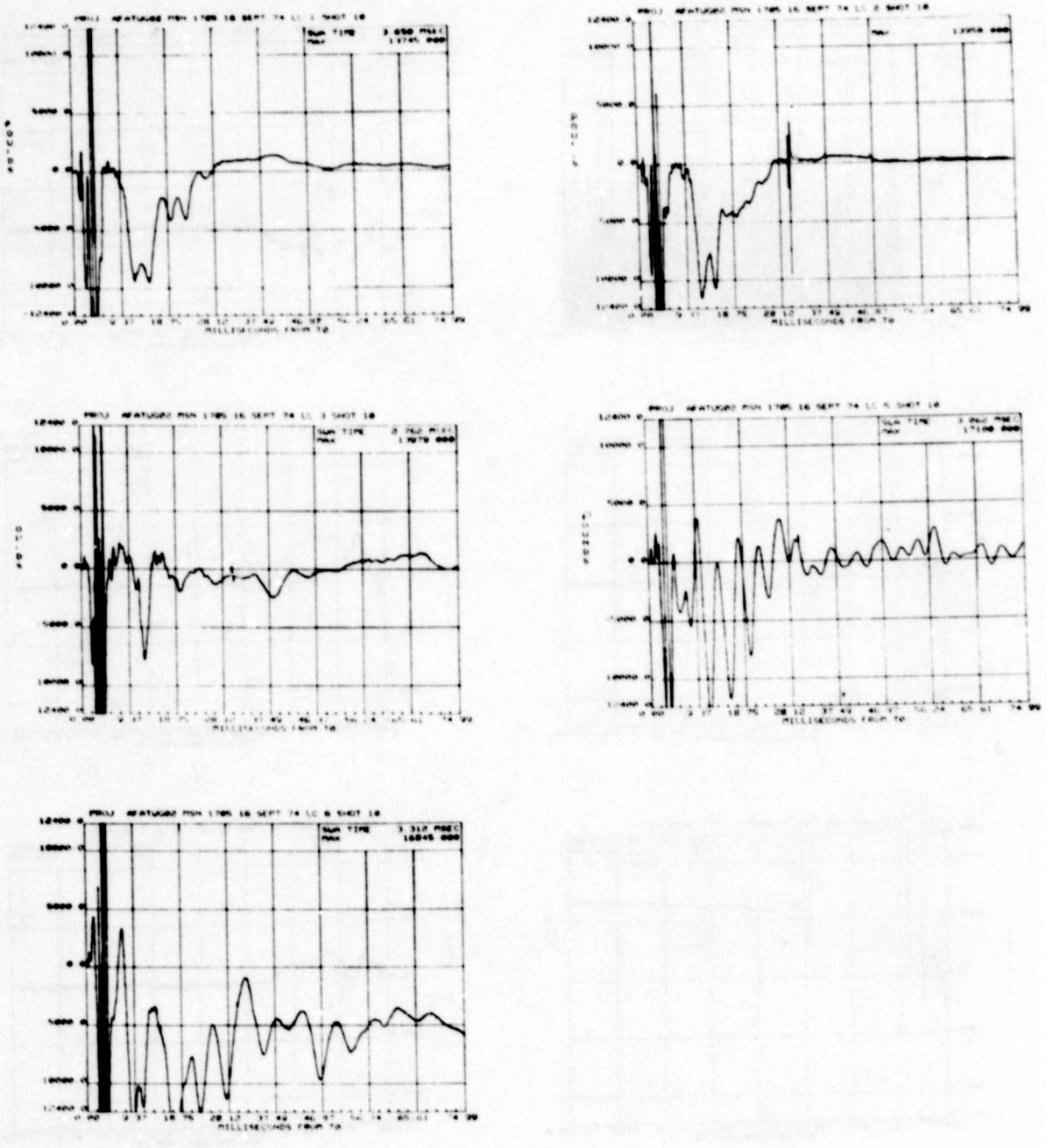

Figure A-10. Data From Impulse Test No. 10, Beam 9, 16 September 1974 (Continued)

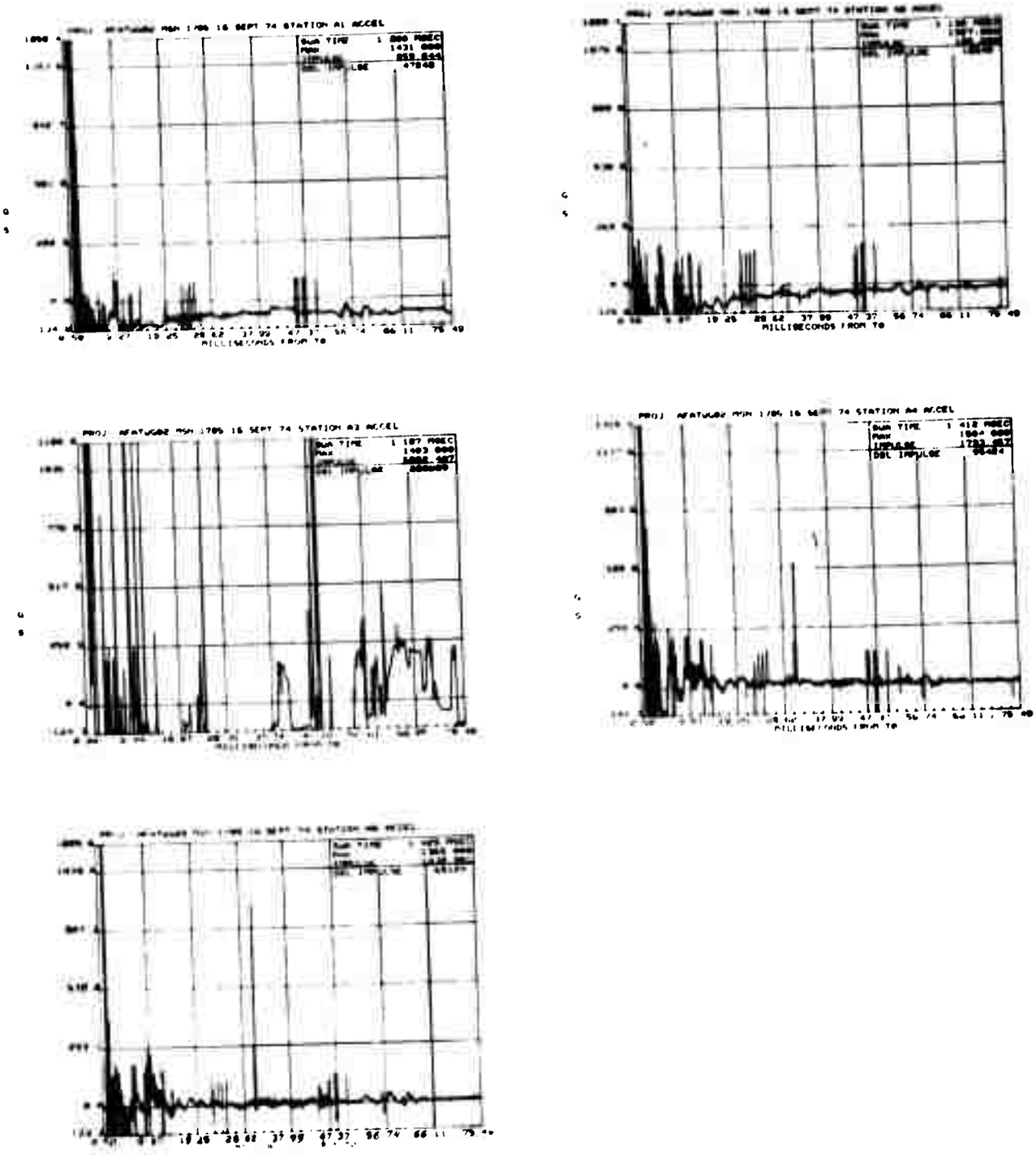

Figure A-10. Data From Impulse Test No. 10, Beam 9, 16 September 1974 (Concluded)

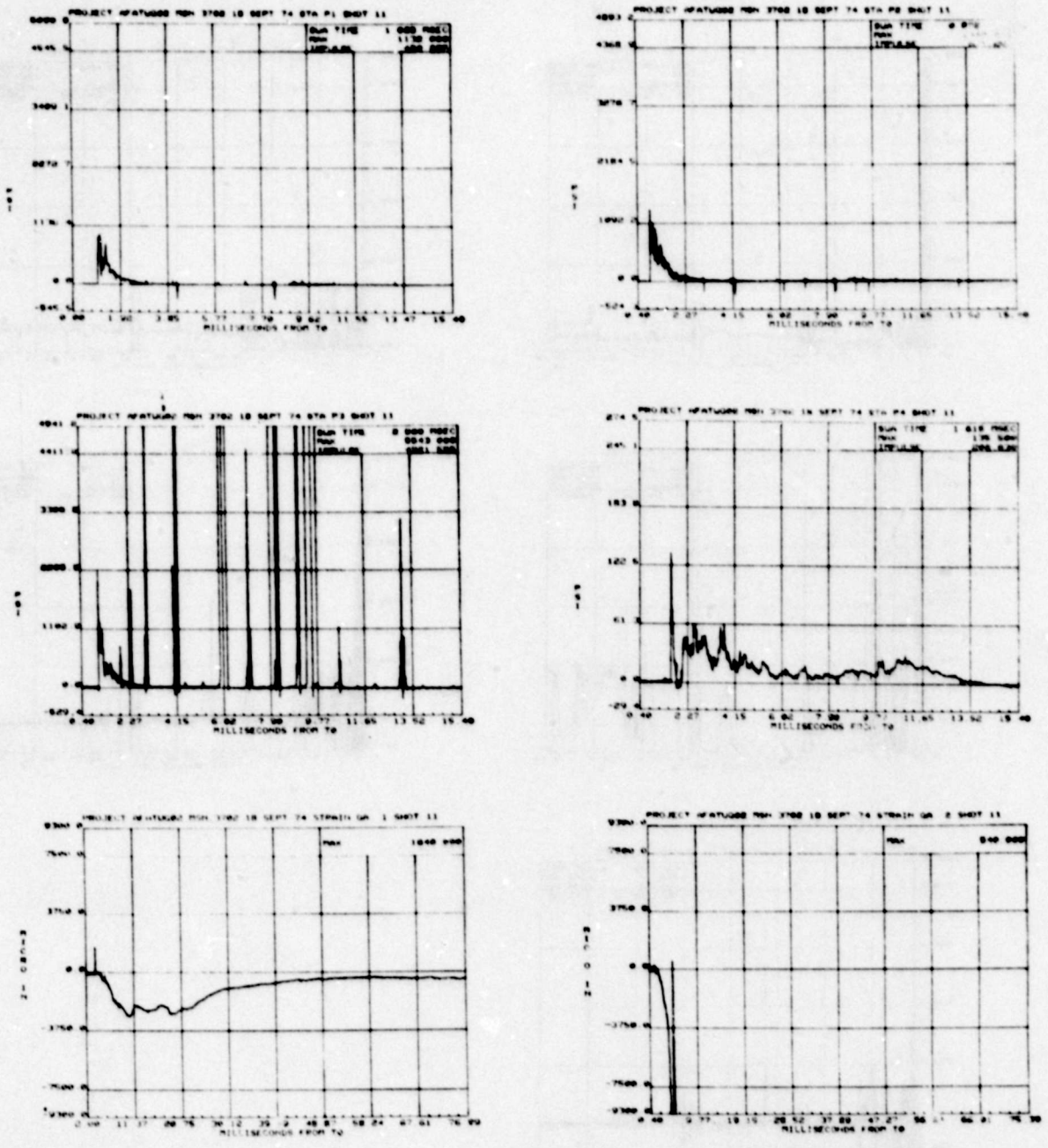

Figure A-11. Data From Impulse Test No. 11, Beam 3, 18 September 1974

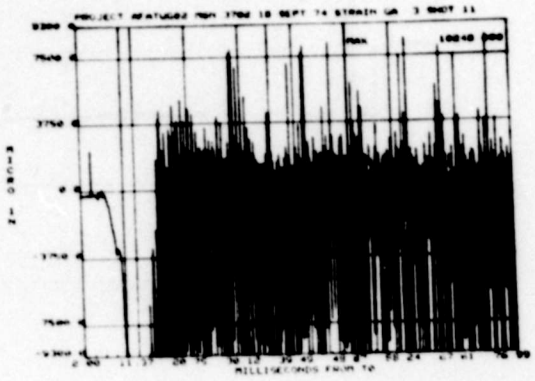

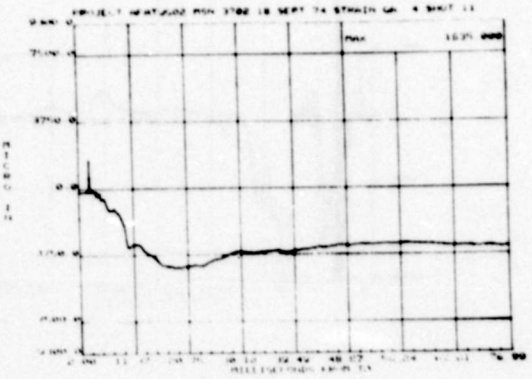

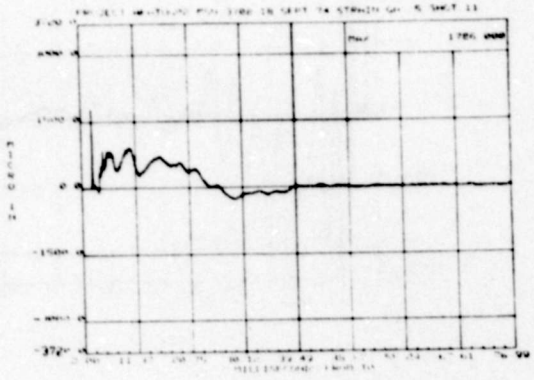

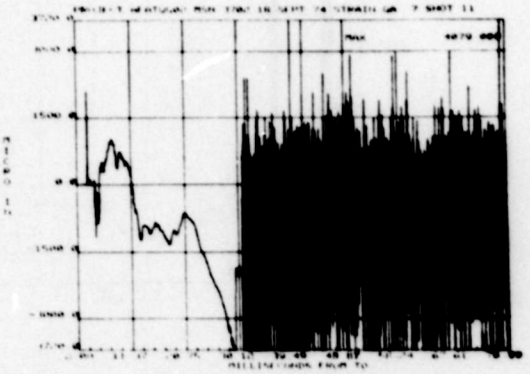

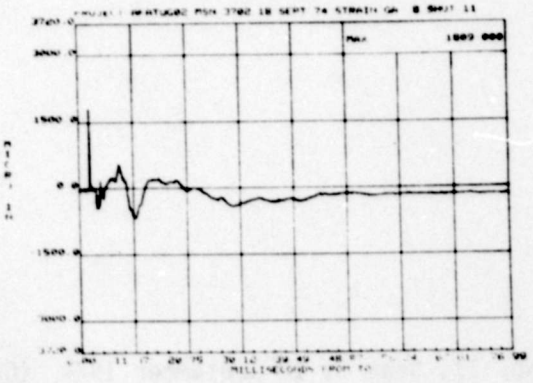

Figure A-11. Data From Impulse Test No. 11, Beam 3, 18 September 1974 (Continued)

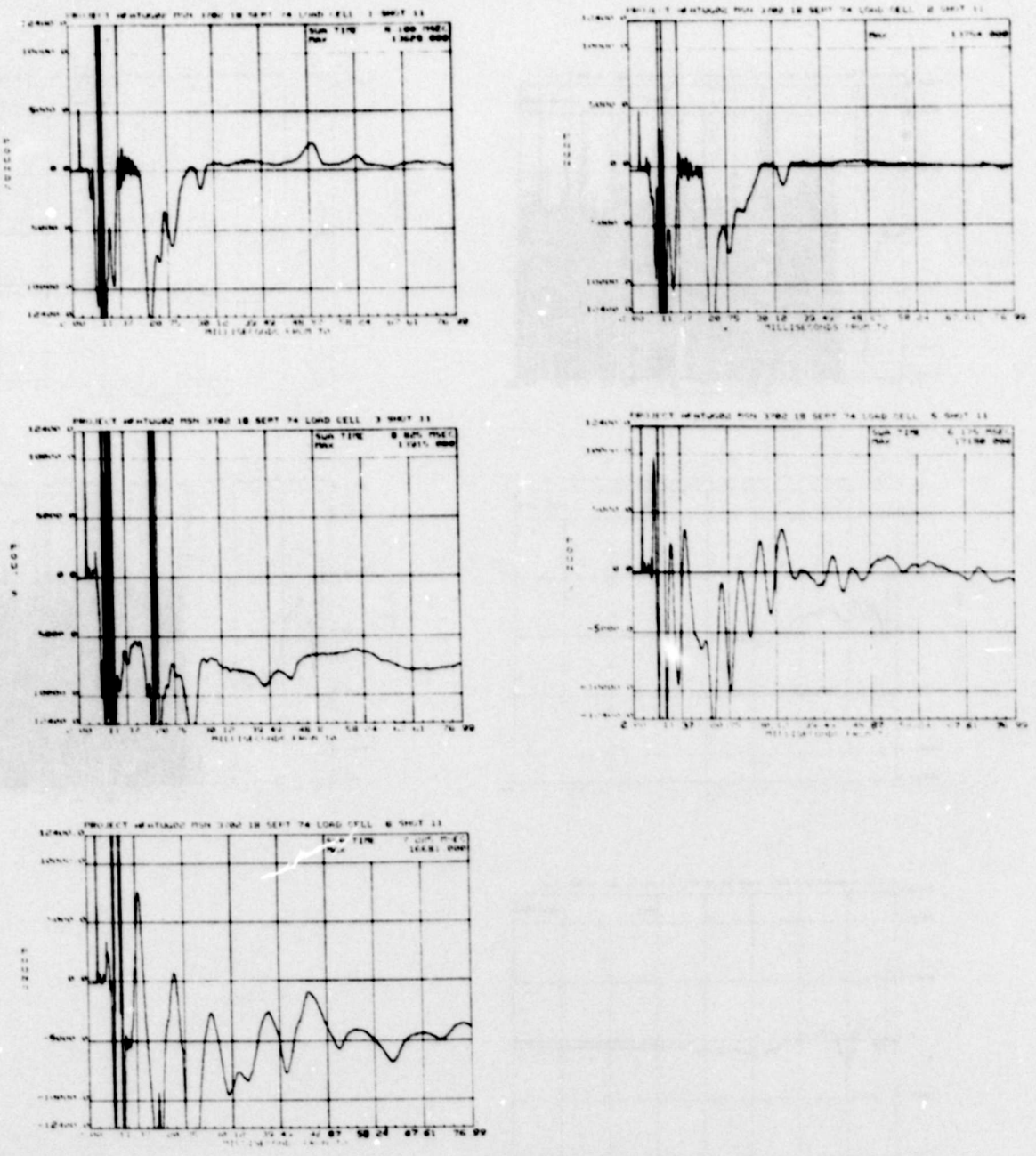

Figure A-11. Data From Impulse Test No. 11, Beam 3, 18 September 1974 (Continued)

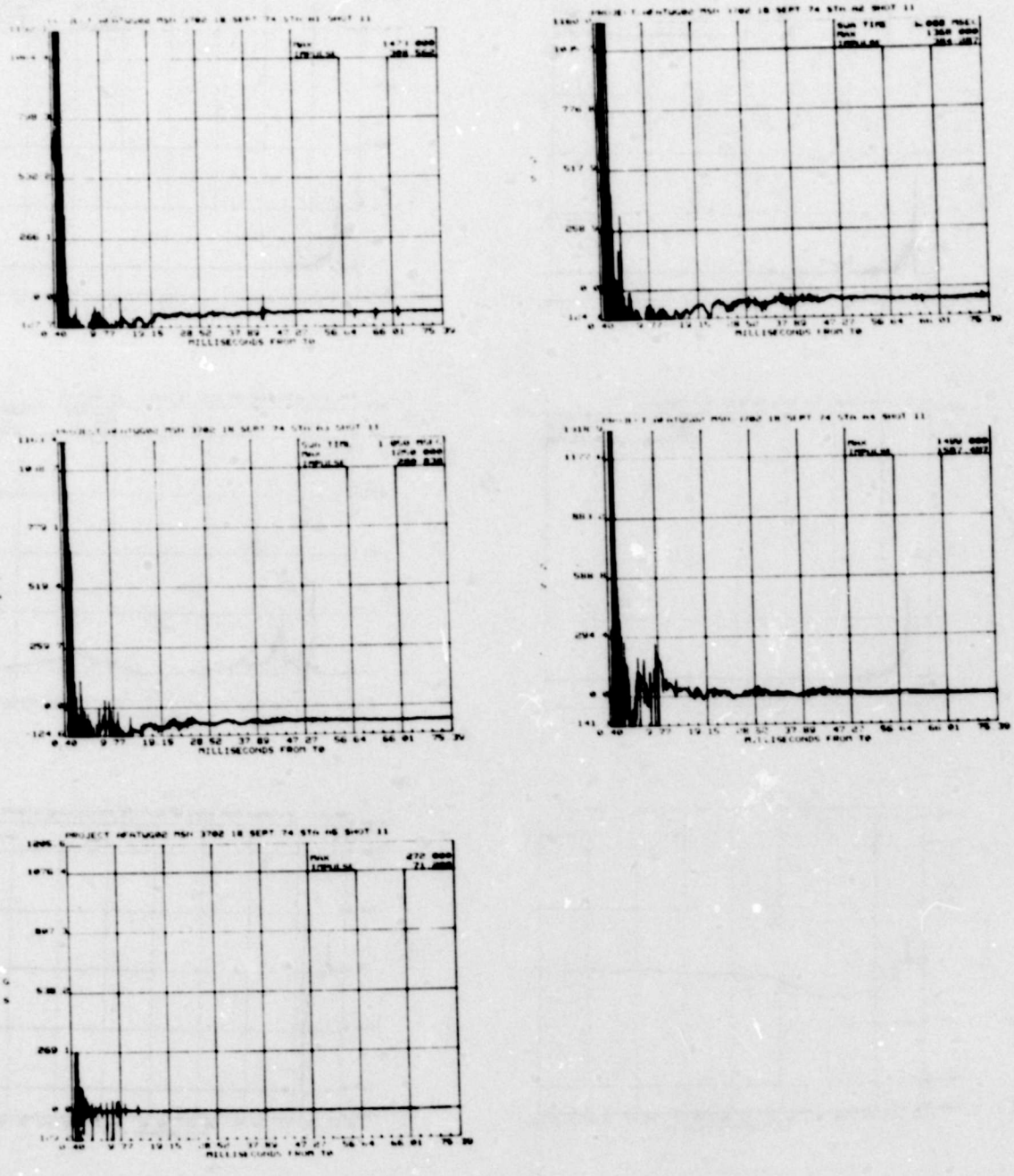

Figure A-11. Data From Impulse Test No. 11, Beam 3, 18 September 1974 (Concluded)

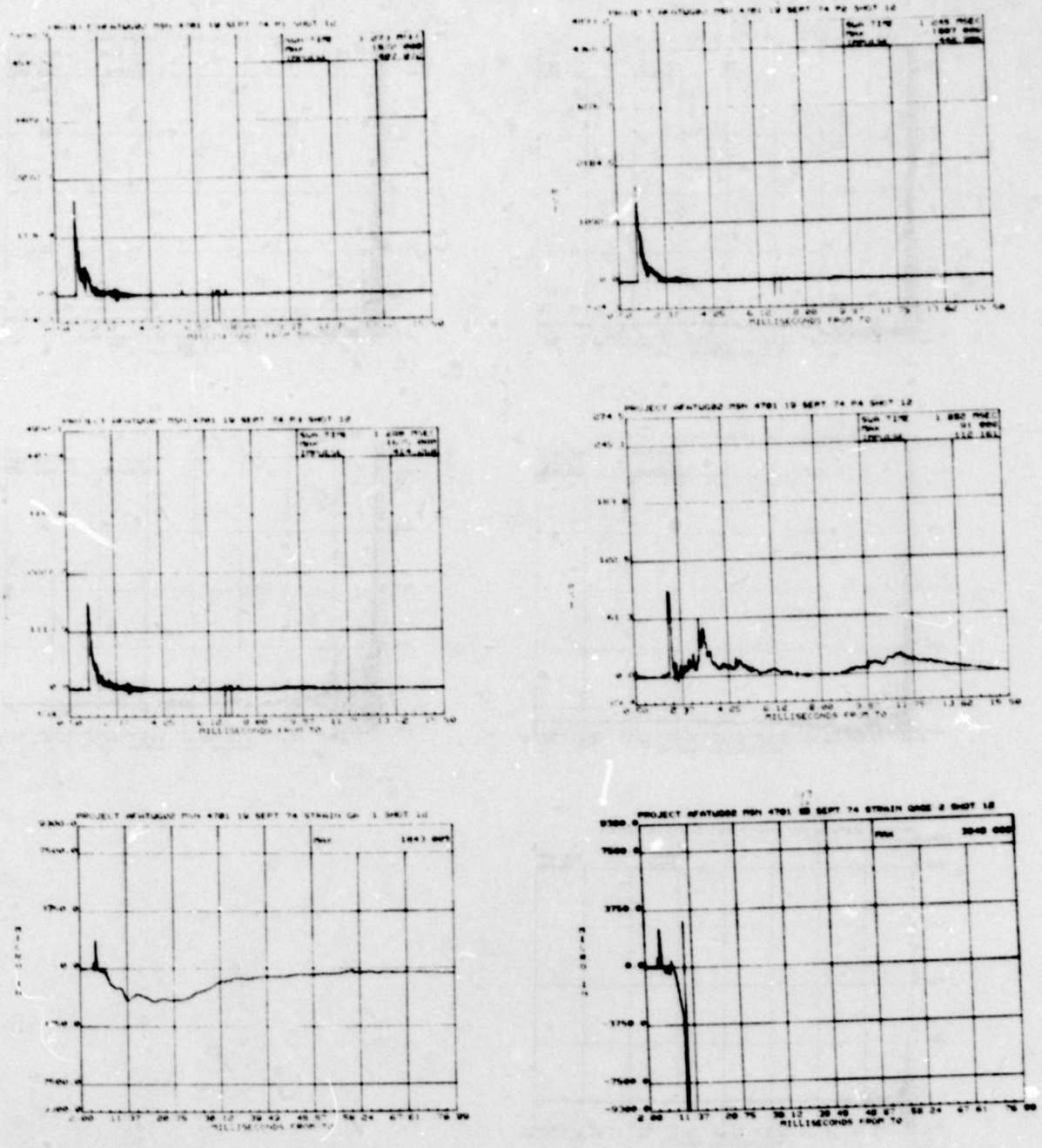

Figure A-12. Data From Impulse Test No. 12, Beam 11, 19 September 1974

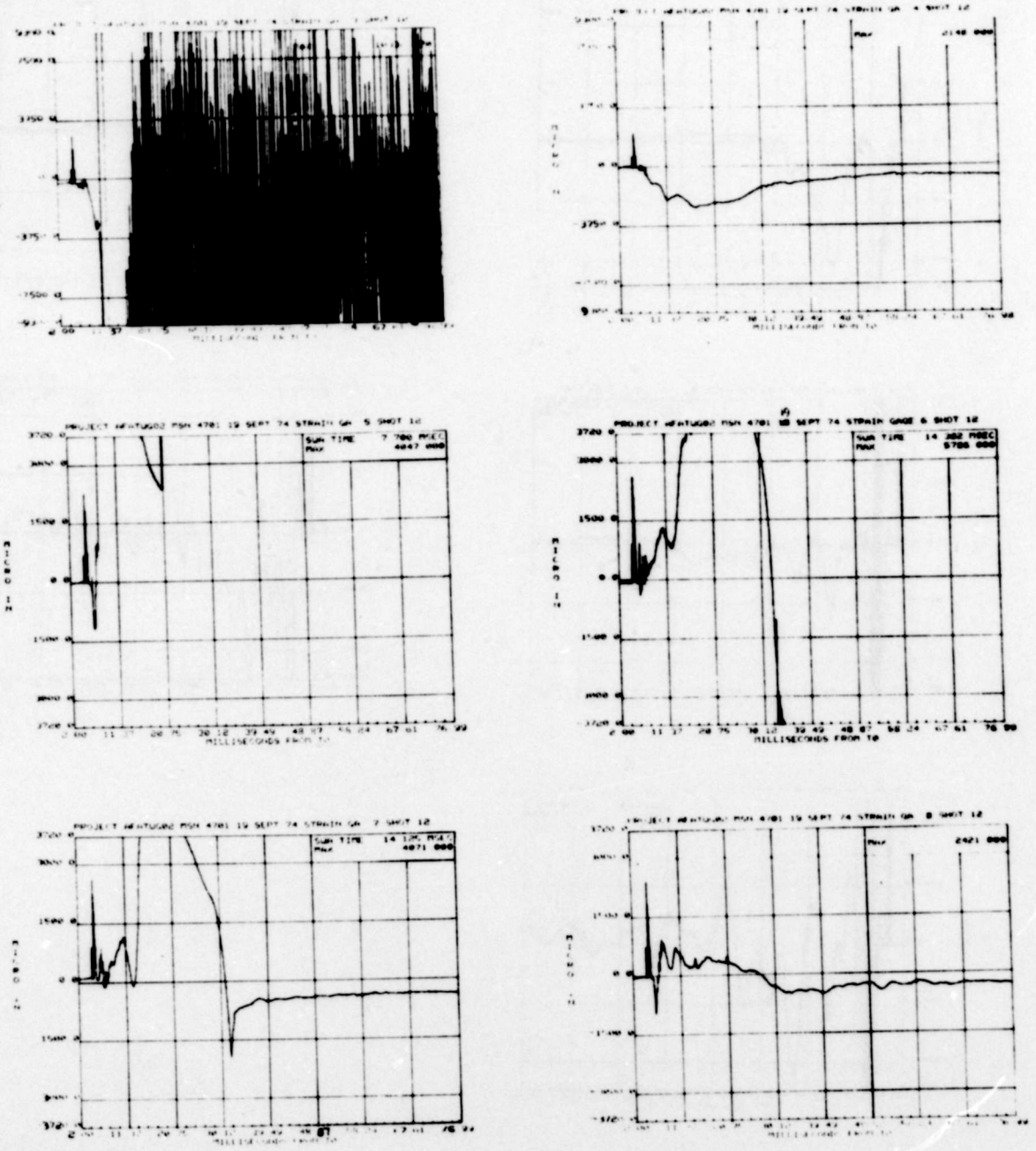

Figure A-12. Data From Impulse Test No. 12, Beam 11, 19 September 1974 (Continu

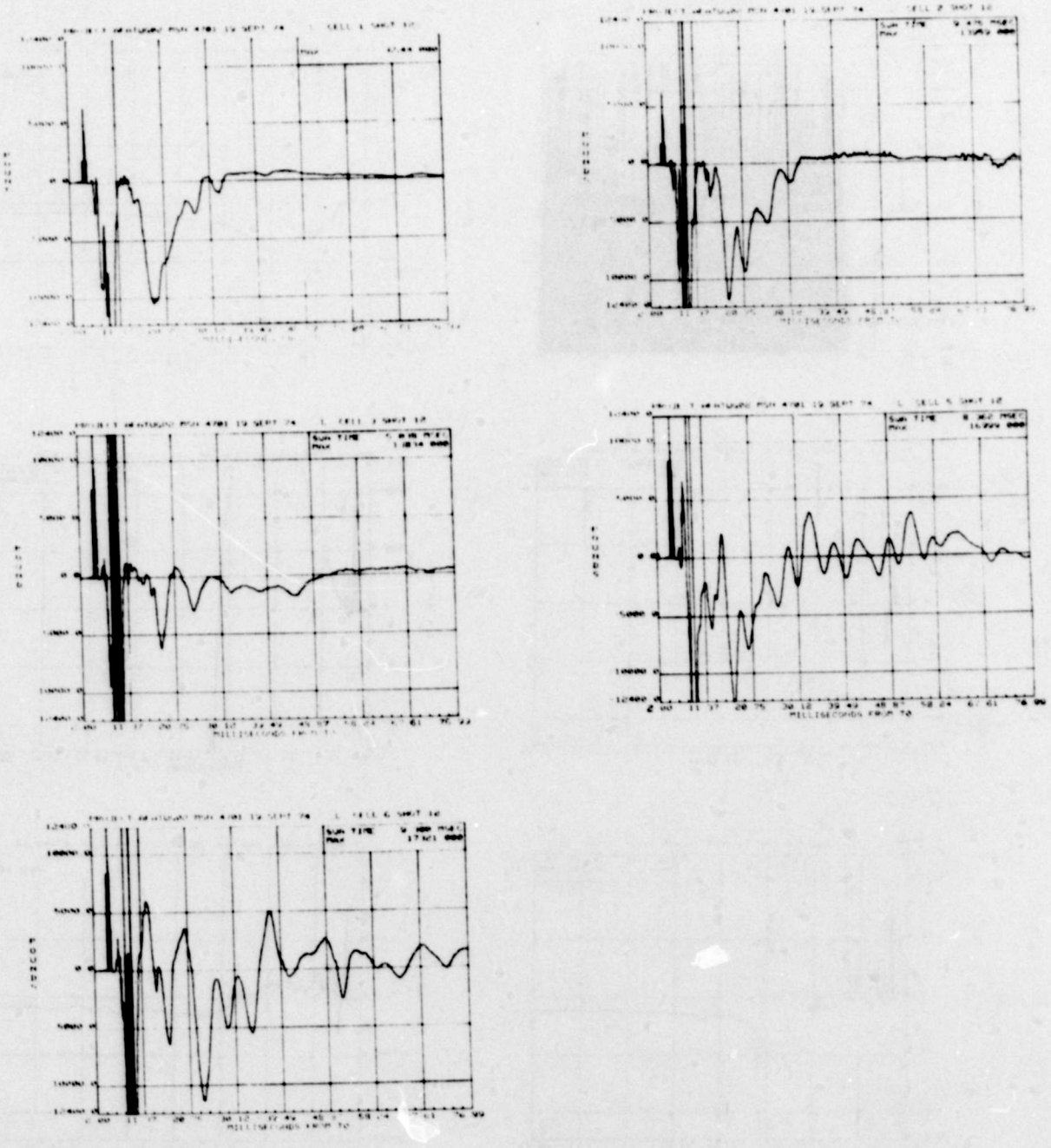

Figure A-12. Data From Impulse Test No. 12, Beam 11, 19 September 1974 (Continued)

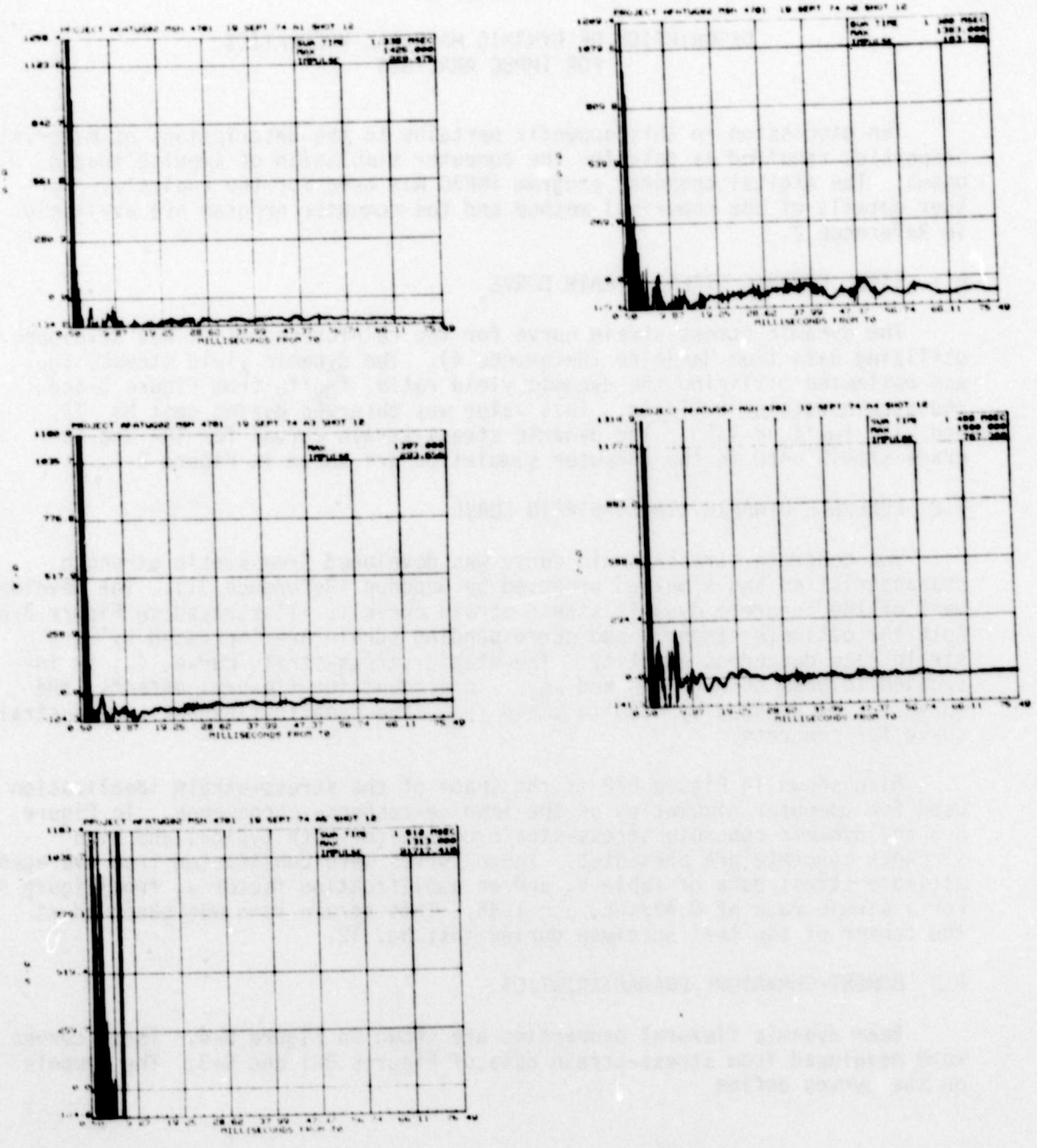

Figure A-12. Data From Impulse Test No. 12, Beam 11, 19 September 1974 (Concluded

APPENDIX B

DESCRIPTION OF DYNAMIC MATERIAL PROPERTIES FOR IMPBC ANALYSIS

The discussion in this appendix pertains to the descriptions of material properties required as data for the computer simulation of impulse loaded beams. The digital computer program IMPBC was used for the analysis. Further details of the numerical method and the computer program are available in Reference 2.

B.1 STEEL DYNAMIC STRESS-STRAIN CURVE

The dynamic stress-strain curve for the reinforcing steel was developed utilizing data from Manjoine (Reference 4). The dynamic yield stress, f_{Dy}, was estimated utilizing the dynamic yield ratio, f_{Dy}/f_y from Figure 3 and the strain rate of 2.01/sec. This value was observed during test No. 12, and gave $f_{Dy}/f_y = 1.55$. The dynamic stress-strain curves for 40- and 60-grade steels used in the computer simulation are shown in Figure B-1.

B.2 CONCRETE DYNAMIC STRESS-STRAIN CURVE

The concrete stress-strain curve was developed from static strength characteristics and a method proposed by Gupchup (Reference 31). The development of the concrete dynamic stress-strain curve is illustrated in Figure B-2. Both the ultimate strength and corresponding strain are increased by α, a strain rate dependent quantity. The static stress-strain curve, f_c, is increased to pass through f'_{Dc} and ε'_{Dc}. To account for flexural effects, the curve f_{Dc} is reduced by 0.85 to yield f_{FDc}, the dynamic flexural stress-strain curve for concrete.

Also shown in Figure B-2 is the shape of the stress-strain idealization used for computer simulation of the impulse-response phenomenon. In Figure B-3 the dynamic concrete stress-strain curves for both typical and high strength concrete are presented. These curves were constructed from averaged ultimate stress data of Table V, and an amplification factor α, from Figure 4. For a strain rate of 0.43/sec, $\alpha = 1.46$. This strain rate was observed at the center of the test specimen during test No. 12.

B.3 MOMENT-CURVATURE CHARACTERISTICS

Beam dynamic flexural properties are shown in Figure B-4. These curves were developed from stress-strain data of Figures B-1 and B-3. The symbols on the curves define

ϕf_{Dy} = the curvature related to onset of steel yield;

$\phi f''_{Dc}$ = the curvature producing ultimate concrete stress in the top fiber; and

$\phi \varepsilon'_{Dc}$ = the curvature which produced failure strain in the concrete.

Several important features of these curves have been discussed in Sections VII and VIII. First, the calculated flexural stiffness, EI, compares very favorably with measured values, Table VI. The measured flexural stiffness for typical beams, beams with high strength concrete, and high strength steel varies from 1.32×10^9 to 1.53×10^9 lb-in^2. An exception is beam 13 with an average flexural stiffness of 1.17×10^9 lb-in^2. In Figure B-4 little difference is noted between the flexural stiffness of these members, which have an average EI of 1.55×10^9 lb-in^2. This difference was anticipated and is due to the adjustment of concrete material properties to reflect increased strain rate. Furthermore, the calculated ultimate moment capacity of the typical beam is 625 kip-in. compared with a measured ultimate moment of 462 kip-in. for beam 13. The 35 percent increase in the calculated over-measured strength was anticipated due to increased strength of the concrete and steel for strain rate effects.

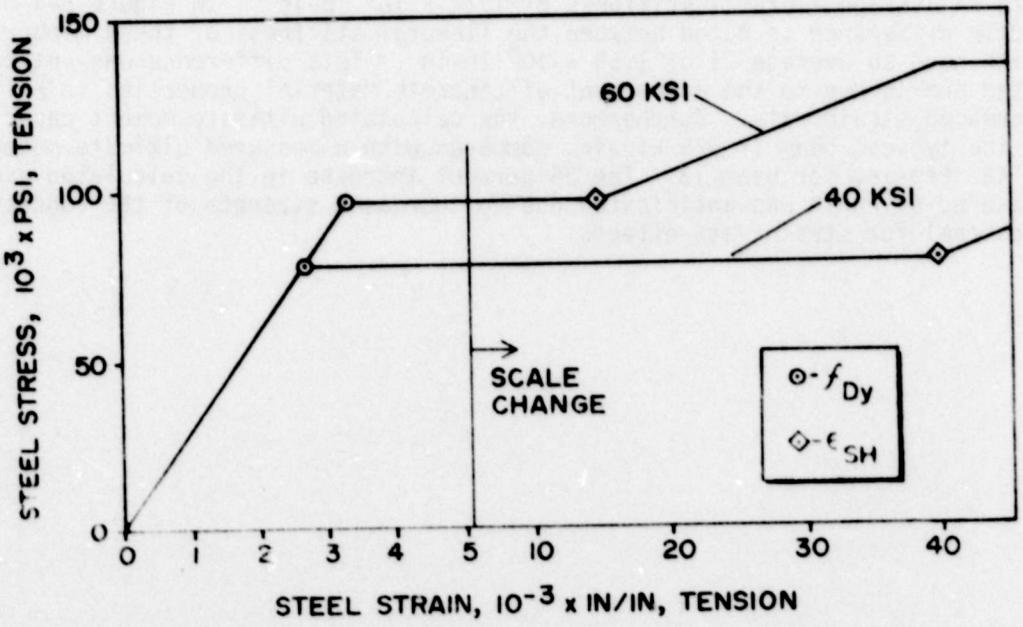

Figure B-1. Steel Stress-Strain Curves Used in IMPBC Simulations

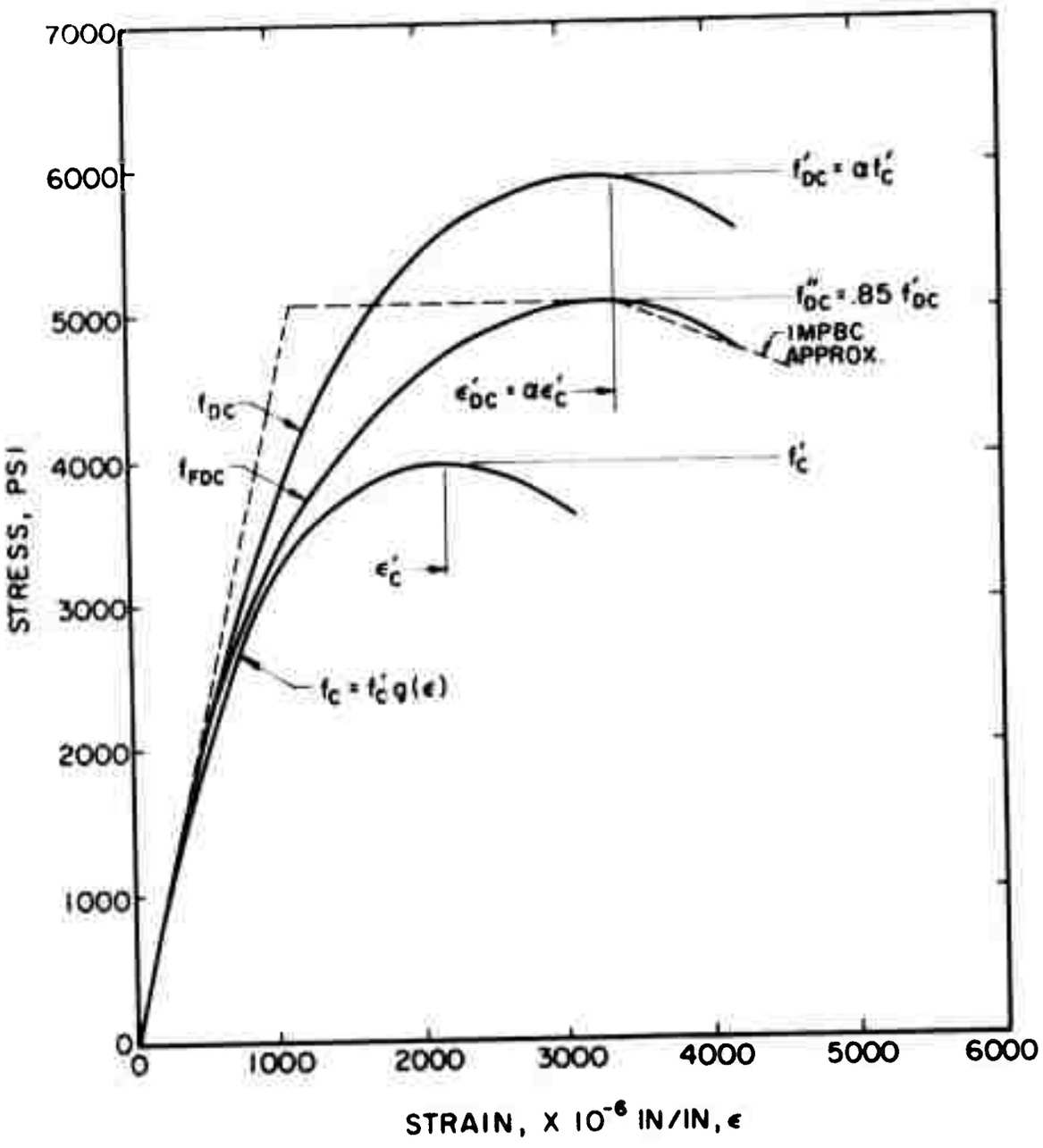

Figure B-2. Adjustments of Concrete Cylinder Stress-Strain Curve to Account for Dynamic and Bending Effects

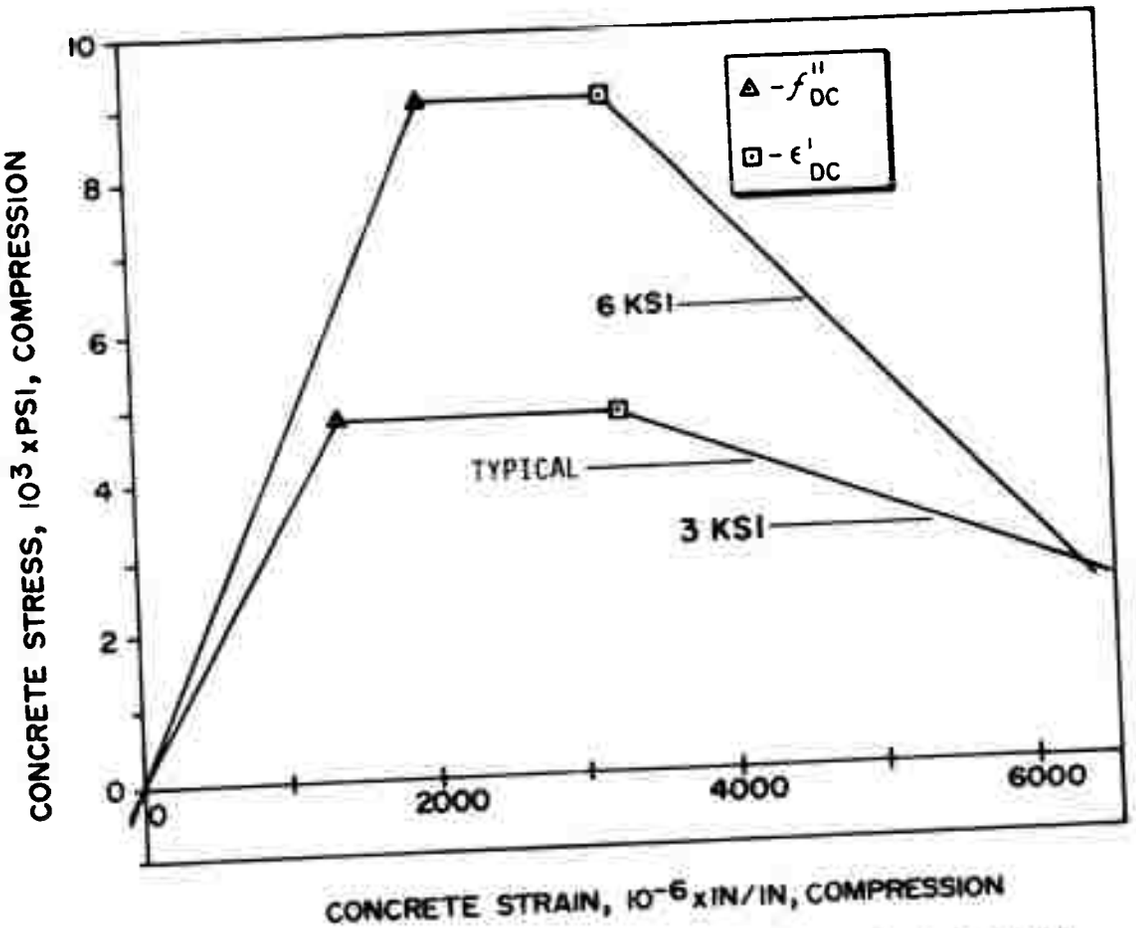

Figure B-3. Concrete Stress-Strain Curves Used in DIPSC Simulations

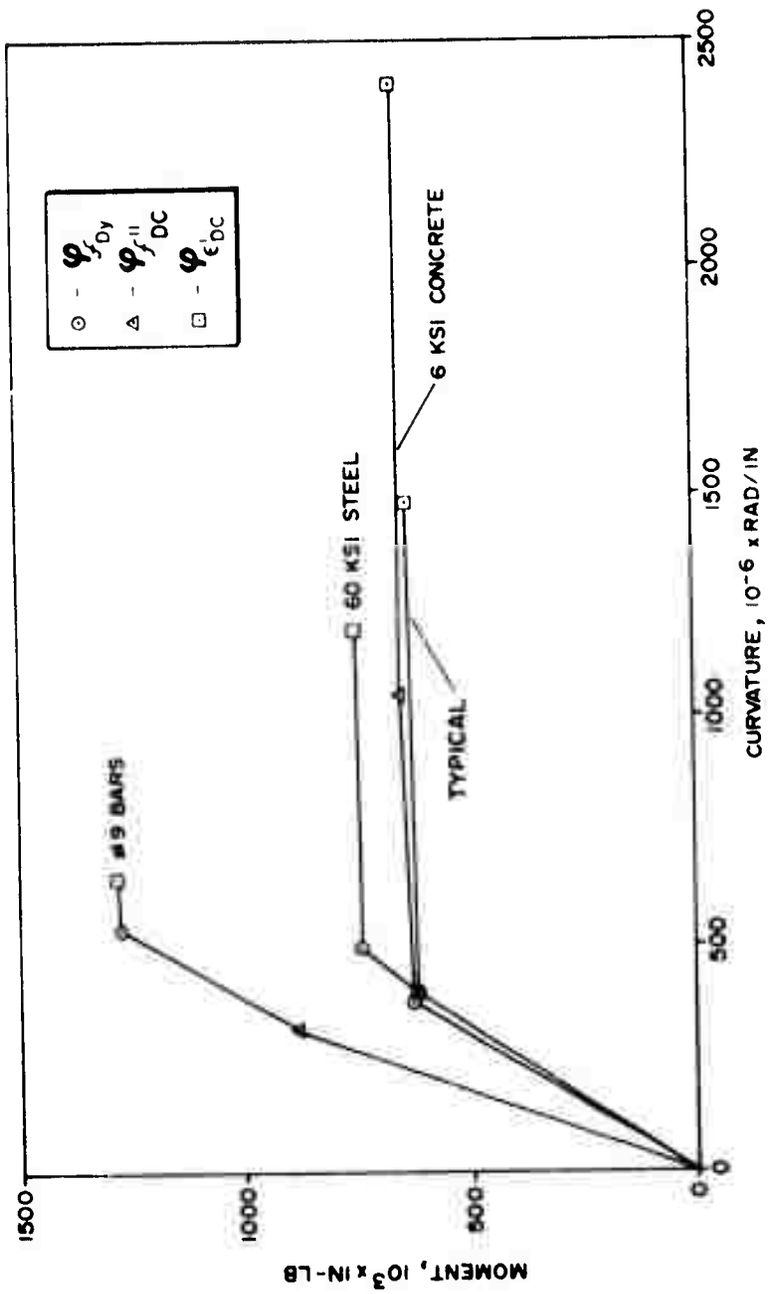

Figure B-4. Predicted Variation of Moment with Curvature for IMPBC Model

(The reverse of this page is blank)

INITIAL DISTRIBUTION

Hq USAF/SAMI	1
Hq USAFE/DOQ	1
Hq PACAF/DOOFQ	3
Hq TAC/DRA	1
ASD/ENFEA	1
AUL/LSE 71-249	1
OO/ALC/MMWMP	2
AFIS/INTA	1
DDC	2
AFATL/DLODL	9
AFATL/DL	1
AFATL/DLY	1
ASD/ENFEA	1
US Army TRADOC Sys Analysis Activity ATAA-SL (Tech Lib)	1
ASD/XRP	1
COMIPAC/I-232	1
AFATL/DLODR	1
AFATL/DLYW	2
AFATL/DLYV	1
Defense Intell Agcy/DB-4	1
AFSC/SDW	1
USNWC/Code 317	2
OASD/SA	1
AFSWC/SA	1
Comdr USA BRL/DRXBR-VL	1
Oklahoma State Univ	2
USAMSAA/DRXSY-J	1

(The reverse of this page is blank)